T.C.
SÜLEYMAN DEMİREL UNIVERSITY
GRADUATE SCHOOL OF NATURAL AND APPLIED SCIENCES

THE PREPARATION OF Au/Zn-NANOPARTICLE-DOPED PVA/n-SiC (MPS) STRUCTURES AND THE INVESTIGATION OF THEIR ELECTRICAL AND DIELECTRIC PROPERTIES AS FUNCTION OF FREQUENCY AND TEMPERATURE USING IMPEDANCE SPECTROSCOPY METHOD

Mohammad Hussein Ali Al-DAHROB

Supervisor
Prof. Dr. Ali KÖKCE

THE DEGREE OF DOCTOR OF PHILOSOPHY
DEPARTMENT OF PHYSICS
ISPARTA -2018

APPROVAL OF THE THESIS

"The Preparation of Au/Zn-Nanoparticle-Doped PVA/n-SiC (MPS) Structures and the Investigation of Their Electrical and Dielectric Properties as Function of Frequency and Temperature Using Impedance Spectroscopy Method" submitted by **Mohammad Hussein Ali Al-DAHROB** in partial fulfillment of the requirements for the degree of **The Degree of Ph.D of Science** in **Department of Physics**, Graduate School of Natural and Applied Sciences, Süleyman Demirel University by,

Supervisor	**Prof. Dr. Ali KÖKCE** Süleyman Demirel University
Committee Member	**Prof. Dr. Abdülmecit TÜRÜT** İstanbul Medeniyet University
Committee Member	**Prof. Dr. Şemsettin ALTINDAL** Gazi University
Committee Member	**Prof. Dr. Ahmet Faruk ÖZDEMİR** Süleyman Demirel University
Committee Member	**Prof. Dr. Nazım UÇAR** Süleyman Demirel University

Director	**Prof. Dr. Yasin TUNCER**

COMMITMENT

I hereby declare that all information in this document has been obtained and presented in accordance with academic rules and ethical conduct. I also declare that, as required by these rules and conduct, I have fully cited and referenced all material and results that are not original to this work.

Mohammad Hussein Ali Al-DAHROB

TABLE OF CONTENTS

Page

ABSTRACT

Doctor of Philosophy

THE PREPARATION OF Au/Zn-NANOPARTICLE-DOPED PVA/n-SiC (MPS) STRUCTURES AND THE INVESTIGATION OF THEIR ELECTRICAL AND DİELECTRIC PROPERTIES AS FUNCTION OF FREQUENCY AND TEMPERATURE USING IMPEDANCE SPECTROSCOPY METHOD

Mohammad Hussein Ali Al-DAHROB

Süleyman Demirel University
Graduate School of Natural and Applied Sciences
Department of Physics

Supervisor: Prof. Dr. Ali KÖKCE

In order to obtain the detailed information of the effect of (Zn-doped PVA) interfacial layer, density of surface states (*N_{ss}*) and series resistance (*R_s*) on electrical and dielectric characteristics, Au/n-SiC (MS) structure with and without (Zn- doped PVA) interfacial layer were fabricated. In this work, Zn doped PVA nano- fiber with interfacial layer of 50 nm thickness was deposited by electro-spinning method. Their electrical and dielectric properties as function of frequency, voltage and temperature have been investigated by using impedance spectroscopy method. The main electrical parameters such as ideality factor (n), barrier height (*BH*), *R_s* and rectification rate (*RR*) were evaluated and the energy dependent profile of surface states (*N_{ss}*) was also obtained from the forward bias current-voltage (I-V) data by taking into account voltage dependent *BH* and n. The sources of observed negative capacitance (NC) at the accumulation region for the MS and MPS structures were also evaluated. From capacitance-voltage (*C-V*) and conductance-voltage (*G/ω -V*) data measurements, the profile of *R_s* and *N_{ss}* were also investigated depending on the voltage for low (1 kHz) and high frequency (1 MHz) by using Nicollian-Brews method respectivly .

In addition, the charge transport mechanisms (CTMs) of the Au/ (7%Zn-doped PVA)/n-4H-SiC (MPS) structures were studied by applying forward bias current-voltage (*I-V-T*) measurements in a temperature domain of (100-320 K). Two distinct linear regions for each temperature were obtained from lnI-V plot which are corresponding to low barrier region (LBR) ($0.05V \leq 0.4V$) and moderate barrier region (MBR) ($0.4 \leq V \leq 0.8V$), respectively. The reverse-saturation current (I_0), n, zero-bias barrier height (Φ_{B0}) and structure resistance (*R_i*) show a strong temperature dependendence. Double Gaussian distribution (DGD) of BH was obtained from Φ_{B0} vs *n*, Φ_{B0} vs q/2kT and (n^{-1}-1) vs q/2kT plots for LBR and MBR at low temperature (LTR) (100-200 K) and high temperature regions (HTR) (220-320 K), respectively.
The values of (nT) or n(kT/q) especially at MBR are found almost constant indicating that the field emission (FE) theory is possible CTM rather than other transport mechanisms. Also, the higher values of n at low temperatures can not be explained only by FE theory. $\overline{\Phi}_{B0}$ and A* values for LBR were calculated from the

values of the slope and intercept of these plots as 0.730 eV, 114.12 $A.cm^{-2}K^{-2}$ at LTR and 1.304 eV, 97.33 $A.cm^{-2}K^{-2}$ at HTR, while for MBR, as 0.687 eV, 144.97 $A.cm^{-2}K^{-2}$ at LTR and 1.165 eV, 122.11 $A.cm^{-2}K^{-2}$ at HTR, respectively. The values of A* for MBR at LTR approach to the 146 $A.cm^{-2}K^{-2}$which represent the theoretical value of for n-4H-SiC. As a result the CTM in Au/ (7%Zn-doped PVA)/n-4H-SiC (MPS) structure can be explained on the base of TE mechanism with the double GD of BHs

In the last part of this study, the effect of voltage and temperature on the values of dielectric constant (ε'), dielectric loss (ε''), tangent loss (tan δ), real and imaginer part of electric modulas (M' and M'') and AC conductivity (σ_{ac}) were calculated at 1 MHz and large voltage and temperature range. These results show a considerably effect of temperature and applied bias voltage especially in depletion and accumulation regions. Negative capacitance (NC) behavior has shown in C–V-T; hence ε'–T plots for all temperatures with negative value especically at high forward biases due to the series resistance, interface states and interfacial layer. The experimental values of ε' shows an incerasing with temperature increasing furthermore, ε'', tan δ and σ_{ac} show an increasing espically at higher temperature than T= 230K at 0.5 V forward bias region. M' and M'' show a strong temperature and applied voltage dependence due to the existence of N_{ss}, dipole polarizations, R_s and interfacial layer. Thus, we can say that the dielectric characteristics and ac conductivity of Au/ modified Zn-doped PVA doped/ n-4H-SiC (MPS) structure has a strong function of temperature and voltage.

Keywords: MS and MPS structures; Passivation effect of Zn-doped PVA interlayer, surface states, negative capacitance, conduction mechanism, barrier hight, barrier inhomogeneties, double Gaussian distribution, electric and dielectric characteristics, electric modulules**.**

2018, 103 pages

ÖZET

Doktora Tezi

Au/Zn-NANOPARÇACIKLA-KATKILI PVA/n-SiC (MPS) YAPILARIN HAZIRLANMASI VE ELEKTRİK İLE DİELEKTRİK ÖZELLİKLERİNİN EMPEDANS SPEKTROSKOPİ METODU KULLANILARAK FREKANS VE SICAKLIĞA BAĞLI İNCELENMESİ

Mohammad Hussein Ali Al-DAHROB

Süleyman Demirel Üniversitesi
Fen Bilimleri Enstitüsü
Fizik Anabilim Dalı

Danışman: Prof. Dr. Ali KÖKCE

Zn-katkılı PVA arayüzey tabakasının, yüzey durumlarının yoğunluğunun (**N_{ss}**)ve seri direncin R_s elektriksel ve dielektrik karakteristikler üzerindeki etkisinin ayrıntılı bilgisini elde etmek için, hem arayüzey tabakasız ve hem de arayüzey tabakalı(Zn-katkılı PVA**)** Au/n-SiC (MS) yapısı üretildi. Bu çalışmada, 50 nm kalınlığa sahip Zn katkılı PVA nano-fiber arayüz tabakası elektro-spin yöntemi ile n-SiC üzerine biriktirildi. Empedans spektroskopisi yöntemi ile frekans, gerilim ve sıcaklığın fonksiyonu olarak elektrik ve dielektrik özellikleri araştırıldı. İdealite faktörü (n), engel yüksekliği (BH), seri direnç (R_s) ve doğrultma oranı (*RR*) gibi temel elektriksel parametreleri değerlendirildi ve aynı zamanda enerjiye bağlı yüzey durumlarının (N_{ss}) profili, voltaja bağlı BH ve n hesaba katılarak doğru beslem akım-volaj (*I-V*) verilerinden elde edildi. MS ve MPS yapıları için birikim bölgesinde gözlenen negatif kapasitans (NC) kaynakları da değerlendirildi. Kapasitans-voltaj (*C-V*)ve iletkenlik-voltaj *(G/ω-V*) veri ölçümlerinden voltaja bağli R_s ve N_{ss} profilleri sırasıyla, düşük– yüksek frekeuns (1kHz -1MHz) Nicollian-Brews yöntemi kullanılarak elde edildi.

Ek olarak, (Au / % 7 Zn-katkılı PVA / n-4H-SiC) (MPS) yapılarının akım-iletim mekanizmaları (CTM), (100-320 K) sıcaklık bölgesinde doğru beslem akım-voltaj *(I-V-T*) ölçümleri uygulanarak incelendi. Düşük gerilim bölgesi (LBR) (0.05V≤0.4V) ve orta gerilim bölgesine (MBR) (0.4≤V≤0.8V) tekabül eden, lnI-V çiziminden her sıcaklık için iki ayrı doğrusal bölge elde edildi. Ters doyum akımı I_0, *n*, sıfır beslem engel yüksekliği Φ_{B0} ve R_s değerleri güçlü bir sıcaklığa bağımlılık gösterdi.

BH'nin double Gauss dağılımı, sırasıyla düşük sıcaklık bölgesi (LTR) (100-200 K) ve yüksek sıcaklık bölgesinde (HTR) (220- 320 K), LBR ve MBR için *n*' ye karşı Φ_{B0}, *q/2kT* ye karşı Φ_{B0} ve *q/2kT* ye karşı (n^{-1}-1) grafiklerinden elde edildi. Özellikle MBR'deki (nT) veya (nKT/q)' nin değerleri neredeyse sabit bulunmakta olup, bu durum alan emisyon FE teorisinin, diğer transport mekanizmalarından ziyade yük transport mekanizmasının CTM mümkün olabileceğini gösterir. Ayrıca, düşük sıcaklıklarda n'nin daha yüksek değerleri sadece FE teorisi ile açıklanamaz. LBR için $\bar{\Phi}_{B0}$ ve A* değerleri, bu grafiklerin eğimleri ve düşey ekseni kestiği değerlerden sırasıyla LTR'de 0.730 eV, 114.12 A.cm^{-2}K^{-2} ve HTR'de 1.304 eV, 97.33 A.cm^{-2}K^{-2}

olarak hesaplandı. Buna karşılık aynı değerler MBR için sırasıyla LTR'de 0.687 eV, 144.97 $A.cm^{-2}K^{-2}$ve HTR'de 1.165 eV, 122.11 $A.cm^{-2}K^{-2}$ olarak hesaplandı. LTR'de MBR için A*' ın değerleri, n-4H-SiC'nin teorik değerini temsil eden 146 $A.cm^{-2}K^{-2}$'ye yaklaşır. Sonuç olarak, Au/%7Zn katkılı PVA/n-4H-SiC MPS yapısındaki CTM, BH'lerin çift GD'si ile TE mekanizmasına dayanılarak açıklanabilir.

Bu çalışmanın son bölümünde, 1 MHz'de geniş bir voltaj ve sıcaklık aralığında, dielektrik sabiti (ε'), dielektrik kaybı (ε''), dielektrik kayıp tanjantı ($\tan\delta$), elektrik modülünün gerçek ve sanal kısımları (M') ve (M'') ve alternatif akım iletkenlik (σ_{ac}) değerleri üzerindeki etkisi hesaplanmıştır. Bu sonuçlar, özellikle tükenme ve birikim bölgelerinde sıcaklık ve uygulanan ön beslemin önemli bir etkisini göstermektedir. Negatif kapasitans NC davranışı (C-V-T)'de dolayısıyla (ε'-T) grafiklerinde seri direnç, arayüz durumları ve arayüzey tabakası nedeniyle özellikle yüksek doğru beslemlerde tüm sıcaklıklar için negatif değerli gösterilmiştir. ε'' nün deneysel değerleri artan sıcaklıkla artış gösterir, ayrıca ε'', $\tan\delta$ ve elektrik iletkenliği σ_{ac} özellikle (T=230K) den daha yüksek sıcaklıklarda (0.5V) önbeslem bölgesinde sıcaklıkla yükselir. M' and M'', N_{ss}, dipol kutuplanması, R_s ve arayüzeyin varlığından dolayı kuvvetli bir sıcaklık bağımlılığı gösterir. Bu nedenle Au / Zn nanopartikülleri PVA/n-4H-SiC (MPS) yapısının dielektrik karakteristikleri ve ac iletkenliğinin hem sıcaklığa hemde voltaja bağlı olduğunu ifade edebiliriz.

Anahtar Kelimeler: MS and MPS yapılar, Zn-katkılı PVA arayüzey tabakasının passivasyon etkisi, yüzey durumları, negative kapasitans, iletim mekanizması, engel yüksekliği, engel homojensizliği, double Gaussyen dağılım, elektrik ve dielektrik karakteristikler, elektrik modulu.

2018, 103 sayfa

ACKNOWLEDGMENT

I would like to express my deep gratitude and appreciation to my supervisor Prof. Dr**.** ALİ KÖKCE for supervising me on a day-to-day basis, for his great patience in introducing me to equipment and Prof. Dr. Şemsettin Altındal, Prof. Dr. Ahmet Faruk ÖZDEMİR for them continuous scientific concepts and understanding that equipped me for the task advice, support, help and guidance through this work. To Dr. Drmush, who was help me a lot during my work.

My thanks to Suleyman Demirel University /Scientific Research Project in (Project No: 4614-D2-16) for supportting this project.

My thanks to staff of Physics Department in Gazi University for their valuable assistant, advice and support and for making all facilities necessary for the research available

I am grateful to the Chairman of the Physics Department and the staff of Physics Department for their valuable support and for making all facilities necessary for the research available

My deepest appreciations are expressed my Ministry of industry and minerals in Iraq that give me this chance to complete my study in one of international universities in the world.

Finally, it will be unfair on my part if I don’t mention the patience and assistance of my **family** who supported me throughout this work.

Mohammad AL-DAHROB

ISPARTA, 2018

LIST OF FIGURES

Page

LIST OF TABLES

LIST OF SYMBOLS AND ABBREVIATION

A^*	Effective Richardson constant
BH	Barrier hight
C	Capacitance
CTM	Conduction transport mechanism
d_i	Interfacial film thickness
DGD	Double Gaussian distribution
e	Elementary charge
E	Electric-field
ε'	Dielectric constant
ε	Dielectric losses
E_C	Bottom of conduction band
E_F	Fermi energy level
eV	Top of valence band
FE	Field emission
G/ω	Conductance
GD	Gaussian distribution
h	Reduced Plank's = h /2π
HOMO	Highest occupied molecular orbital
HTR	High temperature region
I	Current
J	Current density
k	Boltzmann's constant
LBR	Low barrier region
LED	Light-emitting diode
LTR	Low temperature region
LUMO	Lowest occupied molecular orbital
M'	Real electric moduls
Φ_m	Work function of metal
M″	Imaginary electric moduls losses
m^*	Effective mass
MBR	Moderate barrier region
MIS	Metal/insulator/semiconductor
MOS	Metal/oxide/semiconductor
MPS	Metal/polymer/semiconductor
NC	Negative capacitance
NDR	Negative differential resistance
NP	Nanoparticle
N_d	Donor concentration atoms
N_{ss}	Surface state density
OFET	Organic field-effect transistor
OLED	Organic light-emitting diode
PVA	Poly-4-vinylphenolalchol
q	Electronic charge
R_i	Structure resistance
R_s	Series resistance
SCLC	Space-charge-limited current
T	Temperature
$\tan\delta$	Loss tangent

TE	Thermionic emission
TFE	Thermionic field emission
V	Voltage
V_{bi}	Built-in potential
V_F	Forward bias
V_R	Reverse bias
W_D	Depletion width
γ	Electric-field coefficient
ΔE_{ae}	Activation energy of electron
ΔE_{ai}	Activation energy of ions
ε	Permittivity
μ	Mobility
σ	Width of the energetically disorder distribution
Σ	Width of the positional disorder distribution
σ_{ac}	Ac conductivity
Φ_{B0}	Zero-bias barrier hight
Φ_{Bn}	Barrier height of metal-semiconductor
χ	Electron affinity of semiconductor

1. INTRODUCTION

1.1. Organic Semiconductor

A discovering of electrical conductivity of organic materials which was thought in the past to be insulating materials opened up a new interesting research field (Stella, 2006). The using of organic materials in electronics applications have some difficulties such as the stability of electronic devices during the manufacturing or operation towards the ambient environment that contain some elements such as oxygen, uv light and moisture that in most cases effect the organic semiconductors (Chang, 2015). Organic semiconductor materials show superior physical and chemical properties, mechanical flexibility, low cost, deposition over large substrate, and easy fabrication processes such as electrostatic spraying, super-critical fluid (SCF), deposite electrochemically and etching, sol-gel and growth hydrothermally, dip and spin coating, etc. (Tang et al.,1987 ; Burroughs et al., 1990). Design, optimization, specifications and characteristics of metals, semiconductors and polymers materials hold the key for future nanoscience and nanotechnologies. Doped nanoparticles of polymers compared with conventional organic or inorganic semiconductors are one of the important materials belonging to a rich variety of new concepts of the interplay between their π-electronic structure and their geometric structure (Tang et al., 1987). Semiconducting polymers are conjugated polymers taht refer to the alternate single and two bonds between the carbon atoms on the polymer backbone. In case of organic semiconductor, there are HOMO and LUMO levels. The band edge of valance band is referred to as "Highest Occupied Molecular Orbital" (HOMO) and edge of conduction band is called the "Lowest Unoccupied Molecular Orbital" (LUMO). The energy gap between HOMO and LUMO levels in conjugated polymer is generally within range of visible photon. When the incoming photon is absorbed electron is promoted to LUMO level, leaving behind hole in HOMO layer (Koehler et al., 1997; Champbell et al., 1997). This electron and hole remains on the same polymer chain and are bound to each other by their electrostatic force, commonly known as excitons Nowadays, organic semiconductors have found commercial application such as organic light-emitting diodes (OLEDs), PLED's, photovoltaics, photodetectors, FET's and organic memory devices (Choueib et al., 2011; Tascioglu et al., 2011; Gilliot et al., 2015; Tanrıkulu E et al., 2015).

1.2. PVA Polymer

Among polymer materials, polyvinyl alcohol (PVA) is one of the largest volume synthetic resins produced in the world. It is unique among polymers due to not building up from polymerization reaction from single-unit precursor molecules known as monomers. PVA is one of the few linear, non halogenated alphabetic polymers. PVA has two dimensional hydrogen-bonds network sheet structure (Anis et al., 2007; Bouropoulos et al., 2008). The physical and chemical properties of PVA depends a great extent on the method of preparation. In additon these proerties depend on the degree of polymerization and the degree of hydrolysis. PVA is a polymer with exceptional properties used in the synthetic fiber, textile coating and binding industries due to its good both the physical and chemical properties such as good chemical resistance, water-soluble polymer, non-toxicity, biodegradability, high dielectric strength, good storage capacity, etc. Also it has excellent film forming and adhesive properties, high resistant to different kinds of oil, grease and solvent. PVA films have high tensile strength and abrasion resistance and hence are used as binder in electrochemical windows and double layer capacitors etc. (Subba et al., 2006; Anis. et al., 2007; Pawde et al., 2008). PVA is a potential material having very high dielectric strength (>1000 kV/mm) , charge storage capacity is good, besides its important physical properties that arise due to the presence of OH groups and hydrogen bond formation. PVA, henceforth, as one of the most important polymers is used as interfacial organic layer material and has attracted great attention especially in the case of disperse of material-dependent on electrical and optical properties (Khanna et al., 2005). PVA offers a good balance of properties, including excellent outdoor weather ability, a complete absence of plasticizer migration (especially important for medical applications) and improved low-temperature capacity. These properties recommend PVA copolymer for outdoor and medical applications. PVA is normally a poor electrical conductor, but it can be a conductor by doping it with some metal ions. It is also known that PVA reacts with other organic and an inorganic compound because of it's from hydroxyl group. The electric and dielectric properties of PVA are also quite changed with doping concentration donor or acceptor atoms and doping process (Shehap et al., 1998; Subba, et al 2006; Anis et al., 2007; Pawde et al., 2008).

1.3. SiC Semiconductor

The first report about SiC itself which is scarce in nature and composition of a compound material containing silicon–carbon bonds was published by Berzelius in 1824.The formating of synthetic SiC is credited to Edward Goodrich Acheson (in 1880) who attempted to create diamond from carbon and corundum ended up creating SiC (Guichelaar, 1997). Lely in 1955was developed the first successful growth of high purity SiC crystal by using sublimation method (Kimoto et al., 2014). Then it was improved by producing the first single crystal of SiC by Tairov and Tsvetkov in 1978 and became the most grown method for bulk SiC growth. A study deals with growthing method of silicon carbide single-crystalline ingots grown from seeds at a temperature range of 1800- 2600°C (Tairov et al., 1978). Moissan discovered naturalist SiC and considered it as a mineral .This is why SiC is named "Moissanite" in mineralogy or in the field of gem stones (Moissan, 1905).

Because SiC semiconductors have unique physical and chemical properties, it has been developed for important applications such as (i) high power electronics operating at several kV and capable of MW power handling, (ii) high frequency devices in the mobile telecommunication field (iii) new types of sensors that can endure maximum environments conditions such as high temperatures, high pressures or corrosive environments (Harris et al., 1999). The strong chemical bonding between Si and C atoms gives these material important properties such as very high hardness, chemical inertness and high thermal conductivity. With this unique properties of SiC which has ten times the dielectric breakdown field strength (600V and up) and yet with very low resistance, three times the bandgap and work at high temperature as compared with Si semiconductor. SiC devices can be made to have much thinner drift layer and/or higher doping concentration. Therefore SiC has become an attractive material for manufacturing power devices instead of Si semiconductors. SiC exists in a many different polymorphic crystalline structures called polytypes e.g., 3C-SiC, 6H-SiC, 4H-SiC. Presently 4H-SiC is generally preferred in power device manufacturing, due to its identical mobilities along the two planes of the semiconductor, while 6H-SiC exhibits anisotropy that means the mobilities of the material in the two planes are different. Theortically SiC can decrease the resistance per unit area of the drift layer to 1/300 compared to Si at the same breakdown voltage. n- and p-type SiC control over a wide doping domain is comparatively easy, this makes SiC extraordinaryl between wide bandgap semiconductors. The capability of SiC to form silicon dioxide (SiO2) as a native oxide is an important advantage for manufacturing device. For these properties, SiC is a favourable semiconductor for high-power and high-temperature electronic motivations for switching, microwave power applications, low noise amplifiers (LNAs) and mixers (Okojie. et al., 2002 ; Aydin et al., 2007; Oder et al., 2007; Lee et al., 2008; Gupta et al., 2012; Kang et al., 2012).

200 different kinds of SiC polytypes are exist in the nature until yet (Pensl, Choyke, 1993). The electronic properties of SiC were investigated shortly afterward and the first LED was produced in 1907 from SiC. The commercial release of 4H-SiC wafers and devices substantiation are preferred choice for manufacturing electronic device in the mid-1990s.The distinguished potential of SiC-based power devices was proposed in 1989 by Baliga. After fixed amelioration of MOS channel mobility and oxide accuracy, 4H-SiC power DIMOSFETs have also been commercially obtainable since 2010 (Kimoto et al., 2014) . (Scozzie et al., 1998) have shown the deleterious effects for SiC because of interface-trapped charge. Y.Zeng et al. 2001 have shown a process of extracting energy dependent interface trap density for 6H and 4H-SiC MOSFETs in the subthreshold region of operation MOSFET characteristics. (Arnold et al., 2001) have shown the effect of interface traps in SiC on decrease in trans conductance, lower mobile inversion charge density and low drift mobility of inversion layer electrons. (Suzuki et al., 2002) have shown a description in SiC MOSFETs for correlation between channel mobility and interface traps. Infineon Technologies and Cree Inc. introduced the first commercial SiC Schottky diodes as power devices in 2001 and 2002. In 2013, Gene SiC Semiconductor released its SiC super junction transistor (SJT), and Fairchild Semiconductor is developing its SiC bipolar junction transistor (BJT). These SiC devices experience quite different characteristics as compared to their Si counterparts, such as high current gains and fast switching speeds.

1.4. MPS Structure

Braun (1874) was the first researcher to report on rectifying properties of the asymmetric nature of electrical conduction for metal-semiconductor contacts. He had recognized that this anomalous phenomenon caused by a thin interfacial layer exhibiting a large electrical resistance. (Schottky, 1938 and Mott, 1938) were the first to suggest a model for barrier heights in metal-semiconductor contacts. They suggested that the bands of the metal and the semiconductor in contact control in order to bring both vacuum levels in coincidence. Schweikert (1939) measured the barrier heights in metal-selenium rectifiers and obtained an increase in the barrier height approximately linear with decreasing metal work function. Bardeen (1947) was the first to recognize that electronic interface states in the band gap of a semiconductor might account for the reduced slope in figures of the metal work function versus barrier height (Monch, 1990). Japanese chemist (1954) was discovered the first organic semiconductor. In 1960s the first solid conducting polymer was investigated with the charge transfer complex TCNQ (Yongfang, 2015).

The MOS structure was first suggested by Varactor (1959) and its properties were analyzed in 1961-62. The MOS diode was first utilized in the study of a thermally oxidized silicon surface in 1962-63 (Sze, 1981; Nicollian, 1982). The studies of semiconductor materials and devices were increased since the early nineteenth century (Sze, 1981). Table (1.1) shows the major semiconductor devices and Table (1.2) shows the key semiconductor technologies through development stages. During 1960s many important researches and developments on Schottky barrier diodes were made. Then in 1970s these studies were developed in two directions. Firstly, the knowledge acquired from research and development studies in the previous decade has been utilized in industrial applications of devices using Schottky barriers. Secondly, acquire more complete understanding of metal-semiconductor interface have been made by more intensive efforts (Sharma, 1984). Also, in 1970s, the innovative evolution of nanoparticles is causes by an incorporation of theory and experiments in the fields of physics, chemistry, materials science, and biosciences. Specific phenomena (chemical properties and physical properties), instead of the optical feature of a nanoparticle, have lead to new possibilities in different fields.

Huge research efforts have been toward to organic semiconductors and devices result more interest of organic electronics. (Heeger et al., 1977) were discovered the first highly conducting polymer, chemically doped polyacetylene, which pretend that polymers able to use as a good electrical active materials (Chiang et al., 1977). Furthermore in the mid-1970s were first produced of polyacetylene conducting polymers as a novel generation of organic materials with the same electrical and optical properties of metals and inorganic semiconductors, which received significant attention from both science and engineering communities. This culminated in 2000 when Nobel Prize in Chemistry was awarded to A. J. Heeger, H. Shirakawa, and Alan G. MacDiarmid, for their discovering and development of electrically conductive polymer. This remarkable observation opened up an entire new field called organic electronics, and a new range of applications for conducting and semiconducting organic materials (Yun, 2009). After it became obvious that the future of electronics will be based on the basis of conducting organic polymer with advanced specifications to produce low cost, high volume and flexible electronics as compared with conventional semiconductors, so it became important to study the electric, dielectric, mechanical, optical, thermal and magnetic properties of metal/ polymer/ semiconductor and metal/metal-doped-polymer/semiconductor structures at different conditions such as temperature, voltage and frequency,…ect. Many studies deal with this field during the last 20 years. A study including the physics of metal-semiconductor interfaces exhibits that almost all metal-semiconductor or Schottky contacts exhibit rectifying behavior which is caused by a depletion layer on the semiconductor side of the interface. The electronic properties of a Schottky diode are characterized by its barrier height which is the energy difference between the top of the valence band of the semiconductor and the Fermi level at the interface (Monch, 1990).

Organic electronics generally refers to electronic devices and systems that are based on organic semiconductors, particularly conjugated polymers, and generally it is applied to different application technologiesl such as organic light-emitting devices (OLEDs), organic photovoltaic solar cells, and organic electronic circuits based on organic thin layer field effect transistors (OTFTs or OFETs) (Yun, 2009). Organic electronics is basically electronic devices which are made by organic materials (organic dielectrics, conjugated and small molecule semiconductors). This interest and augmentation in research activities for using organic electronics devices are due to their new promise electronics fields fabricated on flexible substrates using low-cost and unconventional means such as electrospinning, spin coating, low/room temperature printing, and roll-to-roll processing... ect (Liu, 2002).The existence of π-orbitals in organic materials is responsible for carrier transport and semiconducting properties in these materials. Interestingly, some of the best OFETs have shown performances that compare favorably well with amorphous silicon thin film transistors (Klauk, 2007). However, considerable challenges still need to be addressed in order to reap the full benefits of organic electronics. Such challenges include the inherent problems of polymer dissolution and solvent-selectivity particularly encountered in the fabrication of all-polymer devices as well as the difficultly in fabricating stable and low-operating voltage OFETs owing to the low dielectric constants of conventional polymer dielectric materials. In this work facile strategies are given for overcoming these above-mentioned organic electronics problems (Yun, 2009).

Recently much attention attracted for synthesis of metal organic polymer and polymer inorganic nanoparticles due to their interesting properties has potential use in technological applications. These nanoparticles affect on the advantageous properties of metals and polymers and also exhibit many new characters that do not exist in single-phase materials (Karim et al., 2007). The key issue in using of novel properties is controlling on the shape and size of nanocrystalline material. Important efforts have focused on the design of synthesize nanostructure methods such as nanowires, nanofibers, nanobelts and nanotubes due to the unique properties of these structures. Different kinds of polymer-assisted synthesis such as PVA, PANI, PVP and PAA have been investigated In order to improve the uniformity and capability of photonic catalysis (Xiaa et al., 2008). Two prepartion methods to obtain nanocomposite materials: casting of films from a mixture of preformed polymer and nanoparticles, or in- situ formation of metal particles in the polymer to a metal complex. In addition, final dispersion of nanoparticles with adjusted size, size distribution, and spatial distribution in the polymer matrix can be obtanied due to interactions between the polymer and the metal or metal precursor. A chemical reduction based on the use of a sodium borohydride solution has been also proved to be efficient to form from an aqueous metal salt solution (Clemenson et al., 2007). In this kind of semiconductor contact structure, an organic interfacial layer is inserted between semiconductor and metal., and this layer used as active layer plays an important part in the electrical characteristics of these structures. There are different types of polymeric interfacial layer such as poly (4-vinyl phenol), polyaniline, polyvinyl alcohol (PVA), poly (alkylthiophene) polypyrrole, polythiophene, and poly (3-hexylthiophene) (Özden et al., 2016). The surface energy of organic materials generally is lower than that of inorganic materials due to dangling bounds on the surface of inorganic based thin film, therefore the organic materials have been used as an interfacial layer at M/S interface for electronic devices in order to match surface energies between two layers (Forrest et al., 1982; Gupta et al., 2004; Çakar et al., 2005; Aydoğan et al., 2005).The formation of barrier height (BH) between metal and semiconductor and current conduction/transport mechanism (CCM or CTM) usually depend on the existence of interfacial layer and its homogeneity, the concentration of doping atoms in semiconductor, surface preparation process, surface states localized between interfacial layer and semiconductor and series resistance of the structure (Aydemir et al., 2013).The main advantage of polymer/organic interfacial layer is numerous proposals for its application in microelectronics, as well as packaging textile and food products, due to their unique electrical, optical, magnetic properties and its high clarity, lack of charge density properties, excellent durability and thermally stable over a large temperature range.

1.5. Electrospinning

There are many fabrication processes to prepare organic semiconductor. The electrospinning is a low-cost, multiple and efficient technique to produce continuous nanofibers from submicron to nanometer diameters by using a high applied voltage**.** The obtained fibers have smaller diameter (2 nm to several micrometers), smaller pores and higher surface area than fibers obtained with standard fiber-spinning techniques such as melt spinning, wet spinning and dry spinning that usually lead to fibers with diameters between 10 and 50 μm (Saito et al., 1994; Salama et al., 2004; Pan et al., 2006; Uslu et al., 2007). Electrospinning technique is the simplest technique for fabricating nanofibers with both solid and hollow interior that are exceptionally long in length, uniform in diameter and varied in composition from polymer solutions or melts which is an easy of use, preparation and arrangement and installation requirements and for that reason it becomes easier to use this technique on a laboratory scale and can be expand their scope to an industrial process and many potential applications (Li et al., 2004). Electrospinning is a direct expansion of electrospraying, as the two processes have the same physical and electrical mechanisms with a difference of forming of continuous fibers in electrospinning while at electrospraying produce small droplets. The spun fibers are mostly deposited on electrode collectors in the form of nonwoven nanofiber mat. By using controlled fiber deposition techniques, it is also possible to obtain range nanofibers. Optimal nanofibers can be manfuctured by controlling the properties of solution such as (solubility, glass-transition temperature, melting point, crystallization velocity, molecular weight distribution, entanglement density, solvent vapor pressure, PH value, electrical conductivity, viscosity or concentration, surface tension of solvent), process parameters such as (strength of electric field, the distance between spinneret and collector, the nutrition rate for polymer solution as well as the humidity and temperature of the surroundings), and ambient parameters It is very important to avert the apperance of beads, particularly for smaller nanoparticles. A lot of interest to control fiber morphology by control of these parameters (Saito et al., 1994; Salama et al., 2004; Pan et al., 2006; Uslu et al., 2007). The main requirements of ideal electrospinning process are controlling of some parameters such as (1) consistent and controllable of the diameter of fibers, (2) the defect-controllable fiber surface and (3) collectable continuous single nanofiber (Huang et al., 2003). Electrospinning can be used for a wide range of materials such as synthetic and natural polymers, polymer alloys, polymers loaded with nanoparticles or active agent, as well as to metals and ceramics metals as well as ceramics and composite systems. A variety of natural or synthetic polymers and composite materials can be fabricated by electrospun from solutions or melts, and non-woven fabrics made of nanofibers are produced this way. The advantages of control the nanofiber synthesis are to attain the coveted property or functionality, offering more resilience in surface functionalities. These superior properties make the polymer nanofibers to be good nominee for many applications, which extend to filtration, environment, biomedical, catalysis, bioengineering, tissue engineering, scaffold constructions, wound dressings, energy conversion and storage, catalysts and enzyme carriers, protective clothing, sensors, drug delivery, cosmetics, electronic and semi-conductive materials (Huang et al., 2003; Xu et al.,   2009).

Table 1.1. Development stages of some major semiconductor (Sze, 1981; Nicollian, 1982).

Year	**Semiconductor Device**	**Author(s)/Inventor(s)**
1874	MS contact	Braun
1907	LED	Round
1947	Bipolar transistor	Bardeen, Brattain, and Shockley
1949	p-n junction	Shockley
1952	Thyristor	Ebers
1954	Solar cell	Chapin, Fuller, and Pearson
1957	Heterojunction bipolar transistor	Kroemer
1958	Tunnel diode	Esaki
1960	MOSFET	Kahng and Atalla
1962	Laser	Hall et a1
1963	Heterostructure laser	Kroemer, Alferov and Kazarinov
1963	Transferred-electron diode	Gunn
1965	IMPATT diode	Johnston, DeLoach, and Cohen
1966	MESFET	Mead
1967	Nonvolatile semiconductor memory	Kahng and Sze
1970	Charge-coupled device	Boyle and Smith
1974	Resonant tunneling diode	Chang, Esaki, and Tsu
1980	MODFET	Mimura et al
1994	Room-temperature single-electron memory cell	Yano et al.
2001	20 nm MOSFET	Chau

Table 1.2. Key Semiconductor Technologies (Sze, 1981; Nicollian, 1982).

Year	**Technology**	**Author(s)/Inventor(s)**
1918	Czochralski crystal growth	Czochralski
1925	Bridgman crystal growth	Bridgman
1952	III-V compounds	Welker
1952	Diffusion	Pfann
1957	Lithographic photoresist	Andrus
1957	Oxide masking	Frosch and Derrick
1957	Epitaxial CVD growth	Sheftal., Kokorish, and Krasilov
1958	Ion implantation	Shockley
1959	Hybrid integrated circuit	Kilby
1959	Monolithic integrated circuit	Noyce
1960	Planar process	Hoerni
1963	CMOS	Wanlass and Sah
1969	MOCVD	Manasevit and Simpson
1971	Dry etching	Irving, Lemons, and Bobos
1971	Molecular beam epitaxy	Hoff et al.
1989	Chemical mechanical polishing	Davari et al.
1993	Copper interconnect	Paraszczak et al.

CVD, chemical vapor deposition; CMOS, complementary metal-oxide-semiconductor field-effect transistor; DRAM, dynamic random access memory; MOCVD, metalorganic CVD.

2. METAL - POLYMER - SEMICONDUCTOR STRUCTURE AND CONDUCTION MECHANISMS AND DIELECTRIC PROPERTIES

2.1. Introduction

Recently, understanding of the physical features and the performances of MPS structure due to the electric and dielectric characteristics of MPS devices is of great importance in the electronics applications. The occurring of an interfacial reaction between the metal and the semiconductor which form deleterious silicide in conventional MS contact, this reaction causes movement of interface to the semiconductor bulk, this will make the barrier height is independent on properties of the surface and the metal work function. Generally, the barrier heights of MS contacts are dependent on the heat of formation of the silicide linearly. In these cases, the properties of the silicides control barrier formation, which prevents the true barrier height of the MS contacts to be determined.

In a metal-polymer-semiconductor (MPS) structure, a thin-film insulator has been used as an interfacial layer since the mid-90.s. A native of enough thin polymeric layers on the surface of semiconductor causes a tunneling for a lot of electrons through it, and it also satisfies the dangling bonds and thus decreases the intrinsic surface state density.

In a thin layer of polymer, some metals can also permeate through it and react with the semiconductor to form silicide. Now the thicknesses of this layer can be control easly until angstroms scale, where an increases in the thickness of this layer lead to reducce in the current tunnel through it (Sharma, 1984).

2.2. MS Contact

In order to understand the characteristic parameters of Schottky contact, the conductivity properties of the insulator and semiconductor crystals must be known. When a semiconductor is contacted with a metal, the resulting contact determines the contact function of the selected metal and semiconductors, which is the Ohmic or rectifying contact. Three fundamentally different contacts are described for metal -

semiconductors contact depending on barrier height. The barrier height is due to the difference between the work functions (Φ_M, Φ_S) of metal and semiconductor materials as following:

(1) When the metal work-function is larger than the semiconductor work-function ($\Phi_M > \Phi_S$) the electrons are depleted from the semiconductor. It is a rectified contact for n-type semiconductor and Ohmic contact for p-type-semiconductor. Because of the electron-depletion, then a difficult in contact region for providing enough charge carriers to the bulk of the semiconductor, and this kind of contacts is called blocking or injection-limited for electrons. Also, in this region excess of holes are exist that can provide any charge flow demanded by the bulk of the semiconductor, and this kind of contacts is called Ohmic or bulk-limited for holes.

(2) When $\Phi_M = \Phi_S$, for contact semiconductors, the Fermi levels already are lined out and no need for redistribution charge that contact. This is called a neutral connection: in both the electron and the hole contact it has an interstitial concentration of charge equal to the intrinsic free carrier concentration.

(3) When the metal work-function is like the semiconductor work-function ($\Phi_M < \Phi_S$), it is Ohmic contact for n-type semiconductor and rectifier contact for p-type semiconductor.Table 2.1 show the ohmic and rectifier behavior for MS contact due to the work function of metal and semiconductor

Table 2.1 Work functions of metals and semiconductors for ohmic and rectifier contact formation in MS contacts

	n-type	**p-type**
$\boldsymbol{\Phi_M > \Phi_S}$	Rectifying	Ohmic
$\boldsymbol{\Phi_M < \Phi_S}$	Ohmic	Rectifying

Furthermore, when a metal is brought into intimate contact with n or p type of semiconductors, a definite energy relationship between the conduction and valence band of the semiconductor and the Fermi level in the metal will be built. In the semiconductor,this relation is serves as a boundary condition of the Poisson equation

, which can be proceeded in same pattern of p-n junctions. The energy-band diagrams for metals for n-type and p-type materials at equlibirum and different applying bias as in Fig. 2.1.

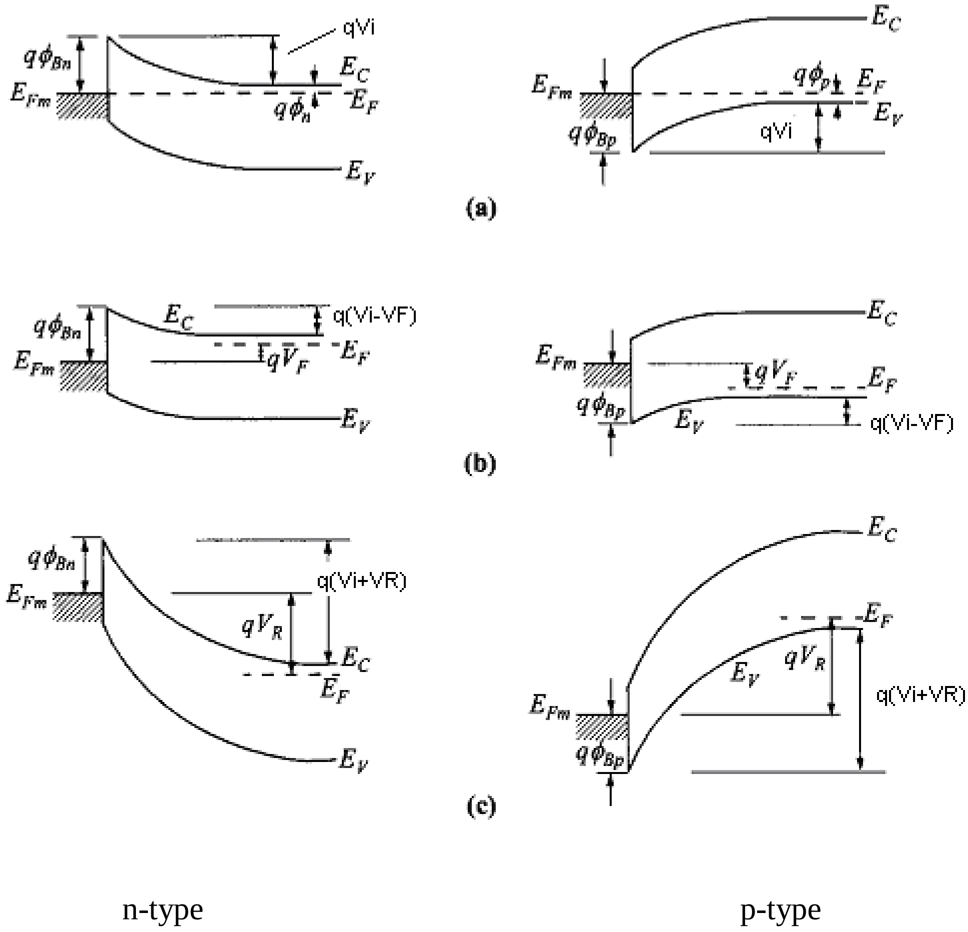

Figure 2.1 Energy-band diagrams of metal n-type and metal p-type semiconductors under different biasing conditions (a) Thermal equilibrium. (b) Forward bias. (c) Reverse bias.

2.3. Schottky- Mott Theory in Metal-Semiconductor (MS) Contacts

According to the Schottky-Mott theory, the potential barrier formation process is caused by contacting metal with semiconductor and the barrier results from the difference in the work function of the two substances. After the metal contact with n-type semiconductors amount to the equilibrium state, the electrons in the conduction band of the semiconductor have greater energy than the electrons of the metal and these electrons continue in flow to the metal until the Fermi levels are equalized.

With this flowing from the semiconductor to the metal decreases in free electron concentration of semiconductor nearthe boundary region. The difference between conduction band edge E_C and Fermi level E_F increases with decreasing electron concentration and the value of E_F remains constant in thermal equilibrium throughout the semiconductor. Conduction band electrons pass through the metal and leave ionized positive charges behind them (donors). As a result, the transferring electrons in the semiconductive region close to the metal are exhausted and cause the depletion of mobile electrons. Extra conduction electrons contained within the Thomas-Fermi screen distance (0.5Å) on the metal side of the interface. The electron charges created by the electrons passing through the metal are basically a surface charge and form a thin negative layer in the metal, an electric field is generated from the semiconductor to the metal. Also, the width of the space-charge region of the semiconductor is to be recognized because the donor concentration in the semiconductors is smaller than the electron concentration in the metal.

Now, the extent to which the energy levels of the semiconductors will curvature can be examined. It is clear that the forbidden energy range of the semiconductor ($E_g = E_c\text{-}E_v$) does not change after small or tight contact with the metal, so that the edge of the conduction band (E_c) will move upwards parallel to the valence band (E_v). In addition, the vacuum level in the semiconductor will follow the same variations as E_c.

An important factor determining the barrier height (Φ_B) for a MS contact in thermal equilibrium state is that the vacuum level remains constant throughout the transition region. For this reason, the vacuum level of the semiconductor side must approach the level of vacuum on the side of the metal to maintain continuity. The size of the curvature in the bands seen on the semiconductor side is equal to the difference between the two vacuum levels, i.e. the difference between the work functions. This difference is ($qV_i=\Phi_M - \Phi_S$) and V_i is the potential difference contact in volts. Here, qV_i is the potential barrier height of the electrons passing through the semiconductor to the metal. However, the barrier height seen from the metal to the semiconductor is higher than that of the semiconductor as much as the difference between bottom of the conduction band and the Fermi level E_F (Φ_n) seen from the semiconductor to the metal. This difference can be explained as following (Sharma, 1984).

$$\Phi_B = (\Phi_M - \chi_S) \quad (2.1\ a)$$

Since

$$\Phi_S = (\Phi_n + \chi_S) \quad (2.1\ b)$$

By substituting qV_i value and using the equations 2.1 (a) and (b) above, then the value of Φ_B occurs as;

$$\Phi_B = (qV_i + \Phi_n) \quad (2.1.c)$$

where $\Phi_n = (E_c - E_F)$ which is the penetration of Fermi level of the semiconductor in the band gap.

Equation 2.1.b was first demonstrated independently by (Schottky, 1938 and Mott, 1938), which is also known as the Schottky limit. Here, when Equation 2.1.b is obtained, it is assumed that the surface dipole contribution in Φ_M and Φ_S does not change after the contact between metal and semiconductor. From the charge distribution in the space charge layer, the exact shape and magnitude of the potential barrier can be calculated. In general, the Φ_B value is much larger than the amount of thermal energy ($= kT/q$) for each temperature, so that the semiconductor space charge region is transformed into a highly resistive depletion zone devoid of moving charges. Thus, in this case, the inhibition can be obtained from the distribution of donor atoms in the form of semiconductor (Schottky, 1938). Supposing that the semiconductors are homogeneously doped into the metal interface, this led to a regular charge density in depletion region. For these stationary space charges, the electric field strength increases linearly with distance from the boundary of the space charge layer, and the resulting parabolic barrier which is known as Schottky barrier (Sharma, 1984). (Mott, 1938) supposes that a thin zone/layer that is doped homogeneously at the M/S interface and free of any moving charges. In this thin layer, the electric field value remains constant and the potential linearly increases throughout the region. This type of barrier is called Mott barrier and this barrier is faced in case of thin layer of low doped between the metal and the highly doped semiconductors.

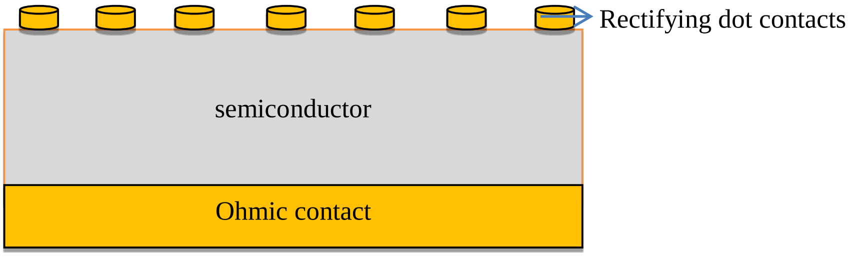

Figure 2.2 Schematic diagram of MS structure

2.4. MS Contacts with Insulating or Polymeric Interface (MIS, MPS) and Interface States

If a naturally or artificially interfacial layer is formed at a semiconductor interface with a metal, Schottky barrier diodes (SBDs) of the MS type will be converted into metal-polymer-semiconductor (MPS) type SBDs. However, if the thickness of this interfacial layer is greater than 100 Å (≥100 Å), these structures are called metal-oxide-semiconductor (MOS) structures or MOS capacitors in order not to lead to any concept confusion. In general, for this interfacial layer different polymeric material such as sheet polymer polyvinyl alcohol (PVA), polyindole, perylene, is used (Altuntaş et al., 2009; Tecimer et al., 2013). Fig. 2, 3 shows a schematic diagram of the (MPS) structure and Figure 2.4 shows an energy-band diagram of an ideal MPS structure at V = 0 for p and n –types semiconductor

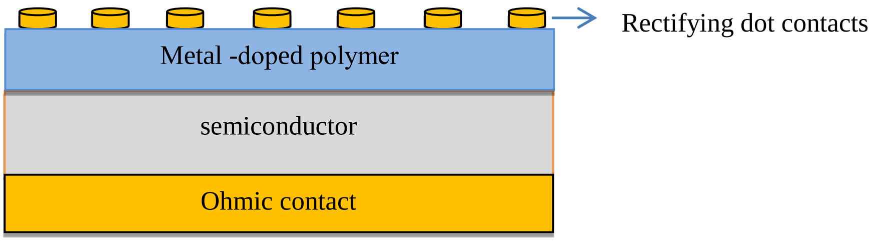

Figure 2.3 Schematic diagram of the MPS structure.

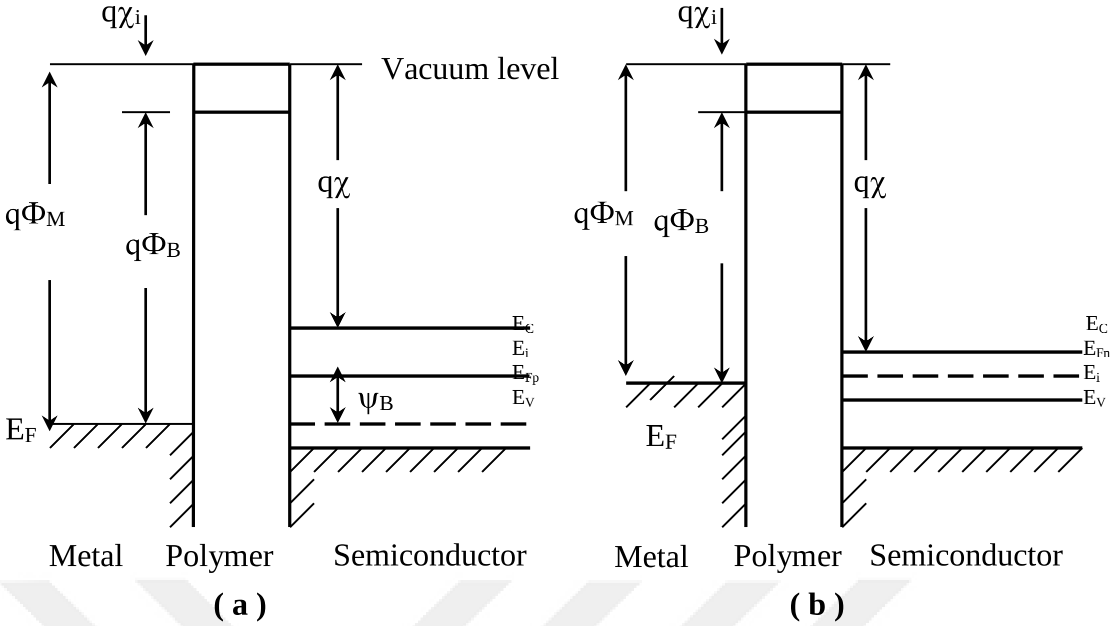

Figure 2.4 (a, b) An energy-band diagram of an ideal MPS structure at V = 0 for p and n-type semiconductors respectively (Sharma,1984).

where: Φ_M: Metal work function, Φ_B: Potential barrier between metal and insulator, χ: Electron affinity of the semiconductor, χ_i: Electron affinity of the insulator, E_V: Valence band energy level, E_C: bottom of conduction band , E_i: Intrinsic Fermi energy level ($(E_C - E_V)/2$), E_F: Fermi energy level, ψ_B: the difference between Fermi and intrinsic Fermi energy levels.

An ideal MIS structure can be defined by the following features (Nicollian et al., 1984; Neamen, 1997):

1. The difference between the work functions ($\Phi_M - \Phi_S$) at zero supply is zero. In other word ($\Phi_{MS} = \Phi_M - \Phi_S = 0$) and given for n-type and p-type semiconductors as follows (Sze, 1981; Cooke, 1990)

$$\Phi_{MS} = \Phi_M - \left(\chi + \frac{E_g}{2q} - \psi_B\right) = 0 \quad \text{for n-type-semiconductor} \qquad (2.2)$$

$$\Phi_{MS} = \Phi_M - \left(\chi + \frac{E_g}{2q} + \psi_B\right) = 0 \quad \text{for p-type-semiconductor} \qquad (2.3)$$

Where E_g is the forbidden energy of the semiconductors and ψ_B is the energy difference between the Fermi energy level. In other word at zero applied voltage it is flat-band condition .

2. At any biasing conditions, the only charges that can occur in the structure are those in the semiconductor that have equal values but opposite sign on the metal surface adjacent to the insulator.

3. The carrier transport through the insulator is zero at applying dc biasing condition or the insulator resistivity is infinity.

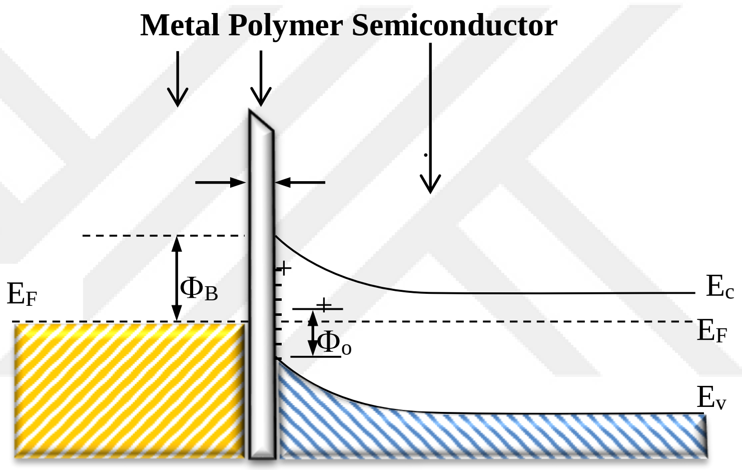

Figure 2.5. The energy band diagram of the Metal-polymer-Semiconductor (MPS) structure for (n-type semiconductor).

The electrons must firstly transform from the inner of semiconductor to the interface, and then they can be emitted over the barrier into the metal. In crossing the depletion region of semiconductor, their motion is governed by the usual mechanism of diffusion and drift in the electric field of the barrier (Rhoderick et al., 1988). In semiconductor the flowing of current can happen in two methods, the first one at applying electric field causes a current flow because of carrier drift and the second one at keeping gradient in the carrier concentration causes a current flow due to carrier diffusion (Sharma, 1984).

When the carriers reach at the interface, then emission into the metal can be calculated from the rate of transform of electron across the boundary between the metal and semiconductor. These two processes are effectively in series, and the current is measured predominantly by the large impediment to the flow of electrons. Due to diffusion theory of Wanger and Schottky and Spenke the first of these processes is the limiting factor whereas according to the thermionic theory of Bethe (1942) the second is the more important (Rhoderick et al., 1988).

2.5. Biasing of MPS Structure

Accumulation, Depletion and inversion cases may occur when a MOS, MIS and MPS structures is biased depending on the type of the substrate and bias direction. A general review for these modes of operation and the relationships between band-bending, charge, and electric field for a MOS, MIS and MPS structure on an n-type and p-type substrate. The analysis for these substrates is similar, with obvious changes for different doping type, doping and Fermi level etc.

2.5.1. Accumulation

Accumulation happens when an external positive bias is applied to the metal gate while the semiconductor surface substrate in MPS structure is grounded the structure behaves like a parallel-plate capacitor where the two electrodes are the semiconductor and the metal, and the polymer interfacial layer is the insulator between them**,** the carrier densities change accordingly in its surface region which is high than the flat band voltage. The minority carriers on the gate attract majority carriers from the substrate to the polymer semiconductor interface. With large positive bias applied to the gate, electrons are attracted by the positive charges to form an accumulation layer. Only a small amount of band curvature is required to build up the accumulation charge so that almost all of the potential variation is within the oxide (Colinge et al., 2002).

2.5.2. Depletion

When flat band voltage is lower than negative voltage which applied to the gate, a positive charge builds up in the semiconductor. Initially this charge is caused by the depletion of the semiconductor starting from the interfacial layer-semiconductor interface. The majority carriers are fended away from the surface causing foundation of a depletion region. The width of depletion layer rises more with rising in gate voltage. As a result of band bending, the intrinsic Fermi level moves toward the Fermi level **(**Colinge et al., 2002).

2.5.3. Inversion

As a larger negative voltage is applied to the gate the surface potential will continue to increase, the electron concentration near the surface decreases while the hole concentration increases. When the potential across the semiconductor rises beyond double the bulk potential, another type of positive charge engenders at the polymeric interfacial layer-semiconductor interface, this charge is caused by minority carriers that form inversion layer. With more rising in the gate voltage, the depletion layer width hardly rises more since the charge in the inversion layer rises exponentially with the surface potential(Colinge et al., 2002).

2.6 Current Transport Mechanism in Metal - Semiconductor and Metal – Insulator- Semiconductor Contacts

2.6.1. Charge transport in insulating layer

In ideal MS structure with insulator or polymer interfacial layer, the conductance of the insulating layer must be zero. Realistic insulators, however, carrier conduction can be seen at applying electric field and at high temperature. The amount of free charge carriers exist in the organic semiconductors materials with high purity can be negliglected. Thus, in some kinds of organic semiconductors are represent trap-free dielectric materials, and theories of carrier conductions or injections across dielectric interfaces have been applied. Table 2.2 summarizes the basic conduction processes in insulators and shows that the conduction process is a function of temperature and voltage, where Schottky emission, Pool-Frenkel, ohmic conduction and ionic conduction are temperature and voltage dependence, while Direct tunneling , Fowler Nodheim tunneling and spase charge limited are a function of voltage only, in other word they are temperature independent.

Table 2.2. Summary of basic conduction processes in dielectric film (kondo, 2007).

Conduction process	**Expression**	**Temperature dependence**	**Voltage dependence**
Schottky emission	$J=A^*T^2\exp\left(\frac{-q(\phi_B-\sqrt{q(V/d)/4\pi\varepsilon i}}{KT}\right)$	$\ln(J/T^2)\sim 1/T$	$\ln(J/V^2)\sim 1/V^{1/2}$
Poole-Frenkel emission	$J\sim V/d \exp\left(\frac{-q(\phi_B-\sqrt{q(V/d)/\pi\varepsilon i}}{KT}\right)$	$\ln(J)\sim 1/T$	$\ln(J/V^2)\sim 1/V^{1/2}$
Direct tunneling	$J\sim V \exp\frac{(-2d\sqrt{2m*\phi_B}}{h}$	None	$\ln(J/V^2)\sim 1/V$
Fowler Nordheim tunneling	$J\sim (\frac{V}{d})^2 \exp\left(\frac{(-4d\sqrt{(2m*\phi_B^{\frac{3}{2}})}}{3qhV}\right)$	None	$J\sim V^2$
Space charge limited	$J=9/8\ \frac{\varepsilon i\mu V^2}{d^3}$	None	$J\sim V$
Ohmic conduction	$J\sim \frac{V}{d}\exp\left(\frac{-\Delta E_{ae}}{kT}\right)$	$\ln(J)\sim 1/T$	$J\sim V$
Ionic conduction	$J\sim \frac{V}{dT}\exp\left(\frac{-\Delta E_{ae}}{kT}\right)$	$\ln(JT)\sim 1/T$	$J\sim V$

A^* = effective Richardson constant, Φ_B = barrier height, ε_i = insulator dynamic permittivity, k = Boltzmann's constant, $\hbar$ = Reduced Plank's constant (= h /2 π), m^* = effective mass, d = insulator thickness, μ = charge carrier mobility, ΔE_{ae} = activation energy of electron, and ΔE_{ai} = activation energy of ions.

The Schottky emission caused by emitting electrons over the barrier at high field in depletion region and it depend on temperature and voltage. Poole-Frenkel emission can be happen because the trapped electrons excited to the conductance band due to field-enhanced thermal energy. While the trap states with coulomb potentials, the term is basically perfect to the Schottky emission. The depth of the trap potential wall is known as barrier height and the quantity $\sqrt{\frac{q}{\pi\varepsilon_i}}$ is larger than in the case of Schottky emission by a factor of 2, since the barrier lowering is double that caused by the immobility of the positive charge. The tunnel emission is due to field ionization of trapped electrons in the conductance band or by tunneling of electrons from the Fermi level of metal to the insulation conductance band. The tunneling emission dependence strongly on the applied voltage but is basically separate of the temperature. Thus, generally there are two processes of tunneling emission (1) direct tunneling, (2) Fowler-Nordheim tunneling and the difference between the two prosess is the shape of barrier and the value of voltage which in first one with square barrier at low voltage and the second one with triangular barrier at high voltage part. The ionic conduction is like diffusion process. Generally, the dc ionic conductivity reduces at appling electric field, due to the difficulty for injection into or extraction of ions from the insulator side. After flow of current initially, two different sign space charges will gathering near the interface of contact causing a deformation in the distribution of potential. After removing applied field, large internal fields stay that because some charges return to toward their balance position that causes hysteresis effects. In some kinds of insulator, different conduction process may be controled in different temperature and voltage domains and may be independent of each other (Kondo, 2007).

Two different processes of transport mechanisms are found in dielectric films, electrode-limited and bulk-limited transport mechanism. The electrode-limited transport mechanism depends on the electrical, dielectric properties which can be extracted from the barrier height and the effective mass of the conduction carriers in dielectric layers and the physical properties of the electrode-dielectric interface, while the bulk-limited transport mechanism depends on the electrical properties of the dielectric itself. Many other important physical parameters in the dielectric layers can be measured from analyses the transport mechanisms of bulk-limited, such as trap spacing, trap level, trap density, dielectric relaxation time, mobility of carrier drift, and density of states in the conduction band. Table 2.3 shows the classification of transport mechanisms in dielectric layers (Chien, 2014).

Table 2.3Transport mechanisms classification in dielectric layers (Chien, 2014)

Transport mechanism	
Electrode-limited transport mechanism	Bulk-limited transport mechanism
• Schottky emission • Fowler-Nordheim tunneling • Direct tunneling • Thermionic-field emission	• Poole-Frenkel emission • Hopping conduction • Ohmic conduction • Space-charge-limited conduction • Ionic conduction • Grain-boundary-limited conduction

There are various ways in which current can be transported through a metal - semiconductor contact or metal –insulator- semiconductor contacts under forward bias as shown in Fig 2.6 where:

(a) Transmition of electrons from the side of semiconductor into the metal over the potential barrier (predominant process for Schottky contacts with middling dopping semiconductors or thermionic emission over the barrier that leads to the ideal current - voltage characteristics) (Sharma, 1984)..

(b) Quantum -mechanical tunneling of electrons through the barrier (predominant process for high doped semiconductors (Ohmic contacts) (Sharma, 1984).

(c) Carrier recombination in the depletion part (Sharma, 1984).

(d) Hole injection from the side of metal to the semiconductor (equal to recombination in the neutral region) (Sharma, 1984).

Processes (b) and (c) cause the departure from the ideal behavior. At a forward bias which is not very large, process (d) is not important as the minority -carrier injection is negligible. The dotted line shows the quasi - Fermi - level according to the diffusion theory and the dashed line according to the thermionic - emission theory (Sharma, 1984).

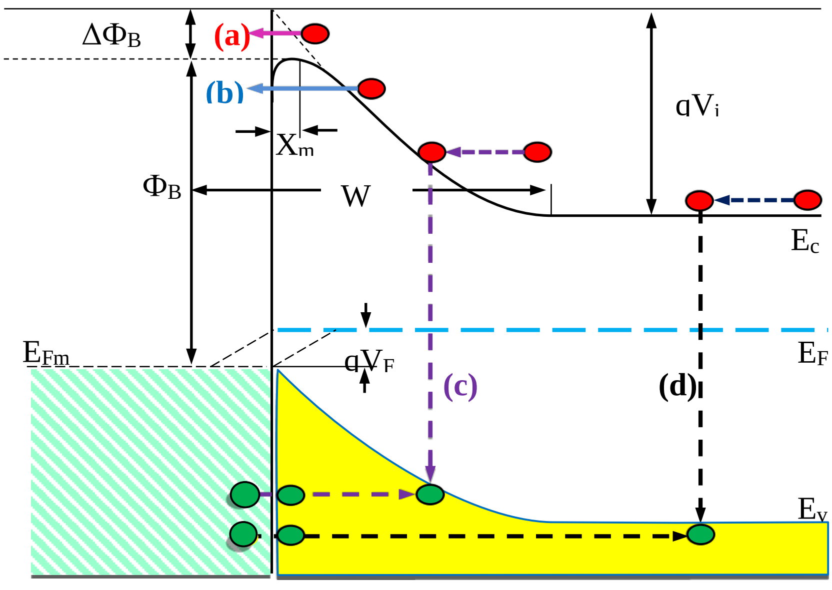

Figure 2.6. Energy band diagram of a forward biased Schottky barrier junction on a n-type semiconductor.

The current across MS contact is mainly caused by majority carriers. Three clearly kinds of mechanisms can be occur: diffusion of carriers from the side of semiconductor into the metal, thermionic emission of carriers over the Schottky barrier, and quantum-mechanical tunneling through the barrier.

Thermionic emission process (TE) in metal-semiconductor contacts occurs when the semiconductors exceed the potential barrier (Φ_B) due to the thermal energy, the carriers of the semiconductors pass through the metal. In Schottky diodes generally the current can be supplied by majority carriers. In general, the TE theory is a standard model commonly used to measure barrier height in Schottky diodes. Furthermore, in this theory the effect of drift and diffusion in the depletion region can be neglectable and the barrier height is very low from kT/q ($\Phi_B << kT/q$) and the carrier collisions in the clearing zone are assumed to be very small, so that the Maxwell-Boltzmann approach can be implemented and the thermal equilibrium state is not affected. According to Maxwellian distribution of velocities, the number of electrons n^* per unit volume in semiconductor which have enough energy to move over the barrier to the metal

$$n^* = n_o \exp\left[\frac{-q(V_i - V)}{kT}\right] \tag{2.4}$$

n_o is the electron concentration in the neutral semiconductor outside the depletion region. Under voltage, the barrier for electrons flowing from metal to the semiconductor remains practically unchanged and remains at Φ_B. Thus, the current (I_{MS}) generated from electron flowing from the metal to the semiconductor is I_o, which is known as the saturation current. However, the current generated from semiconductor to metal (I_{SM}) at low or intermediate voltage ($V \geq 3kT/q$) can be analyzed according to thermionic emission (TE) theory (Rhoderick, 1978; Sze, 1981; Sharma, 1984) is expressed as follows:

$$I_{SM} = I_o \, exp(qV/kT) \tag{2.5}$$

The net current is obtained by combining the currents flowing in both direction:

$$I = I_0\,[\exp(\frac{qV}{kT}) - 1] \tag{2.6}$$

where V is the voltage drop across the junction , n is the ideality factor (Rhoderick, 1978) and I_o is the saturation current which can be express as

$$I = AA^{*}T^2\exp(\frac{-q\,\Phi_B}{kT}) \tag{2.7}$$

where A * is a Richardson constant and is expressed as

$$A^{*} = (4\pi m_e^{*} qk^2)/h^3 \tag{2.8}$$

where m_e * is the effective mass of the electron, h is the Planck constant, and k is the Boltzmann constant. Also for a semiconductor with spherical energy surfaces such as SiC, m_e* is independent of the direction, The Richardson constant unit (A/cm^{-2}K^{-2}) is 146 for n- type 4H- SiC (Kimoto, 2014). The TE theory is based on the assumption that electron collisions in the depletion zone are neglected, and this assumption applies only to high mobility semiconductors. Then by substituting Equation (2.8) in Equation (2.5) we can get

$$I = \underbrace{AA^{*}T^2\exp(-\frac{q\Phi_{B0}}{kT})}_{I_o}\left[exp\left(\frac{qV}{nkT}\right) - 1\right] \tag{2.9}$$

2.6.2. Tunneling through the barrier

Field emission (FE) and thermionic-field emission (TFE) become quite effective for semiconductors with high doping and low temperatures. That is besides the TE mechanism, electrons can also be transported along the barrier by quantum mechanical tunneling when the barrier width (depletion zone width) is not thicker. The tunneling of the electrons takes place either through the electron barrier (FE) of electrons at low temperature or through the thermal energy (TFE) of the electrons which can tunnel through the narrow triangular potential at high temperature. The quantum-mechanical (TFE and FE) tunneling phenomenon occurring in the MS contacts and it occurs in the forward direction only in degenerate semiconductor, and except for very low forward biases and the current-voltage relationship can be expressed as (Sze, 1981; Nicollian, 1982; Sharma, 1984; Rhoderick et al., 1988).

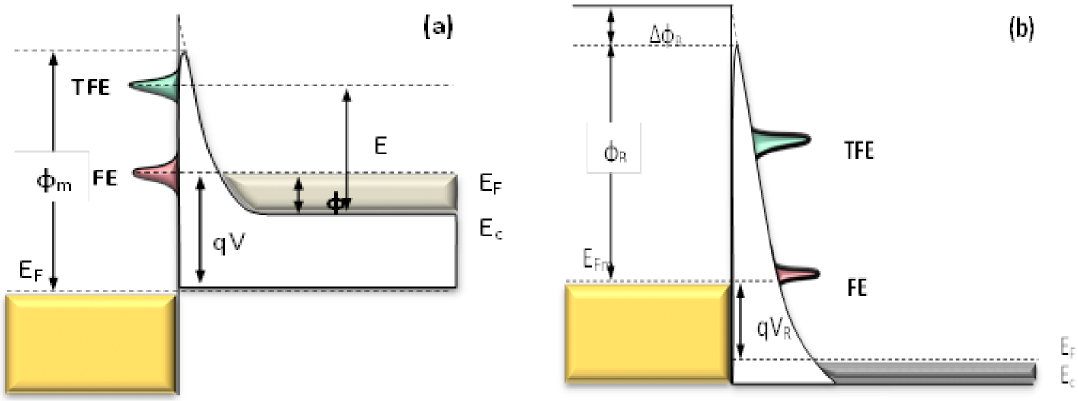

Figure 2.7. Field emission (FE) and thermionic - field emission (TFE) tunneling through a Schottky barrier on n - type semiconductor at (a) forward bias and (b) reverse bias.

$$I = I_{tun}\left(exp\left(\frac{q(V-IR_S)}{E_o}\right) - 1\right) \tag{2.10}$$

and

$$n_{tun} = \frac{E_{oo}}{kT} coth\left(\frac{E_{oo}}{kT}\right) = \frac{E_o}{kT} \tag{2.11}$$

where E_{oo} is an energy parameter related to tunneling and is expressed as

$$E_{oo} = \frac{h}{4\pi}\left(\frac{N_D}{m_e^{*}\varepsilon_s}\right)^{1/2} \tag{2.12}$$

where (h= 6.626x10^{-34} Js) Planck constant, m_e* (=0.067m_e) is the effective mass of electrons.,ε_s is the permittivity of the semiconductor (=9.7 for 4H-SiC), ε_o (=8.85x10^{-12} F/m) is the permittivity of free space and N_D is the density of doping donor atoms that was used as about 7.07x10^{23} m^{-3} in this study .According to the effect of tunneling in Schottky contacts, it is possible to explain the mechanism of the carrier which is dominant in the contact as follow: The current mechanism is

- TE if $E_{oo} << kT / q$,
- FE if $E_{oo} >> kT / q$.

- TFE if $E_{oo} \approx kT / q$. (Kondo, 2007).

In this case Eq. 2.12 can be written as follows, taking into account the potential barrier height constant, β (=$d\Phi_{Bo}/dV$), depending on the voltage (Padovani 1965; Sze 1981 ; Rhoderick et al., 1988);

$$n = \frac{E_o}{kT\,(1-\beta)} \tag{2.13}$$

which of the above-mentioned stream-transmission mechanisms are active alone or together is defined in Figure 2.8

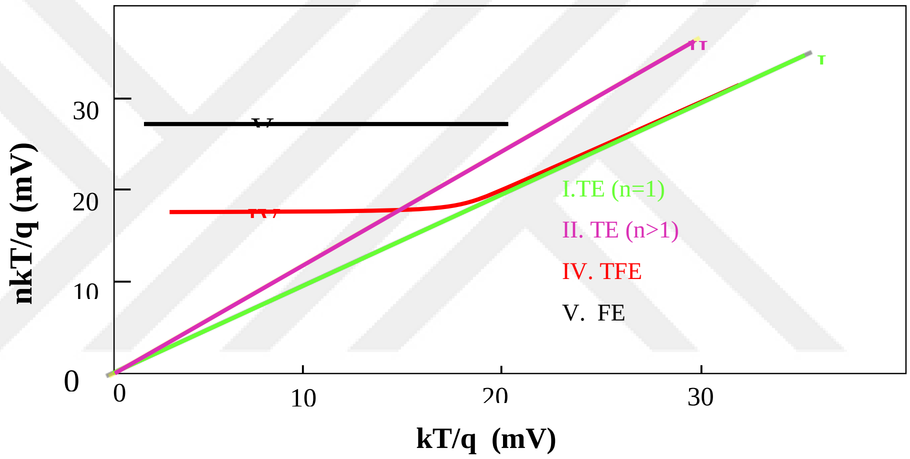

Figure 2.8. *nkT /q* vs *kT /q* shows different current conduction mechanisms (Sharma, 1984).

If the ideality factor is greater than one, it is now independent of the temperature if it is usually manifested by imaginary force, insulator interface layer or interface states. But if n is greater than one, it is due to the the ideality factor temperature and TFE or the recombination currents in the consumption zone. Schottky depends on the temperature in the majority of diodes.

2.6.3. The effect of inhomogeneity in the metal-semiconductor interface

The above-mentioned transmission mechanisms cannot be elucidated by the thickness of the insulating interfacial layer and the presence of interfacial states, since the ideality factor is more than one. The ideality factors greater than one have recently been explained by barrier inhomogenity (Sullivan et al., 1991; Werner, 1991 ; Tung, 1992). This theory is called the Gaussian distribution (GD). That is, the fact that the current-voltage (I-V) characteristics in M/S Schottky contacts are not ideal or that the magnitude 1 of the ideality factor n is large can arise from spatial inhomogeneities in the M/S interface (Sullivan, et al., 1991; Werner, 1991; Tung, 1992). The atomically rough (irregular) interface between the metal and the semi-conductor will result in different spatial variations in the potential of diffusion (V_D) and barrier height (Φ_B), leading to non-uniform dispersion. The atomic structure, dislocations and grain boundaries of the metal as well as the change of the thickness of the metal can cause the interface to become rough. Another reason for these potential changes is there may be a decrease in the local obstacle height due to the area emission. These local changes may also occur with the effect of different metallic phases at the interface. In addition, a regular lattice of donor atoms scattered randomly in semiconductors, irregular distances between donor atoms, may be another reason for such potential changes. Due to these factors, the barrier height is thought to have a Gaussian distribution (Song, et al., 1986; Dimitriadis et al., 1995). At low temperatures, many Schottky diodes were observed to deviate from the ideal TE. It is seen that the ideality factor increases significantly at low temperatures and that the ln (I_o/T^2) *-1/T* curve is not linear (Richardson curve), but that the ln (I_o/T^2) -1/nT curve is linear. It has been found that this image cannot be explained by the image-force effect, the tunneling effect, or the recombination current in the depletion zone (Tung 1992; Wittmer et al., 1994).In the theory proposed by Song (Song et al., 1986), Gaussian distribution has been accepted for the distribution of the barrier heights with a mean value $\overline{\Phi}_B$ and a standard deviation of (σ_s) and the mean value of obstacle height $\overline{\Phi}_B$:

$$P(\Phi_B) = \frac{1}{\sigma_S\sqrt{2\pi}} exp\left[-\frac{(\Phi_B-\overline{\Phi}_B)^2}{2\sigma_S^2}\right] \tag{2.14}$$

Where $P(\Phi_B)$ is the probability for the barrier height to have Φ_B. In a Gaussian distribution, the mean barrier height $\overline{\Phi}_B$ and the square of the standard deviation of the barrier height σ_s application potential are given as:

$$\overline{\Phi}_B = \overline{\Phi}_{Bo} + \rho_2 V \tag{2.15}$$

and

$$\sigma_s^2 = \sigma_{so}^2 + \rho_3 V \tag{2.16}$$

where ρ_2 and ρ_3 are the voltage coefficients.

The total current due to the correct feed-in potential can be obtained by taking following integral:

$$\mathrm{I(V)} = \int_{-\infty}^{\infty} \mathrm{I}(\Phi_\mathrm{B}, \mathrm{V})\mathrm{P}(\Phi_\mathrm{B})\mathrm{d}\Phi \tag{2.17}$$

where $I(\Phi_B,V)$ is the current at a bias voltage for a BH according to theory of ideal thermionic-emission-diffusion (TED) and $P(\Phi_B)$ is the normalization distribution function for BH. Since, carrying out this integration in domain of -∞ to +∞, one can calculate the current $I(V)$ through a barrier at a forward bias voltage as

$$\mathrm{I(V)} = \mathrm{AA^*T^2}\exp\left[-\frac{\mathrm{q}}{\mathrm{kT}}\left(\bar{\Phi}_\mathrm{B}-\frac{\mathrm{q}\sigma_\mathrm{s}^2}{2\mathrm{kT}}\right)\right]\exp\left(\frac{\mathrm{qV}}{\mathrm{n_{ap}kT}}\right)\left[1-\exp\left(-\frac{\mathrm{qV}}{\mathrm{kT}}\right)\right] \tag{2.18}$$

and in the case of exisitance of series resistance Equation (2.18) can be rewritten as

$$I(V) = AA^*T^2\exp\left[-\frac{q}{kT}\left(\bar{\Phi}_{B0}-\frac{q\sigma_o^2}{2kT}\right)\right]\exp\left(\frac{qV}{n_{ap}kT}\right)\left[1-\exp\left(-\frac{q(V-IRs)}{kT}\right)\right], \tag{2.19}$$

In addition, the reverse saturation current, can be obtained as:

$$\mathrm{I_0} = \mathrm{AA^*T^2}\exp\left(-\frac{\mathrm{q}\Phi_\mathrm{ap}}{\mathrm{kT}}\right) \tag{2.20}$$

The Φ_{ap} and n_{ap} are the apparent barrier height and apparent ideality factor, respectively,

$$\Phi_\mathrm{ap} = \bar{\Phi}_\mathrm{B0}-\frac{\mathrm{q}\sigma_\mathrm{s0}^2}{2\mathrm{kT}} \tag{2.21}$$

$$\frac{1}{n_{ap}(T)} - 1 = -\rho_1(T) = -\rho_2 + \frac{q\rho_3}{2kT} \tag{2.22}$$

Substituting Equation (2.21) and take the logarthiom of the both side, then Equation (2.20) can be rewerttina as

$$ln\left(\frac{I_o}{T^2}\right) - \frac{1}{2}\left(\frac{q\sigma_{so}}{kT}\right)^2 = \ln(AA^*) - \frac{q\bar{\Phi}_{Bo}}{kT} \tag{2.23}$$

As a result, according to this theory, the nullity of the zero feed is caused by the presence of the Gaussian distribution of the barrier height to the reduction of the barrier height, and this effect is determined by the standard deviation of the height of the barrier. This effect is especially important at low temperatures. On the other hand, the abnormal increases that occur in the ideality factor also depend on the average barrier height and the change of the standard deviation from the feeder (Tecimer et al., 2014). Fig.2.9 shows the inhomogeneity of the barrier height that made a deviation of the barrier height.

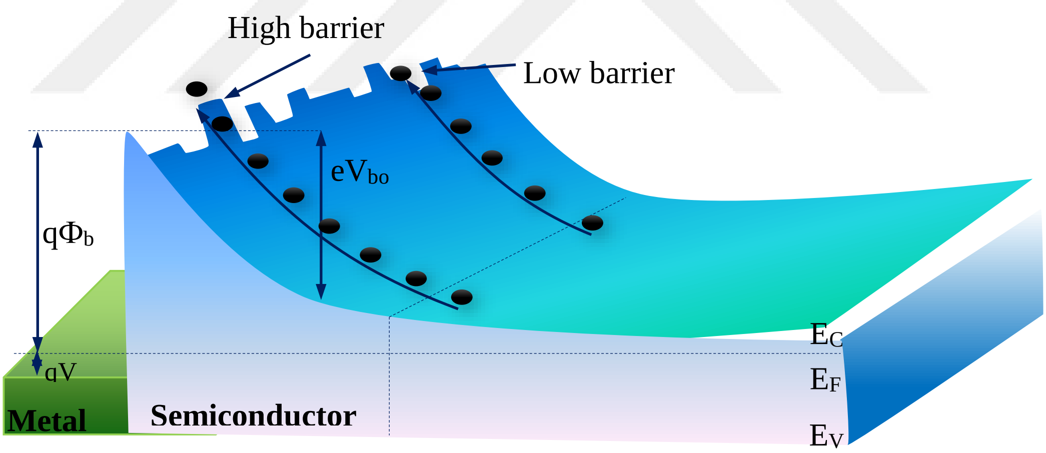

Figure 2.9 Three-dimensional example of potential barrier explain the inhomogeneity of the barrier for a metal- semiconductor rectifier contact.

2.6.4. Most important reasons for deviation from the ideal situation

Many reasons can effect on the behavior of ideal situation of MIS structure and causes a deviation. The most important reasons are as following:

- Image-force (Schottky) effect

- Tunneling effect.
- Serial resistance effect.
- Edge effects.
- Interface states.
- The effect of minority carriers.
- The effect of the interface layer.

2.7. Dielectric properties

Recently, advanced technology increases by using electrical insulators materials to prevent the flow of current in an electrical circuit and exhibiting the property of electrical polarization in electronic application such as high-voltage power system elements and low-voltage high-frequency applications. It is very important for safe operation to know how the electrical properties of these insulators vary within wide boundaries and at different conditions. For this reason, it is necessary to measure the dielectric properties under the conditions in which insulating materials used in different fields and operating conditions are used at the beginning of these properties, dielectric constant and loss factor**.** At applying external electric to the material, this excitation is a dielectric if it has energy storage capability. The dielectric constant (permittivity or electrical permeability) is used under an area effect to determine how much energy is stored in the external electric field and how much energy is lost in the material. The dielectric constant of a material is a parameter that reduces the electrostatic force between two electric charges. Electrons and atoms in the material are displaced by the electric field effect, and as a result, electric charge centers shift and electrical polarization is observed. Formed Electrical dipoles cause charge accumulation on the surface of the dielectric material. Their use as an insulator should not impede the charge transfer in electrical circuits (yudga, 2007).

2.7.1. The effect of static electric field in dielectrics

The difference between the dielectrics and conductors is that the dielectric does not have enough free carriers that can move under an external electric field effect to provide electrical conductivity. In dielectrics, all charges are bound to certain atoms or molecules and their motion is limited within the molecule. The only action of dielectric substance can have when it is placed in an external electric field is the small displacements in the opposite directions under electrostatic force with positive and negative charges. In general, a dielectric becomes polarized when an external electric field is applied to it, which means that acquires a dipole moment.When the electric field effect is removed from the center, these charges return to their former locations and the net dipole moment becomes zero again. It also directs molecules that have a continual dipole moment from the displacement of positive and negative charges under electrostatic force. Such molecules are under the influence of a pair of forces that try to orient themselves in the field. The result is a balanced polarization of a clear orientation. Some dielectric materials have this charge separation inside the electric field. These materials have a net dipole moment. The electrical properties of dielectric materials are generally expressed in terms of dielectric constants. In most materials, this value is independent of the magnitude of the electric field, but depends on the frequency of the electric field effect.

2.7.2. Parallel plate capacitor without dielectric

Two parallel plate capacitors with surface area *A* and spacing *d* are given in Figure 2.10. If a dielectric is placed between the plates, the transition of the charges from one plate to another is limited.

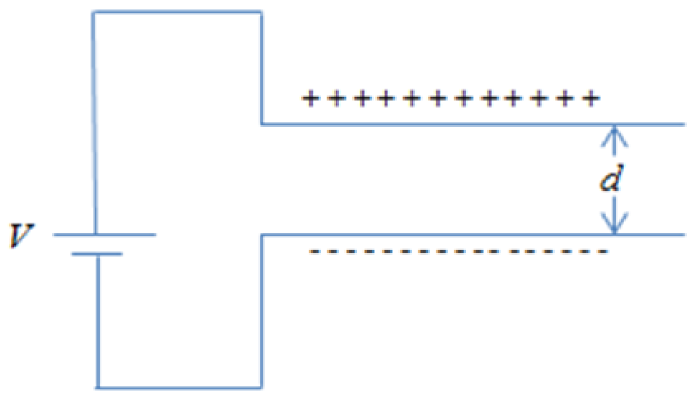

Figure 2.10. Parallel plate capacitor without dielectric

The two parallel plates of the capacitor have charges + Q, and -Q. If an insulator (dielectric material) is puted between the two plates, the charges are prevented from one plate to another. If these plates are connected to the ends of a voltage source, the capacitor can easily is charged Electric field intensity between plates can be represented as the following equation:

$$E = \frac{\sigma}{\varepsilon_o} \qquad (2.24)$$

where, ε_o is the permittivity of free-space, σ is surface charge density. The potential difference between the plates spaced from each other by *d* can be written as :

$$V = E.d \qquad (2.25)$$

and the total capacitance between two parallel plates is

$$C = \frac{Q}{V} = \frac{\varepsilon_o A}{d} \qquad (2.26)$$

2.7.3. Parallel plate capacitor with dielectric

If the gap between the two plates of a capacitor is completely filled with an insulator (dielectric) material, the capacitance of the capacitor increases by the ε' multiplication of the capacitor. The multiplication factor ε' is called the dielectric constants of the insulator.

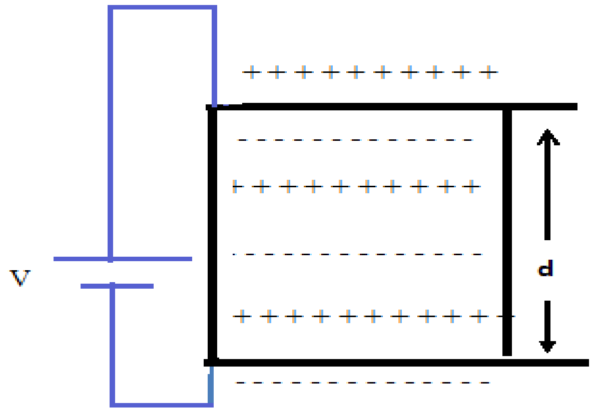

Figure 2.11. Parallel plate capacitor with dielectric interfacial layer

In the absence of a dielectric, the capacity of the parallel plate capacitor the potential difference between the ends of the capacitor and the electric field can be represented as C_o, V_o and E_o respectively. If a dielectric substance is placed between the two plates, then the potential difference and electric field in free space multiplied by 1 /ε', and can be rewritten as :

$$V = \frac{V_o}{\varepsilon'} \tag{2.27}$$

$$E = \frac{E_o}{\varepsilon'} \tag{2.28}$$

Since the charge Q does not change on the capacitor, the value of the capacitance increases by a factor of ε':

$$C = \frac{Q_o}{V} = \frac{\varepsilon' Q_o}{V_o} = \varepsilon' C_o \tag{2.29}$$

Then, when the area between the plates is exactly filled with dielectrics, the parallel plate capacitor capacitance can be rewritten as:-

$$C = \frac{\varepsilon' \varepsilon_o A}{d} \tag{2.30}$$

2.7.4. Dielectric polarization

When applying an electric field to insulators, the electrons are unsettled to each atom opposite the direction of that field, while the nucleus of each atom is unsettled in the same direction of that field. This separation of charges is called polarization or electric polarization.

The reduction in potential when a dielectric is placed between the plates of a capacitor requires reduction of the electric field strength ($E = V/d$). The net charge or effective charge on the unit surface decreases as the electric field intensity ($E = \sigma/\varepsilon_o$) decreases. This is only possible if the dielectric comes to the fore with the opposite signs on the faces of the dielectric facing the plates. Since free charges on the plate do not change with placing a dielectric between plates, the decreasing of electric field can be attributed to increasing of electric permittivity of the medium.

When a conductor is placed in the electric field, the free charges are displaced under the influence of the forces exerted by the field. When electrostatic equilibrium is established, the electric field of the charges on the conductor surface facing on the plates neutralize the outer field at all points and the electric field within the conductor becomes zero (Yudga, 2007).

When a dielectric is placed between the plates of a dielectric capacitor, the charges of the dielectrics against the plates come into play. The molecules of some dielectrics contain a permanent dipole. In these materials called polar, the centers of mass of the positive and negative charges do not overlap, so the loads are separated by a very small amount. When a dielectric is placed in electric field, the electrons make a very small displacement with respect to their nucleus. Thus, the atoms become very small (atomic) dipoles and are polarized electrically. Thus, the dipole moment of the molecule will be parallel to the electric field. When the electric field is removed, the atoms return to their normal state again and the dipoles disappear.

There are several individual mechanisms of dielectric polarizations which are typically described by four major mechanisms: electronic, vibrational, orientation and space charge polarizations, as shown in Figure 2.16 (Hess et al., 1989; Sasidhar, 2011).

- Electronic polarization exsist in a neutral atom when the electric field displaces the electron density proportional to the nucleus it surrounds, inducing a dipole moment that vanishes as soon as the electric field is removed. Electronic polarization is frequency independent and thus continues through the entire frequency range. Electronic polarization is common in all dielectric materials (Dakin, 2006; Maheshwari, 2007; Sasidhar, 2011).

- Vibrational polarization, also called atomic or ionic or displacement polarization, usually happens in ionic substances. At applying electric field to an ionic substance, two ions with different sign are displaced in the opposite directions until the ionic bonding forces stop the process, inducing a dipole moment. This type of polarization is predominant in inorganic crystals, glasses and ceramics and is the principle mechanism for permittivity of inorganic crystals that is observed to be uniform from D.C. through infrared frequencies (Arora et al 1995; Dakin, 2006; Maheshwar, 2007; Sasidhar, 2011).

- Orientational or dipolar type of polarization usually happens in polar dielectrics, which have permanent dipoles, such as polymeric substances and dipolar ceramics. Under normal conditions, dipoles that are exsist in polar dielectrics that have zero net dipole moment and polarization are randomly oriented. At applying external field, the dipoles resort to reorient along the direction of applied field performing a non-zero net dipole moment and polarization. Orientational polarization happens from D.C. through microwave frequencies depending on the presence of dipolar bonds and resistance to molecular rotation. (Arora et al., 1995; Dakin, 2006; Maheshwari, 2007).

- Translational or interfacial polarization is usually associated with existance of migrating charges, by electrons or ions, in an applied field over macroscopic distances. They tend to be straitened and accumulate at physical barriers such as defects, voids, impurities, grain or phase boundaries and also at the electrode interfaces where the material has different charge transport properties, e.g., conductivity. The accumulated charges deform the local electric field and give an increasing to permittivity. Particularly, in heterogeneous or multiphase systems like polymer-ceramic nanocomposites, the interfacial polarization is important. Interfacial polarization, involving a long range ion movement, is usually observed only at lower frequencies, otherwise known as a space-charge or Maxwell Wagner polarization (Dakin, 2006; Sasidhar, 2011).

In general a dielectric medium exhibits more than one polarization mechanism. Thus, the average induced dipole moment per molecule will be the sum of all polarization contributions, depending on which to determine dielectric permittivity of the material. For example, interfacial polarization plays an important part in permittivity of semicrystalline polymers, such as PVA. Also for another example, a polar dielectric having ionic bonding and permanent dipoles possess orientational as well as ionic and electronic polarizations, an ionic and non-polar dielectric, e.g., alkali halides which contain more than one type of bonds but no permanent dipoles, possess both ionic and electronic polarizations (Maheshwari, 2007).

2.7.5. Electric field and dielectric loss in dielectrics

When a sample with a clear and permanent dipole moment is placed in the electric field, the electrical displacement (D) and electric field (E) for this sample can be expressed as a function of time. Time dependence (dipole-relaxation) of the electrical displacement vector (D) is seen in samples with permanent dipoles. This is different from non-dipole specimens. When a static electric field (E) is applied to a crystal at time t = 0 for a certain period of time, the movement of the dipoles in the crystal can have two results: this movement arranges the dipoles simultaneously in the direction of the applied electric field, or causes them to find their final configurations slowly. The first state is known as the static state. The others are caused by the fact that the electric field and the polarization vector are not in the same phase.

The electric displacement in electrostatics can be expressed as follow:

$$D = \varepsilon E \tag{2.31}$$

ε is a real time independent constant. When the electric field is time dependent, the following equation can be written:

$$D + a\frac{dD}{dt} = bE + c\frac{dE}{dt} \tag{2.32}$$

where a, b, c are the correction constants in the added terms. In this equation, second, third etc. order time derivative terms can be added. But high-order derivatives can be neglected for medium-strength electric fields. If the dielectric behavior is examined by considering the conditions given below, it is found that the constants a, b and c are specific to the sample (Wert et al., 1970). When a constant electric field is applied to the sample the electric field and hence the amount of electric displacement does not change over time. This is a static situation.

$$\left(\frac{dE}{dt} = 0 \; and \; \frac{dD}{dt} = 0\right), \text{then Eq 2.30 will be } D = bE \tag{2.33}$$

where b represent the static dielectric permeability constant (ε_s), and then Equation (2.32) can be rewritten as following :

$$D + a\frac{dD}{dt} = \varepsilon_s E + c\frac{dE}{dt} \tag{2.34}$$

When the sample is under a constant electric field, $\frac{dE}{dt} = 0$, then Equation (2.32) can be written as

$$D + a\frac{dD}{dt} = \varepsilon_s E \tag{2.35}$$

Solution of this equation is given by $ln(\varepsilon_s E - D) = \frac{-t}{a}$+constant at t=0 and D=D(0) we get $ln(\varepsilon_s E - D) = \frac{-t}{a}$+constant

$$D = \varepsilon_s E - [-D(0) + \varepsilon_s E]e^{\frac{-t}{a}} \tag{2.36}$$

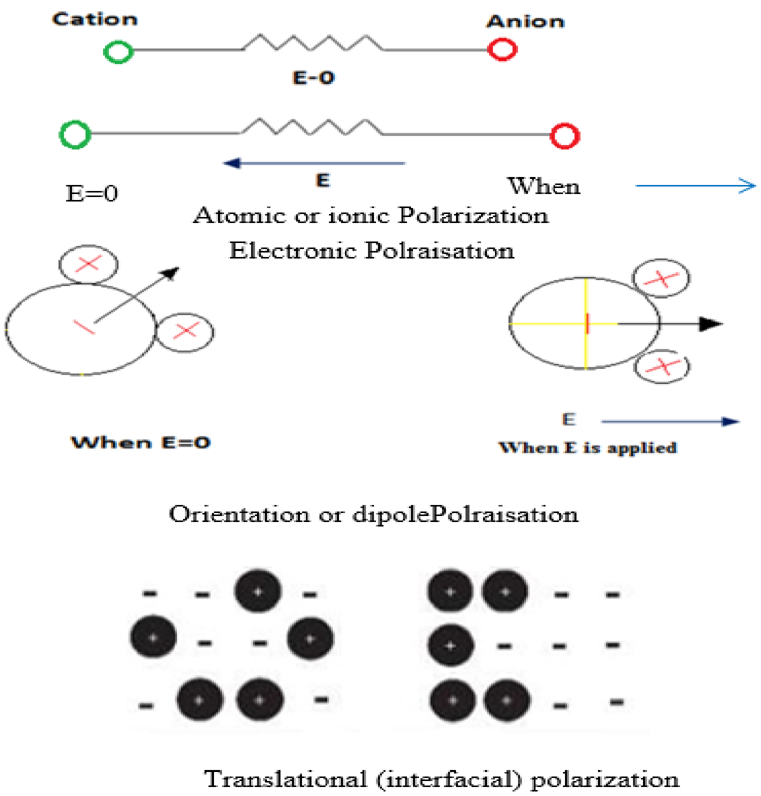

Figure 2.12. Mechanisms of dielectric polarizations

Taking the above equation into consideration, the change in D along time is given in Figure 2.12. It is seen that the first value of the electric displacement is D (0) and the final value is maximum value ($\varepsilon_s E$) that comes with an exponential increase. The value of constant (a) in the Equation (2.36) has an exponential behavior at constant time (relaxation time), and then by substituting it in Eq. 2.32 we can get the following Equation:

$$D + \tau \frac{dD}{dt} = \varepsilon_s E + c \frac{dE}{dt} \tag{2.37}$$

If sample is put in an electric field which has a value of E (0) at t = 0, the electric displacement value D in the sample will be D_1. For D to remain constant at D_1, the electric field will change as a function of time. Then Equation (2.37) will be as following:

$$D_1 = \varepsilon_s E + c \frac{dE}{dt} \tag{2.38}$$

By integrating the above equation we obtained

$$\varepsilon_s E = D + [\varepsilon_s E(0) - D_1] e^{\frac{-\varepsilon_s t}{c}} \tag{2.39}$$

The corresponding graphic for this expression is given in Figure 2.14. The exponential changes with time in In Figures 2.13 and 2.14 occur with different time constants ($\tau_1 = c / \varepsilon_s$). For this reason Equation (2.37) can be written as last form as

$$D + \tau \frac{dD}{dt} = \varepsilon_s E + \varepsilon_s \tau_1 \frac{dE}{dt} \tag{2.40}$$

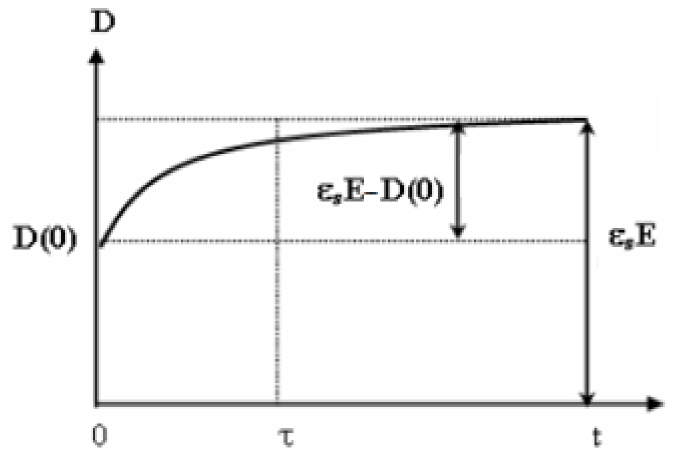

Figure 2.13. The variation of D with time at constant E

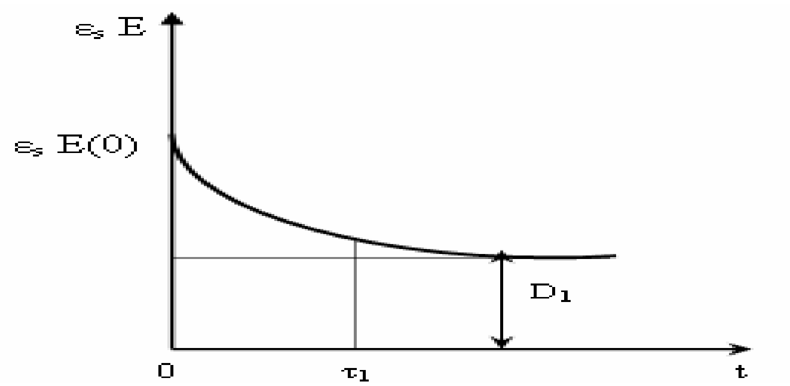

Figure 2.14. The variation of *E* with time at constant D

These results can be characterized by admittance or impedance method which can be rewritten as :

$$Y = \frac{1}{Z} = G + j\omega C \tag{2.41}$$

where *Y* is the admittance, *Z* is the impedance, *G* is the conductance, *C* is thel capacitance, ω is the angular frequency, then

$$Y = G + j\omega\ (C_{o}\varepsilon^{*}) \tag{2.42}$$

Where C_o is the dielectric constant of the capacitor when there is no dielectric material, and ε^* is the relative dielectric constant and can be written as

$$\varepsilon^{*}(\ \omega) = \varepsilon'(\omega\ ) - j\varepsilon''(\omega) \tag{2.43}$$

then by substituting the value of the permittivity, the admittance value can be rewritten as

$$Y = G + j\ \omega C_{o}(\varepsilon' - j\varepsilon'') \tag{2.44}$$

$$Y = \left(G +\ \omega\varepsilon'' C_{o}\right) + j\ \omega C_{o}\varepsilon' \tag{2.45}$$

Then the impedance Z which represents the opposite of admittance can be written as

$$Z = \frac{1}{j\omega C+G} = \frac{1}{j\omega C_{\circ}\varepsilon^{*}} \quad (2.46)$$

Substituting in Equations (2.43) and (2.46) we can get the imaginary part of permittivity as follow

$$\varepsilon'' = \frac{G}{\omega C_{\circ}} = \frac{1}{\omega R C_{\circ}} \quad (2.47)$$

Where is real part of the permittivty was explaind in Equation (2.29). At applying A.C voltage to ideal dielectric, the consuming energy is zero and the phase angle between the current voltage and voltage is 90˚. In general, the phase angle in commercial dielectrics is ϕ > 90˚. Finished angle δ= 90- ϕ is called the dielectric loss angle. This angle can calculate the power which squandered in each cycle.An oscillating field $E = E_0\, e^{j\omega t}$ is applied across the plates. All the displacement field $D = D_0\, e^{j(\omega t-\delta)}$ with phase difference with respect to E – field. These equation leads to a complex quantity as

$$\frac{D_{\circ}}{E_{\circ}} e^{-j\delta} = \varepsilon' - j\varepsilon'' = \varepsilon^{*} \quad (2.48)$$

where the relative permitivity or dielectric constant $\varepsilon' = \frac{D_0}{E_0} cos\delta$ the dielectric loss constant $\varepsilon'' = \frac{D_0}{E_0} sin\delta$ then

$$\tan\delta = \frac{\varepsilon''}{\varepsilon'} \quad (2.49)$$

where tanδ is called loss tangent or squandered of the dielectric. It represents the value of energy that is lost in the dielectric when an A.C applied voltage is across it. Now the complex electric modulus (M^*) or the reciprocal of complex relative permittivity can be significantly sturdy tool for analyzing dielectric demeanor of a polymeric insulating material, particularly at comparatively high temperatures, where complex permittivity commonly becomes very high because of electrode polarization and carrier transport. The complex electric modulus spectrum represents the measure of the distribution of ions energies or configurations in the structure and it also describes the electrical relaxation and microscopic properties of ionic glasses. The modulus formalism has been adopted as it suppresses the polarization effects at the electrode/electrolyte interface. Hence, the complex electric modulus M'' spectra reflects the dynamic properties of the sample alone (Macedo et al., 1972; Provenzano et al., 1972).

The complex electric modulus is defined by the reciprocal of the complex permittivity ε^*.

$$M^* = \frac{1}{\varepsilon^*} = j\, C_o Z^* \tag{2.50}$$

$$M^* = M' + jM'' \tag{2.51}$$

then Equation (2.50) can be rewrritin as flow

$$M^* = \frac{1}{\varepsilon^*} = M' + jM'' = \frac{\varepsilon'}{\varepsilon'^2+\varepsilon''^2} + j\,\frac{\varepsilon''}{\varepsilon'^2+\varepsilon''^2} \tag{2.52}$$

where M^* is the complex modulus, M' is the real and M'' is the imaginary parts of electric modulus.

3. EXPERIMENTAL METHOD

3.1. General Properties of SiC Crystals

Silicon carbide (SiC) consists of chemically stable (Si) and carbon (C) atoms. Each electrons of Si atom are covalently bonded to the C and form different arrangement such as tetrahedral arrangement. SiC has many different crystal structures and is called a multi-structure, but it usually crystallizes in a large number of structures. The most important structures of SiC are three types of double-atomic layers A, B, and C which form a periodical series with a specified repeated unit along the c-axis form a specific polytype of the silicon carbide crystal, such as 3C-SiC, the stacking sequence of the double-atomic layers is ABCABC. The predominant polytypes in SiC are hexagonal. The most three prevalence hexagonal polytypes are 2H, 4H, and 6H and their stacking sequences are ABAB, ABCBABCB, and ABCACBABCACB, respectively, as shown in Fig 3.1. Where, "H" refers to the hexagonal crystal structure and the number before "H" denotes the number of double-atomic layers in one repeating unit. The general properties of 4H-SiC explained in Table 3.1.

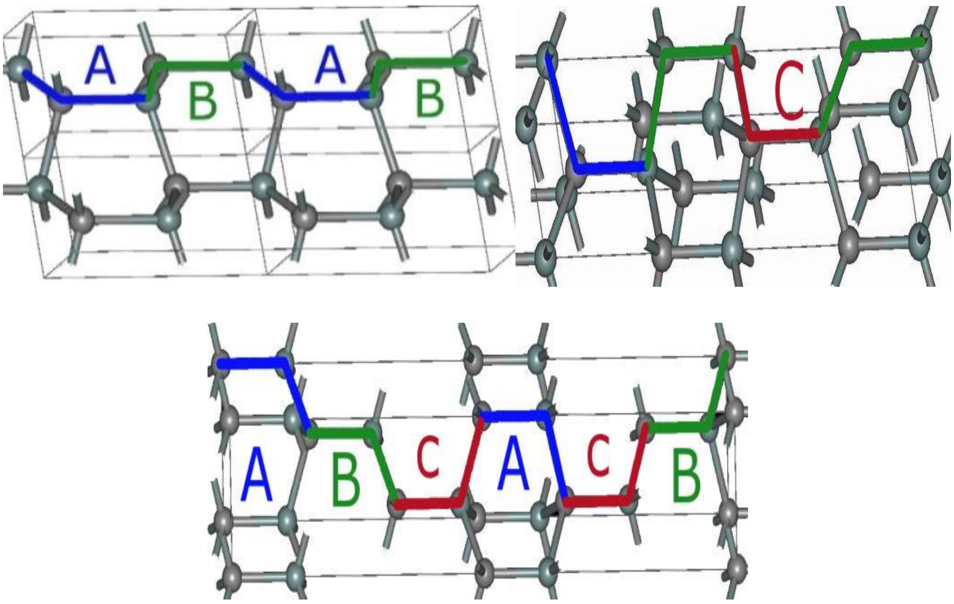

Figure 3.1. 2H-SiC, 4H-SiC and 6H-SiC structures.

Table 3.1. Some properties of 4H-SiC (Casady et al., 1996; Han et al., 2003)

Properties	4H-SiC
Thermal conductivity (W $cm^{-1}K^{-1}$) at 300K doped at ~$10^{17}cm^{-3}$	3.7
Intrinsic carrier concentration at 300K (cm^{-3})	$5x10^9$
Saturation velocity (cm s^{-1}) parallel to c-axis	$2.0x10^7$
Electron mobility ($cm^2V^{-1}s^{-1}$)	1000
Hole mobility (cm^2V^{-1} s^{-1})	115
Band gap (eV) (T<5K)	3.26
Saturated electron drift velocity (10^7 cm s^{-1})	2.0
Breakdown field (MV cm^{-1})	2.2
Thermal conductivity (W cm^{-1} K^{-1})	3.7
Dielectric constant	9.7
Physical stability	Excellent

3.2. General Properties of PVA Crystals

PVA is a polyhydroxy polymer, is the biggest volume, synthetic water-soluble resin produced in the world. It is commercially produced by the hydrolysis of poly (vinyl acetate). PVA refers to the sequence of products which may be considered copolymers of vinyl acetate and vinyl alcohol. The physical properties of polyvinyl alcohol (PVA) depend on the preparation method, crystallinity, molecular weight, humidity ect as in Table (3.2). Their final properties are influenced by the polymerization conditions of polyvinyl acetate, the conditions of hydrolysis, drying and milling. The tensile strength of the unplasticized PVA is dependent on the hydrolysis degree, molecular weight and relative humidity. The degree of hydrolysis and polymerization greatly affects the water solubility of PVA in particular in other word, at high hydrolyzed PVA has low solubility in water. In PVA, the hydroxyl groups provide strong hydrogen bonding between molecules and within the molecule that will reduce the water solubility. The residues of the acetate groups present in the partially hydrolyzed PVA weaken these hydrogen bonds and lead to solubility at low temperatures. As the number of the hydrophilic nature of the acetate groups of the acetate groups increases, it causes an increase in negative heat dissolution. Increasing acetate group ratio causes the critical temperature to drop. It means that when applied temperature on PVA increases with low hydrolysis grade (70-80%), the solubility decreases (Marten, 2000).

Table 3.2 Physical Properties of Poly (vinyl alcohol) (Marten, 2000).

Property	Value	Remarks
Appearance	White to ivory white granular powder	
Specific gravity	1.27–1.31	rises with crystalline degree
Tensile strength, MPa (98–99% hydrolyzed)	67–110	rises with crystalline degree (heat treatment), and molecular weight, reduces with rising humidity
Tensile strength, MPa (87–89% hydrolyzed)	24–79	rises with molecular weight and reduces with rising humidity
Elongation,	0–300	rises with rising humidity
Thermal coefficient of expansion per ◦C	7–12 $\times 10^{-5}$	
Specific heat, J/(g.K)	1.67	
Thermal conductivity, W/(m.K)	0.2	
Glass-transition temperature, K	358	98–99% hydrolyzed
Melting point, K	331	87–89% hydrolyzed
	503	98–99% hydrolyzed
	453	87–89% hydrolyzed
Electrical resistivity,Ω·cm	(3.1-3.8)x10^7	
Thermal stability	Gradual discoloration above100 C; darkens rapidly above 150C; rapid decomposition above 200 C	
Refractive index n_D (20C)	1.55	
Degree of crystallinity	0–0.54	rises with heat treatment and hydrolysis degree
Storage stability (solid)	Indefinite when protected from moisture	
Flammability	Burns similarly to paper	
Stability in sunlight	Excellent	

3.3. Preparation of PVA by Electrospinning Method

Electrospinning method is one of the most effective methods for the production of polymer based nanofibers. Electrospinning is a multi-disciplinary method of fluid dynamics, polymer chemistry, basic physics, electrical physics, machine and textile engineering disciplines. In the electrospinning method, a polymer thin films produce by electric energy. The experimental setup required for the electrospinning method consists of three main fundamentally important parts which are 1-high voltage power supply, 2-syringe pump, 3-electric conductive picker. The syringe pump is one of the important components for obtaining a fixed and adjustable feed rate of the polymeric solution as shown in figure 3.2 (Tecimer et al., 2013).

If we will explain this method in the simplest way;

1. A polymer solution is placed in the syringe and a collector-metal plate is placed a certain distance away from the syringe.
2. The collector plate is grounded while the high voltage supply source of the power supply is tied to the metallic wire of the syringe.
3. A high electric field is thus obtained between the syringe and the collecting plate.
4. As the voltage provided by the power supply is increased, electric field forces reaching a sufficiently high value overcome the viscoelastic and surface tension forces on the solution and the polymer molecules are transported from the syringe to the collector.
5. As a result, nano-sized fibers are formed on the collecting plate.

Before coating, the n-type4H- SiC substrate was washed with 1% hydrofluoric acid to remove silicon oxide on it. Then 0.1 g of Zinc acetate was mixed with 0.9 g of PVA having a molecular weight of 72 and 9 ml of deionized water. After stirring at 50 C for 2 hours, a concentrated solution of PVA was got. Using a peristaltic syringe pump, the precursor solution was distributed at a constant flow rate of 0.05 mL / s with (10 ml) needle syringe with inner diameter of 0.9 mm at rate about 0.05 ml/h constant flow. The needle was tied to a high voltage power supply and a mengenede was placed horizontally. A piece of flat aluminum leaf was placed 15 cm below the needle to collect the nanofiber particles. The n-type 4H -SiC substrate was placed on an aluminum sheet by applying a voltage above 20 kV, the fluid jet was ejected from the tip. The solvent was evaporated and the charged fiber was deposited on SiC substrate.

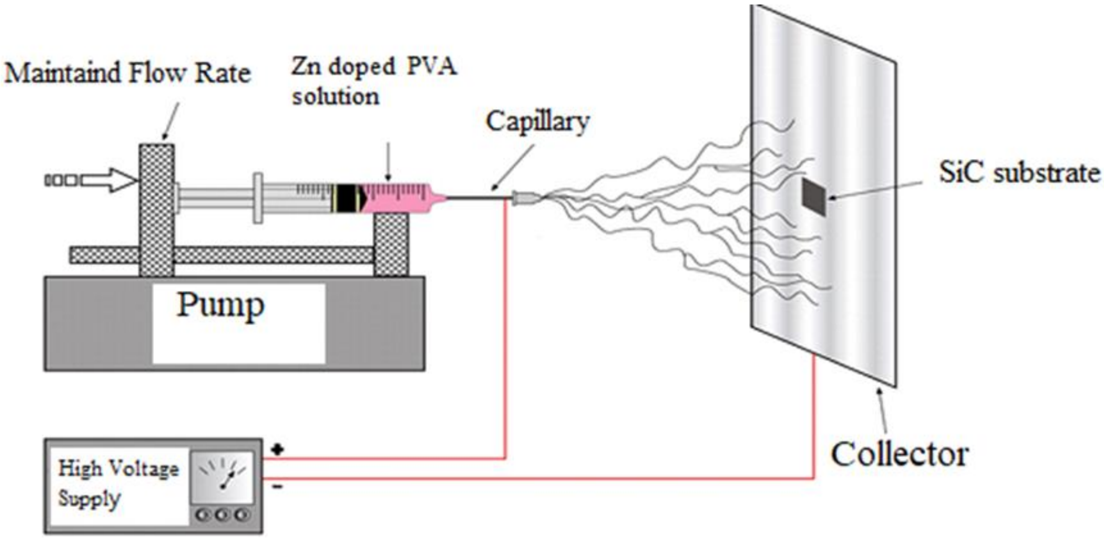

Figure 3.2. Electrospinning process digram

3.4. Preparation of Au / Zn doped PVA / n-4H-SiC structure

Both the Au/n-SiC (MS) and Au/Zn-PVA/n-SiC (MPS) structures were grown on the n-type 4H-SiC (0001) wafer with 7.07×10^{17} cm^{-3} donor concentration atoms (N_d), 0.0314 cm^2 rectifier/Schottky contact area and 250 μm thickness. Firstly, n-type 4H-SiC wafer was degreased in organic solution of peroxide-ammoniac solution in 10 minutes, and then etched in a sequence of H_2O+HCl solution in ultrasonic bath and then quenched in de-ionized water (DI) with 18 MΩ.cm resistivity for ten minutes. Preceding each cleaning step, the wafer was rinsed thoroughly in DI water and then dried with high pure dry nitrogen (N_2) gas. Immediately, n-type 4H-SiC wafer transferred into vacuum chamber and high purity (99.999%) gold (Au) with a thickness of ~1500 Å was thermally evaporated onto the whole back side of it at a pressure of 10^{-6} Torr in the high vacuum metal evaporation system (HVMES). In order to get low resistivity ohmic back contact, both two n type 4H-SiC wafers were sintered at 500 °C for 5 min in nitrogen ambient. Finally, high purity Au dots of ~2 mm diameter with a thickness of ~1500 Å was thermally evaporated onto the front of (Zn-doped PVA) layer with 50 nm in the same high thermal evaporation system. Thus, the fabrication processes of Au/(Zn-PVA)/n-4H-SiC (MPS) type structures were completed. Both the thickness evaporated metal layer and the deposition rates were monitored with the help of quartz crystal thickness monitor.

In order to perform Au/Zn-PVA/n-SiC (MPS) structures, Zn-doped PVA interfacial layer with 50 nm was deposited onto the front of n type 4H-SiC wafer by using electrospinning method. After the formation of the Zn-doped PVA interfacial polymer as in Figure(3.3a) , high purity Au dots of ~2 mm diameter with a thickness of ~1500 Å was thermally evaporated onto the front of n type 4H-SiC wafer in the same high vacuum MES for two structures by using mask as in Figure (3.3b). Thus, both the fabrication processes of Au/n-SiC (MS) and Au/Zn-PVA/n-SiC (MPS) structures were completed as in Fig 3.4 (a and b) . Both the metal thickness layer and the deposition rates were monitored with the help of quartz crystal thickness monitor. Finally, in order to perform electrical measurement of these structures, they were mounted on a copper (Cu) holder with the help of silver paste and electrical measurements were made to the upper electrodes by the use of tiny silver coated Cu-wires with silver paste. The measurement system for the forward and reverse bias *I-V*, *C-V* and *G/ω-V* measurements was also given in Fig.3.5and 3.6. The interfacial layer thickness (d_i) was estimated to be about 500 Å from high frequency (1MHz) *C-V* measurements of the interfacial layer capacitance ($C_i=\varepsilon_r\ \varepsilon_o\ A/d_i$) in the strong accumulation region. The forward and reverse bias C-V and *G/ω-V* measurements were performed by the use of a computerized HP 4192A LF impedance analyzer (5 Hz-13 MHz) in the wide applied bias voltage range of (-6V)- (+6V) by 50 mV steps at 1 kHz and 1 MHz as in figure 3.6. The forward and reverse bias *I-V* measurements were performed by the use of a Keithley 2400 current-voltage source-meter.

In the second step, *I-V-T, C-V-T* and *G/ω-V-T* measurements were performed by using a computerized HP 4192A LF impedance analyzer in bias voltage range and the temperature (−4 V)–(+6 V) and 100–320 K at 1 MHz, respectively. All measurements were carried out in dark with the help of a microcomputer through an IEEE-488 AC/DC converter card in the JANES-475 Cryostat at about 10^{-3} Torr to avoid an external noise or other effects as in Fig.3.7and 3.8.

3.4.1. Materials and measurements devices

- Deionize water source (18 MΩ/cm),
- Some chemical solutions
- Some semiconductor wafers (n-type 4H-SiC)

- Some of pure metals (Au, Zn).
- Liquid nitrogen N_2. dry nitrogen gas (N_2) atmosphere.
- Some of polymer materials (PVA).
- IEEE-488 AC/DC converter card in the JANES-475 Cryostat.
- Copper (Cu) holder with the help of silver paste.
- Tiny silver coated Cu-wires with silver paste.
- Copper base.
- Ultrasonic bath
- Keithley 2400 current-voltage source
- Janis VPF-475 cryostat (77-400 K)
- Hawlett Packard 4192A LF impedans Analyzer (5Hz-13 MHz),

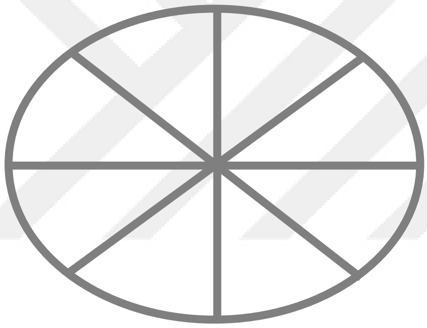

Figure 3.3. (a) The mask used to create the ohmic contact.

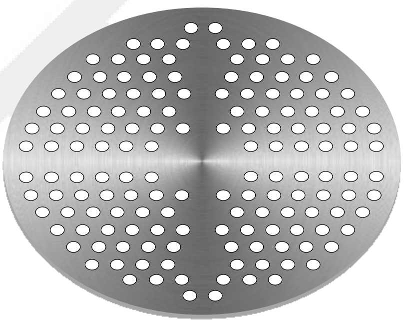

Figure 3.3. (b) The mask used to create a rectifier contact.

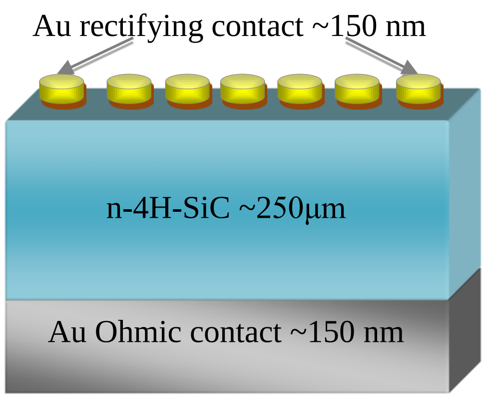

Figure 3.4. (a) schematic diagrams of Au/n-4H-SiC(MS) structure.

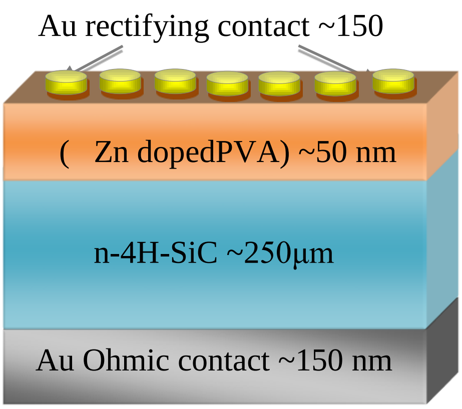

Figure 3.4. (b) schematic diagrams Schematic representation of Au / Zn doped PVA / n-4H-SiC (MPS) structure.

3.5. Experimental Measurement System

1. At room temperature, a schematic view of the experimental measurement system is given in Figures 3.5and 3.6. The devices used in this test system are as follows.
   - HP 4192A LF impedance analyzer
   - Keithley 2400 current-voltage source.
2. At temperature range (100-320) K, a schematic view of the experimental measurement system is given in Figures 3.7and 3.8.The devices used in this test system are as follows.
   - HP 4192A LF impedance analyzer
   - Keithley 2400 current-voltage source.
   - Janis vpf-475 cryostat.
   - Lake Shore model 321 Autotaning Temperature Controller.

3.5.1. HP 4192A LF impedance analyzer

HP 4192A LF impedance analyzer (5 Hz-13 MHz) and 40 mV_{rms} test signal was used to measure capacitance–voltage (*C-V*) and conduction –voltage (*G/ω-V*) measurements at room temperature and wide rage temperature.

Figure 3.5. HP 4192A LF impedance analyzer

3.5.2. Keithley 2400 current-voltage source

A Keithley 2400 current-voltage source was used to measure current-voltage measurements and current-voltage temperature-dependent measurements. The

Keithley 2400 current-voltage meter shown in Figure 3.6 can measure both current-source voltage measurement and voltage-source current measurement. It can measure voltage from ± 1 μV to ± 200 V and current measurement from ± 10 pA to ± 1 A. ± 0.15% sensitivity measurement device has IEEE-488 interface data path.

Figure 3.6. Keithley 2400 current-voltage source device.

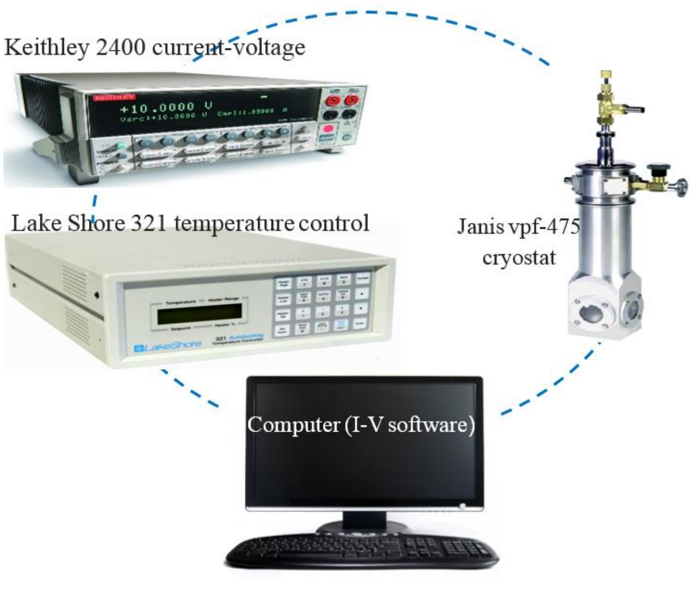

Figure 3.7. A schematic view of the experimental I-V measurement system

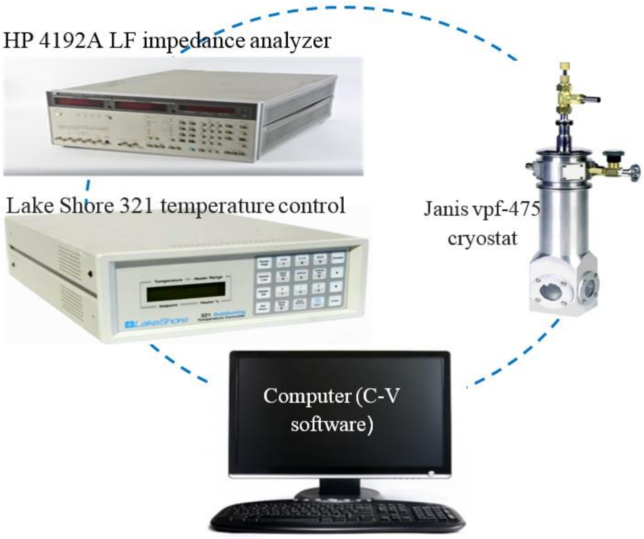

Figure 3.8. A schematic view of the experimental C-V measurement system

3.5.3. Janis vpf-475 cryostat and Lake Shore model 321 temperature control system

I-V measurements of Au / (Zn-doped) PVA / n-4H-SiC structure prepared to reduce external effects on all measurements were performed at a pressure of about 10^{-2} mbar in a Janis vpF-475 cryostat with 4 optical windows. This cryostat has a Lake Shore model 321 temperature control system and is capable of measuring at temperatures ranging from 79 K to 425 K.

Figure 3.9. Photo of Lake Shore model 321 temperature controller device and Janis vpf-475 cryostat.

4. RESULTS AND DISCUSSION

4.1. A Compare of Electric Characteristics of Metal-Semiconductor (MS) and Metal-Polymer-Semiconductor (MPS) Structure at Room Temperature

4.1.1. The forward and reverse bias current-voltage (I-V) characteristics

In order to determine whether MS structure with modified PVA interfacial layer doped by Zn nanoparticles and without an interfacial layer has the ideal diode behavior, its experimental results at forward bias *I-V* characteristics and low or intermediate voltage ($V \geq 3kT/q$) can be analyzed according to thermionic emission (TE) theory and by using Equation (2.6) (Rhoderick, 1978; Sze, 1981; Sharma, 1984).

From Eq. (2.9) , the saturation current (I_o) was calculated from straight line interception of lnI at V=0, A^* is the effective Richardson constant (146 $A.cm^{-2}K^{-2}$ for n-type 4H SiC, A is the rectifier/Schottky contact area, T is the absolute temperature in K, V_D is the voltage drop across the junction ad n is the ideality factor (Rhoderick, 1978), and the other quantities are well known in the literature. Fig. 4.1 shows the experimental reverse and forward bias *I-V* characteristics for MS and MPS type structures at room temperature. As shown in Fig.4.1, both MS and MPS type structures have a rectifying behavior with exponential increase of the current showing in the forward bias and weak voltage dependence in the reverse bias regions. The value of I_o was evaluated from the intercept of the linear region of *lnI-V* plots, whereas the value of n was evaluated from its slope for both structures according to Equation (2.9) by taking the logarthem for both side , then we get the following equation (Sze, 1981; Rhoderick, 1978).

$$n = (\frac{q}{kT})(\frac{dV}{d(lnI)} \tag{4.1}$$

Now, the value of Φ_{Bo} was calculated by taking the logarthem for both sides of Equation (2.7) and using theoretical value of A^* and extrapolated I_o values as following equation for two type structures (Sharma, 1984).

$$\Phi_{B0} = \frac{kT}{q}\ln(\frac{AA^{*}T^{2}}{I_0}) \quad (4.2)$$

Fig.4.1, shows shows lnI vs V plot of the MPS structure having two linear regions with different slopes whereas for MS structure this plot has one linear region in the intermediate biases. For the MPS structure, these regions are belonging to low bias voltages ($3kT/q \leq V \leq 0.55$V) and intermediate bias voltage regions (0.55V≤V≤1.30V), respectively. Such two linear regions for MPS structure are known two parallel diodes model with different BH (Demirezen et al., 2015). In addition, in the enough high forward-bias voltages, Fig.4.1 plot shows for both MS and MPS structure deviation from linearity due to the existence of R_s. Table 4.1, showing the values of I_0, n and Φ_{B0} for MS and MPS structures were found from the first region as $1.90\text{x}10^{-11}$A, 3.854 , 0.906 eV and $7.08\text{x}10^{-10}$A, 3.24, 0.80 eV, respectively. These high values of n for two structures at room temperature can especially be due to the existence of native or deposited interlayer, the spatially distribution of N_{ss}, and the existence of many distribution of low BHs or patches an average BH (Rhoderick, 1978; Sze, 1981; Sharma, 1984; Tunc et al., 2011; Bilkan et al., 2015). These results refer to the values of n and leakage current at (-6 V) for the MPS with (Zn doped-PVA) interfacial layer are lower than those of the MS attributed to the passivity role of Zn-PVA interfacial polymer layer. Similarly, the rectifying rate ($R=I_F/I_R$) at ±6V for the MPS structure is 15.5 times higher than MS structure.

Table 4.1. The experimental results values for some electrical parameters obtaind from the forward bias *I-V* characteristics for MS and MPS structure at room temperature.

Samp.	I_0 (A)	$n(I\text{-}V)$	$\Phi_{B0}(I\text{-}V)$ (eV)	$R_s(dV/dln(I)\text{-}I)$ (Ω)	$R_s(H(I)\text{-}I)$ (Ω)	$RR(\pm 6V)$ ($=I_F/I_R$)	$R_s(I\text{-}V)$ (Ω)	$R_{sh}(I\text{-}V)$ (Ω)
MS	$2.91\text{x}10^{-11}$	3.854	0.806	27.03	89.305	347	49.4	$2.4\text{x}10^{7}$
MPS	$7.08\text{x}10^{-10}$	3.241	0.815	171.72	196.79	5390	22.1	$9.5\text{x}10^{8}$

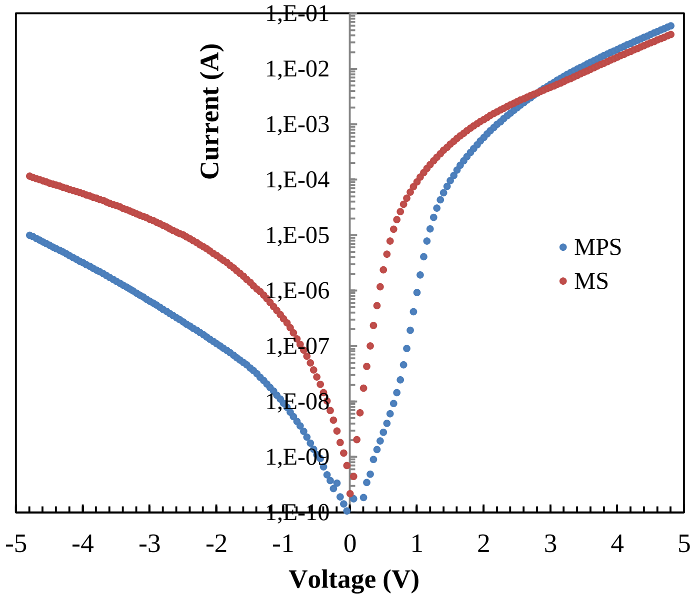

Figure 4.1. Experimental reverse and forward bias *I-V* characteristics for both MS and MPS type structures at room temperature.

As can be seen in Equation (4.1) MPS type structure or diode has N_{ss} in equilibrium state with semiconductor ($d_i \geq 3$ nm) and interfacial layer, the experimental results value of *n* becomes greater than 1 and dependent on applied bias voltage. Thus, N_{ss} can be calculated from the forward bias *I-V* characteristics by taking into account voltage dependent effective BH (Φ_e) and ideality factor $n(V_i)$ by using following relations (Sharma, 1984; Demirezen et al., 2016; Alialy et al., 2014):.

$$n(V_i) = \frac{q}{kT}\left[\frac{V_i}{\ln(\frac{I_i}{I_0})}\right] = 1 + \frac{\delta}{\varepsilon_i}\left[\frac{\varepsilon_s}{W_D} + qN_{ss}(V_i)\right] \quad (4.3a)$$

$$\Phi_e = \Phi_{B0} + \beta(V) = \Phi_{B0} + \left[1 - \frac{1}{n((V_i)}\right] V_i \quad (4.3b)$$

where Where, δ_i represents the thickness of interlayer, W_D represents the depletion layer width, N_{ss} represents the surface states/traps density, ε_i and ε_s represent the permittivity of modified PVA interfacial layer doped by Zn nanoparticles and semiconductor, respectively. β is the voltage coefficient of the effective BH used in the Φ_{B0} (β=dΦ_e/dV=1-1/n(V)). In calculations, the value of δ is taken as 20Å for native SiO_2 and 500 Å for (Zn-doped PVA) layer respectively. W_D is the width of the space charge region (≈3.87×10^{-5} cm which can be obtained from the linear part of reverse bias C^{-2} *vs* V plot at 1 MHz). The value of ε_s was taken as13.1ε_o for 4H SiC, the values of ε_i was taken as 3.8ε_o for SiO_2 and 8.47ε_o for Zn-doped PVA. The voltage dependent $n(V_i)$ values for both structures at room temperature are obtained by using Equation (4.3) and shown in Fig.4.2. The experimental results value of n at intermediate bias voltage (for the linear region of ln$I$ vs V plots) is almost constant, but it increases with increasing voltage almost linearly at enough high forward bias voltages for two diodes. In addition, the expression for the N_{ss} from Equation (4.3a) that is entirely governed by the semiconductor suggested by Card and Rhoderick can be calculated as follows (Demirezen et al., 2016).

$$N_{ss}(V) = \frac{1}{q}\left[\frac{\varepsilon_i}{\delta}\,(n(V) - 1) - \frac{\varepsilon_s}{W_D}\right] \tag{4.4a}$$

The energy level of N_{ss} with respect to the bottom of the conduction band for n-type semiconductor is given by (Card et al., 1971; Altındal et al., 2009)

$$E_c - E_{ss} = q(\Phi_e - V) \tag{4.4b}$$

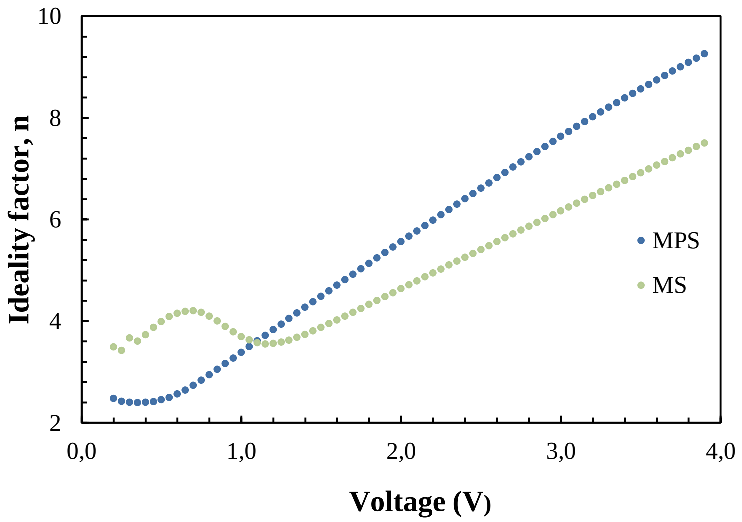

Figure 4.2. n vs V for both MS and MPS structures at room temperature.

From Eqution (4.3 b) it's clear that the value of Φ_e increases by increasing applied forward bias voltage because of the increase in quasi-Fermi energy level of majority carriers on the semiconductor side. Thus, the value of N_{ss} was calculated by using Equation 4.4(a, b) and was given in Fig. 4.3 for both structures. As can be seen clear in Fig. 4.3, the values of N_{ss} increase from the mid-gap of 4H SiC towards the bottom of conduction band (E_c). Thus the values of N_{ss} for the MPS are much lower like n and leakage current compared to the MS because of the saturation of dangling bonds or the passivity role of (Zn doped-PVA) interfacial layer. These results show that a grown of a modified PVA interfacial layer doped by Zn nanoparticles between metal and semiconductor instead of conventional SiO_2 can increase the quality and performance of the MS and MIS type structures.

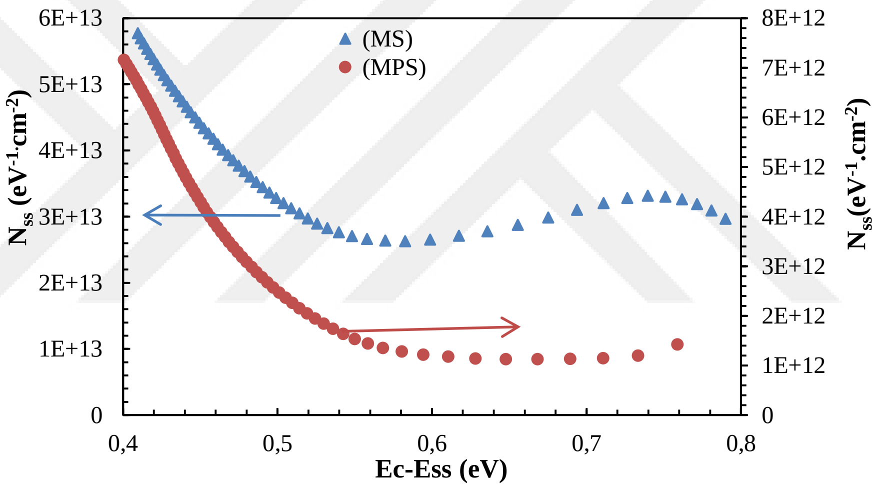

Figure 4.3. The energy dependent density distribution profiles of N_{ss} vs (E_c-E_{ss}) plots for the MS and MPS structures at room temperature.

Usually, the forward bias I-V plot for MS, MIS and MPS structures is linear on semi-logarithmic scale at intermediate forward bias voltage ($V \geq 3kT/q$), but there it becomes deviation from linear state especially because of the existence of R_s and polymeric interfacial layer. Furthermore, the experimental values of N_{ss} and resistance of the interlayer will be added to the resistance of epitaxial and so leads to deviation from linearity at enough high forward biases (Sochacki et al., 2005). There are several methods to determine the value of R_s in the literature (Rhoderick, 1978; Norde, 1979; Sze, 1981; Nicollian et al., 1982; Sharma, 1984; Cheung et al., 1986). In this study, R_s has been calculated by applying the Cheung's method (Cheung et al., 1986). Applying this method and by using Equation (2.9), the forward bias *I-V* relation with R_s value can be expressed as:

$$\frac{dV}{d(lnI)} = n\frac{kT}{q} + IR_s \qquad (4.5)$$

and

$$H(I) = V - n\frac{kT}{q}\ln\left(\frac{I}{AA^{*}T^{2}}\right) = n\phi_B + IR_s \qquad (4.6)$$

Both the d*V*/d(ln*I*) vs I and H(*I*) vs *I* plots were drawn by using Equations (4.5) and (4.6) for the MS and MPS structures ant they were given in figures 4.4 and 4.5, respectively. As shown in Figs. 4.4 and 4.5, these two plots have a good linear range for two structures. Thus, a plot of dv/dln I vs I will give the values of R_s as the slope and *n* values will be obtained from Equation (4.5) determining the y-axis intercept (=*nkT/q*), of these plots respectively. Similarly, the slope of H (*I*) vs *I* plot (Fig.7) will provide a second way for determination of R_s, which produce a check the uniformity of this approach. From Equation (4.6), the values of R_s and Φ_B were calculated and obtained from the slope and the intercept of y-axis (=$n\Phi_B$) of these plots for two structures, respectively. The values of *n* which are calculated from Cheung function acorrding to Equation (4.5) are considerably higher than those extracted from Equation (4.1). Fig.2, shows an expected situation due to the increase of *n* with applied bias voltage. The voltage dependence of structure resistance (R_i) is also obtained by applying Ohm's law ($R_i=dV_i/dI_i$) and represented inset in Fig.4.1 for MS and MPS type structure. As shown in this figure, the real values of R_s and R_{sh} for both two structures agree to enough high forward bias voltage (6V) and enough low or zero bias voltages, respectively. As seen in Table 4.1, the experimental result of R_{sh} value for MPS structure is 39.99 times higher as compare with R_{sh} value for MS structure. The experimental values of R_s that obtained from Cheung's functions and Ohm's law for two structures were represented in Table 4.1. The discrepancy between R_s from these methods is the result of voltage dependence of it like ideality factor and BH.

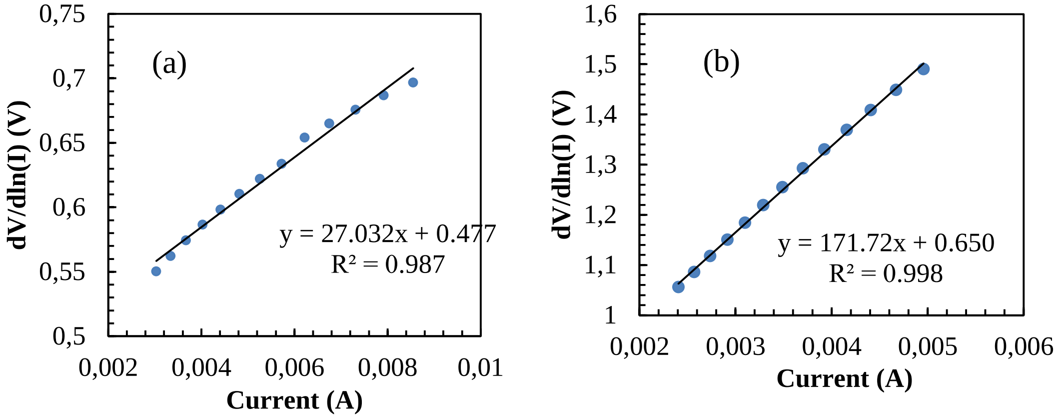

Figure 4.4. (a) dV/dln(I) vs I for MS structure. (b) dV/dln(I) vs I for MPS structure .

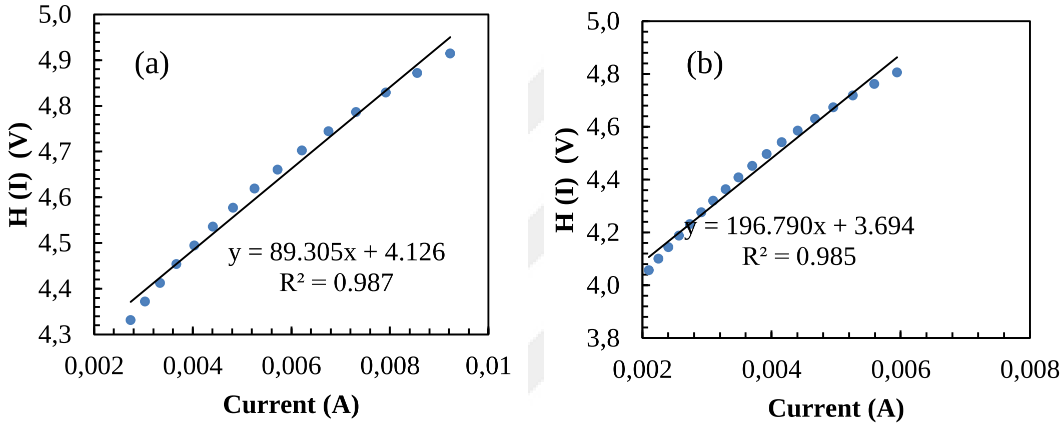

Figure 4.5. (a) H(I) *vs* I for MS structure. (b) H(I) *vs I* for MPS structure.

4.1.2. The Forward and Reverse Bias C-V and G/ω-V Characteristics

The capacitance and conductance measurements *(C-V* and *G/ω-V*) respectively were applied at both low (1 kHz) and high (1 MHz) frequencies by using HP 4192A LF Impedance Analyzer. According to Nicollian and Brews (Nicollian et al., 1982), at enough low frequencies, almost of all surface states can follow the external alternating ac signal easily and so yield an excess $C_{ex.}$ and $G_{ex.}/\omega$ to the real values of them, but at high frequencies it is impossible for these states/traps to follow the ac signal. For this purpose, the *C-V* and *G/ω-V* plots of the MS and MPS structures were drawn at low frequency 1 kHz and high frequency 1 MHz. Fig. 4.6 (a) and (b) shows the *C-V* characteristics for MS and MPS structures at 1 kHz and 1 MHz, respectively, and these plots have three regions (inversion, depletion and accumulation) both low and high frequency. *C-V* characteristic has shown clearly that the anomalous peak at the accumulation region due to the effect of R_s and native

SiO_2 and (Zn-doped PVA) interfacial layer rather than N_{ss}. It is clear that the magnitude of anomalous peak inversely related to frequency due to the effect of N_{ss}. This kind of peak behavior can be attributed to the particular density distribution of N_{ss} and remodeling and restructure of them under applying electric field (Arslan et al., 2011; Uslu et al., 2011; Demirezen et al., 2016). As seen in Fig. 4.6 (a) and (b), the value of capacitance of both structures are extremely sensitive to the N_{ss}, interfacial layer and R_s ,but N_{ss} shows an effective behavior especially at inversion and depletion regions, whereas R_s shows an effective behavior only at accumulation region.

As seen in Fig. 4.5 (b), at 1 MHz, C value increases with increasing voltage until accumulation region after that it suddenly decrease until goes to negative due to the effect of R_s, but at 1 kHz, this negative capacitance (NC) behavior becomes disappear. Because, the effect of R_s on C-V and G/ω-V plots can be neglected at low frequencies, but it becomes very effective at high frequencies contrary to N_{ss}. The general consensus on NC in the accumulation region is due to the existence of N_{ss} and their relaxation time (τ), R_s, the contact injection and minority carrier injection (Ershov et al., 1998; Werner et al., 1988). In addition, according to Butcher (Butcher et al., 1996) and Huang et al. (Huang et al., 1997), NC behavior can be attributed to technical problems of devices, such as parasitic inductance or accuracy of calibration, respectively.

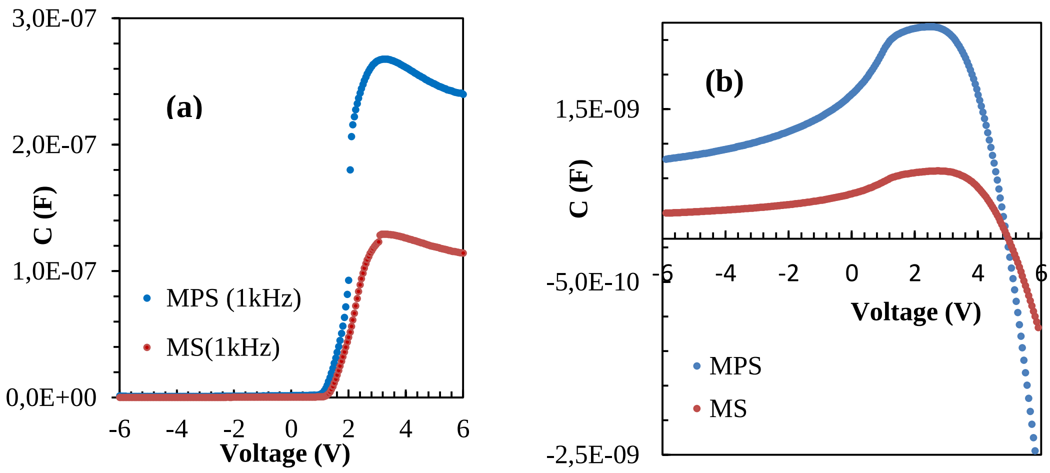

Figure 4.6. (a) C-V characteristics of MS and MPS at 1kHz (b) C-V characteristics of MS and MPS at 1MHz.

In general, the NC has been referred to as "abnormal" or "anomalous" behavior in the literature (Arslan et al., 2011). The C value is a differential effect of charge Q with respect to junction voltage V_j, i.e. C=dQ/dV_j Zhu et al. (Zhu et al., 2009). Furthermore, by increasing forward bias voltage the C value reaches to a maximum value and after certain voltage it starts rapidly to decrease until the negative value reaches (Ershov et al., 1998; Zhu et al., 2009; Bilkan et al., 2015). *C-V* and *G/ω-V* plots for MS and MPS structures at 1 MHz were drawn to see the inductive behavior in these structures in Fig. 4.7(a) and (b), respectively, which explain how the *G/ω* value increases for two structures with increasing frequency both at depletion and accumulation region, but at accumulation region contrary to *G/ω*, the value of C reaches a peak value and then goes to negative value at strong accumulation region. In addition, the lowest value of C represent the highest value of *G/ω*. NC exhibits a decrease in electronic charges on electrodes with an increasing bias voltage and such behavior of C and *G/ω* is known as "inductive behavior" in the literature (Werner et al., 1988; Butcher et al., 1996; Huang et al., 1997; Ershov et al., 1998; Zhu et al., 2009; Uslu et al., 2011; Arslan et al., 2011; Bilkanet al., 2015).

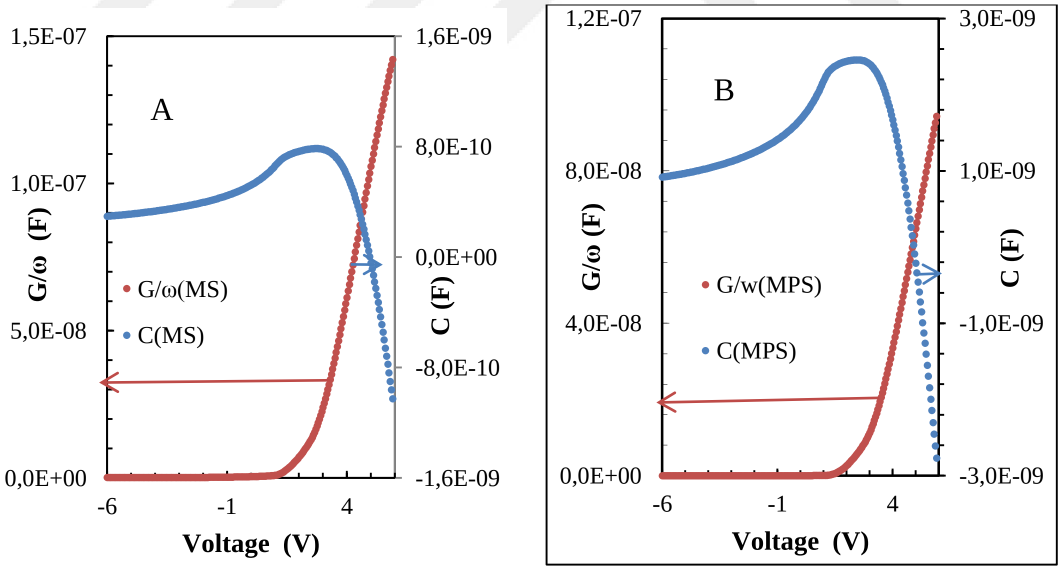

Figure 4.7. (A) *C-V* and *G/ω-V* plots of MS at 1MHz. (B) *C-V* and *G/ω* characteristics of MPS at 1MHz.

The variation in C at the reverse bias or inversion region, the C^{-2}-V plot of the MS and MPS structures for 1 MHz are given in Fig. 4.8. As shown in Fig. 4.8, the C^{-2}-V plots for two different type structures have a perfect linear region in the wide range of reverse bias voltage. At elevated frequencies ($f \geq$ 1MHz), the depletion layer capacitance of MS and MPS type structures can be expressed as follows (Rhoderick, 1978; Sze, 1981; Sharma, 1984).

$$C = \frac{|dQ_{sc}|}{|dV|} = \sqrt{\frac{q\varepsilon_r \varepsilon_0 A^2 N_D}{2(V_{bi}+V)}} \quad \text{and} \quad \frac{1}{C^2} = \frac{2(V_R+V_{bi})}{q\varepsilon_r\varepsilon_0 N_d A^2} \tag{4.7}$$

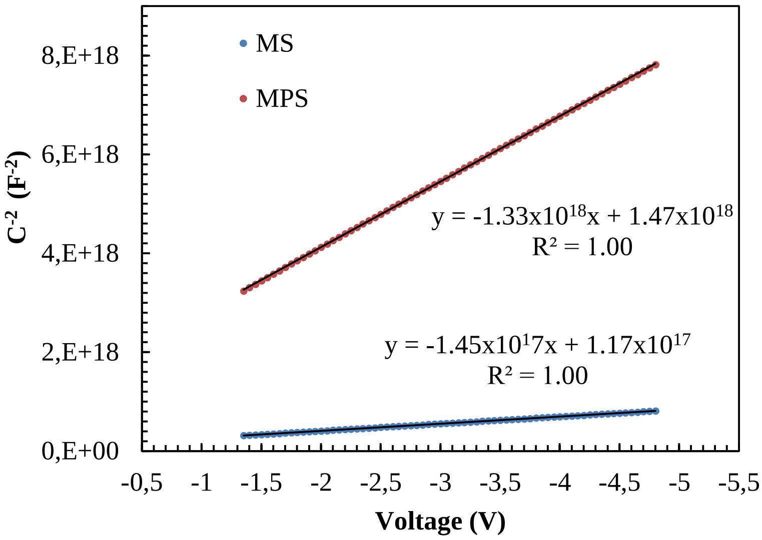

Figure 4.8. C^{-2} -*V* plots for MS and MPS structures for 1MHz at room temperature.

In Eq. 4.7, A, V_R, V_{bi}, N_d , ε_r , ε_o represent the rectification contact area, the reverse-bias voltage, the built-in voltage at zero bias, the donor concentration in 4H SiC, the relative permittivity of semiconductor and the permittivity of free space or vacuum repectively. The values of V_o, N_d, E_F, Φ_b *(C-V)* and depletion layer width *(*W_D) are calculated from the intercepts and slopes of the C^{-2}-*V* plot for each structure using following relations (Card et al., 1971; Rhoderick, 1978; Sze, 1981; Sharma, 1984):

$$V_{bi} = V_0 + \frac{kT}{q} \tag{4.8}$$

$$W_D = \left[\frac{2\varepsilon_r\varepsilon_0(V_R+V_{bi})}{qN_d}\right]^{\frac{1}{2}} \tag{4.9}$$

The value of E_F can be calculated from the conduction band edge for *n*-type semiconductor in the neutral region of n-4H SiC by using following relation as (Rhoderick, 1978; Sze, 1981):

$$E_F = \frac{kT}{q} \ln(\frac{N_c}{N_d}) \tag{4.10}$$

Where, N_c is the effective density of states in n-4H SiC conduction band. The experimental values V_o, N_d, E_F, Φ_B and W_D were obtained and arranged as in Table 2.

Table 4.2. The expermental values of some parameters at the linear parts of the reverse bias C^{-2} vs V plots for MS and MPS structure at room temperature

Sample	V_0 (V)	N_d (cm^{-3})	E_F (eV)	Φ_B (eV)	W_D (cm)
MS	0.807	8.373 x10^{16}	0.123	0.955	1.249x10^{-5}
MPS	1.105	9.128 x10^{15}	0.179	1.309	3.781x10^{-5}

As can be seen in Table 4.1 and 4.2, the $\Phi_{B0}(C\text{-}V)$ value which calculated from the reverse bias *C-V* characteristics is higher than Φ_{B0} *(I-V)* which obtained from the forward bias *I-V* characteristics due to the nature of measurement methods. In other words, the values of BH obtained from two techniques are not always the same in bias voltage. It is well known that the apparent BH from metal side to semiconductor side is higher than from that semiconductor to metal sides at about E_F. This discrepancy between $\Phi_{B0}(C\text{-}V)$ and Φ_{B0} *(I-V)* is also the result of the in-homogeneities of BH and polymeric interfacial layer at M/S interface.

$$R_s = \frac{G_{mi}}{G_{mi}^2 + (\omega C_{mi})^2} \tag{4.11}$$

The voltage dependent R_s profile as was also calculated by using Equation (4.11) for the *C-V* and *G/ω* measurements by applying Nicollian and Brews method at 1MHz to explain how R_s effects both *C-V* and *G/ω-V* characteristics for MS and MPS structure and were given in Fig. 11 (Nicollian et al., 1982).

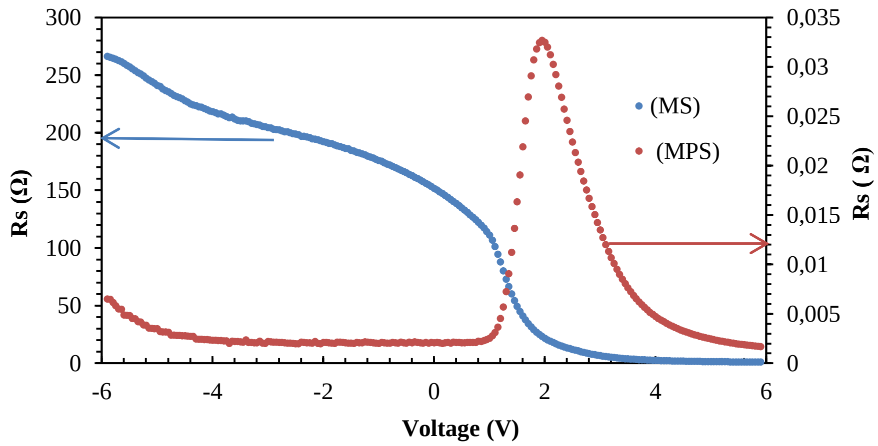

Figure 4.9. R_s *vs* V plots of the MS and MPS structures for 1 MHz at room temperature.

As shown in Fig. 4.9, the value of R_s at accumulation region is almost independent of applied bias voltage and so it is representing to the real value of R_s for two type structures. Thus, the real value of R_s for MS and MPS structure was found as 1.09 Ω and 1.63 Ω at 6 V, respectively. The value of R_s for MPS structure is also lower than the MS structure and these values of R_s are more suitable for an electronic device. The peak behavior in R_s vs V plot for MPS structure can be caused by particular distribution of N_{ss} at (Zn doped-PVA)/n-4H SiC interface. Because, at peak position, the charge carriers may be trapped due to higher value of N_{ss} and at certain high forward biases voltage, the value of R_s will decrease due to decreasing of charge carriers at traps or states. Finally, in order to see the charges at surface states or traps on the *C-V and G/ω-V* plots, the profiles of N_{ss} *vs* V was also calculated from the high-low frequency (1MHz-1 kHz) capacitance (C_{HF}-C_{LF}) technique using following relation for both structures and they were given in Fig.4.10.

$$qAN_{ss}=(1/C_{LF}-1/C_i)^{-1}-(1/C_{HF}-1/C_i)^{-1} \qquad (4.12)$$

In Equation 4.12, C_i is the interfacial layer capacitance and was obtained by using the C_{ma} and G_{ma}/ω values at strong accumulation region at 1 MH by using following relation (Nicollian. et al., 1982).

$$C_i= C_{ma}\,[1+((G_{ma}/\omega)/C_{ma})^2] \qquad (4.13)$$

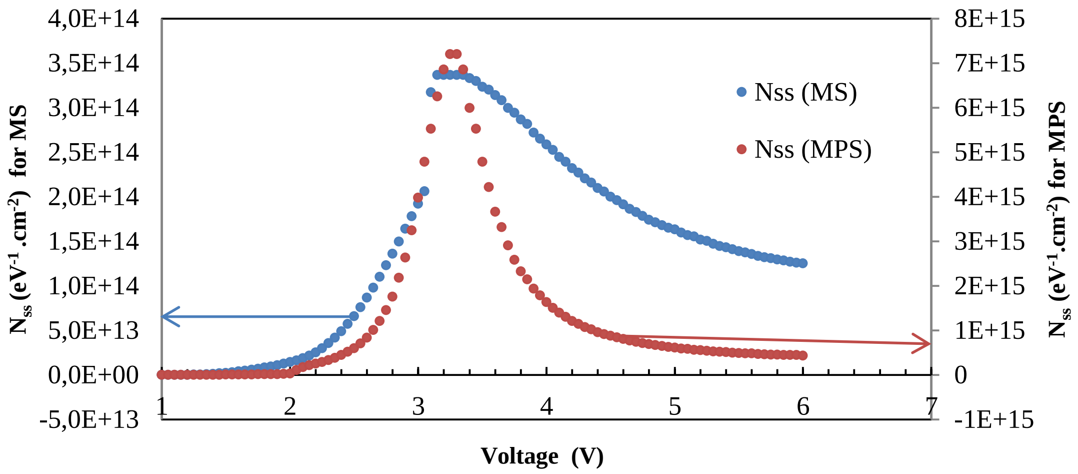

Figure 4.10. Profiles of N_{ss} *vs* V for the MS and MPS structures obtained by the high-low frequency capacitance method at room temperature.

As seen in Fig .4.10, the density of N_{ss} for MS and MPS type structures shows a peak value due to a special density distribution of N_{ss} and their remodeling and restructure under electric field. As a result, the values of N_{ss} was calculated from high-low-frequency capacitance method for MPS structure are also lower than those of MS structure at accumulation region, but the distribution of N_{ss} varies from region to region due to their special distribution between interfacial layer and semiconductor. Fruthermore, Fig. 4.10 shows a peak value of N_{ss} at about 3V for both MS and MPS structures with higher value for MPS 10 times than that of MS structure and then at higher voltage (V≥ 3V) the value of N_{ss} exponentially decreases from conduction band to mid-gap with increasing applied biasing voltage in different ratio for both structures. These results indicated the electrical parameters of these structures to be quite dependent on voltage as well as interfacial polymeric layer. When the main electrical parameters of MS and MPS structure are compared; the values of ideality factor, leakage current, R_s, Φ_{Bo} and N_{ss} for MPS structure are considerably lower than those of MS structure. However, the values of R_{sh} and *RR* for MPS structure are considerably higher than those of MS structure due to the passivity role of Zn-PVA interfacial polymer layer. As a result, we can say that the (Zn doped-PVA) polymer material can be applied as an interfacial layer instead classical SiO_2 insulation layer to get better quality or performance of MS structure.

4.2. *I-V* Characteristics of Metal-Polymer-Semiconductor (MPS) Structure at Wide Temperature Domain (100-320K)

Fig.4.11 shows the semi-logarithmic forward and reverse bias *I-V* characteristics of the fabricated Au/(Zn-doped PVA)/n-4H-SiC (MPS) structure for various temperature. As can be seen in Fig. 4.11, the semi-logarithmic *I-V* at forward bias region has two distinct linear regions with different slopes depending on the bias voltages for each temperature. These two linear regions are corresponding to the low bias voltages (LBR), $0.05V \leq 0.4$V and moderate bias voltages (MBR), $0.4 \leq V \leq 0.8V$, respectively. These two linear regions for MPS structure are known two parallel diodes model with different BH. For high forward-bias voltages (HBR), ln*I* vs *V* plot MPS structure shows a deviation from linearity because of the existence of R_i. The non-saturating behavior of the current at reverse bias region can be commonly explained in terms of the image force lowering of BH and the existence of interfacial layer between metal and semiconductor (M/S). This soft non-saturating reverse characteristic can be also based on the barrier inhomonogeneity at M/S interface.

For MS structure with and without an interfacial insulator or polymer layer (MIS or MPS) and at effective series resistance region,the relation between forward bias current-voltage according to thermionic emission (*TE*) theory ($V>3kT/q$) can be expressed as follow (Padovani et al., 1966; Crowell et al., 1969; Sze, 1981; Tung, 1992):

$$I = AA^{*}T^{2}\exp(-\frac{q}{kT}\Phi_{Bo})\left[\exp\left(\frac{q(V-IR_{s})}{nkT}\right)-1\right] \tag{4.14}$$

The expressions in front of the brackets in Equation (4.14) corresponds to reverse-bias saturation current (I_o) and it is obtained from the interception of the linear region in ln*I*-*V* plot at V=0, Φ_{Bo} is the zero-bias barrier height, V is the applied voltage drop across the diode, A^* is the effective Richardson constant (146 $cm^{-2}K^{-2}$ for n-type 4H-SiC), the term of IR_s is the voltage drop across the R_s and others are well known quantities in the literature. Thus, the value of Φ_{Bo} can be obtained from Equation (4.3) by substituting the values of I_o and rectifier contact area (A) of the diode for each temperature.

The value of n of the MS and MIS type diodes is a decisive parameter that affects the device efficiency by controlling on the charge transportation through interfaces and it can also be calculated from the slope of the linear region in lnI-V plot using Equation (4.1) (Rhoderick, 1978; Sze, 1981).

The experimental values of I_o, n and Φ_{Bo} for both at the LBR and MBR for the fabricated Au/(Zn-PVA)/n-4H-SiC (MPS) structures in the temperature range of (100-320 K) are tabulated in Table 4.3. All these main diode parameters are found a strong function of temperature and they change from 7.70×10^{-9}A, 10.99, 0.24 eV (at 100 K) to 1.68×10^{-8}A, 3.08 and 0.830 eV (at 320 K) for LBR and 2.25×10^{-9}A, 13.31, 0.252 eV (at 100 K) to 9.89×10^{-8}A, 4.15 and 0.767 eV (at 320 K) for MBR, respectively. Such change in Φ_{Bo} with temperature both for LBR and MBR is in-agreement with negative temperature of forbidden band-gap or BH for ideal Schottky diodes. In addition, the high values of n especially at low temperature can be partly explained by the existence of interfacial (Zn-doped PVA) layer, a special density distribution of surface states (N_{ss}) between (Zn-doped PVA) and n-type 4H-4H-SiC and the dominated conduction by interface recombination, but main reason is the in-homogeneities of BH at M/S interface (Song, 1986; Werner et al., 1991; Schmitsdrof et al., 1997; Mönch, 1999; Reddy et al., 2014; Reddy et al., 2015; Marı, 2015; Güçlü et al., 2016; Moraki et al., 2016). The temperature dependence of n and Φ_{Bo} of the Au/(Zn-PVA)/n-4H-SiC (MPS) structure for LBR and MBR are given in Fig.4.12 (a) and (b), respectively. As can be seen in Fig. 4.12, while the value of Φ_{Bo} increases, n decreases with increasing temperature. This decrease in Φ_{Bo} and increase in the n with decreasing temperatures is an evident for the deviation from the TE theory.

In addition, according to TE theory, the value of n should be close to unity and furthermore the value of BH should increase with decreasing temperature due to the negative temperature coefficient of the BH or the forbidden band gap (E_g) of the semiconductor. These lower values of Φ_{Bo} at low temperatures can be attributed to the electrons which are able to surmount the lower barriers or patches and therefore current conduction will be dominated by current flowing through these patches or lower BHs and leads to high values of n (Reddy et al., 2014; Marıl et al., 2015; Güçlü et al., 2016; Moraki et al., 2016). However, when temperature increases, more and too much charge carriers (electron or holes) have enough thermal energy to surmount the high barriers. Therefore, it can be said that the obtained values of Φ_{Bo} are not mean BHs, they are apparent BHs ($\Phi_{ap.}$) for each temperature. In other words, at low temperatures the possible CTMs is more complicate and considerably different from high temperatures. Because, at low temperatures, the BH is lowered due to the patches or pinch-off around the mean value of BH between metal and semiconductor (Moraki et al., 2012; Alialy et al., 2015; Güçlü et al., 2016).

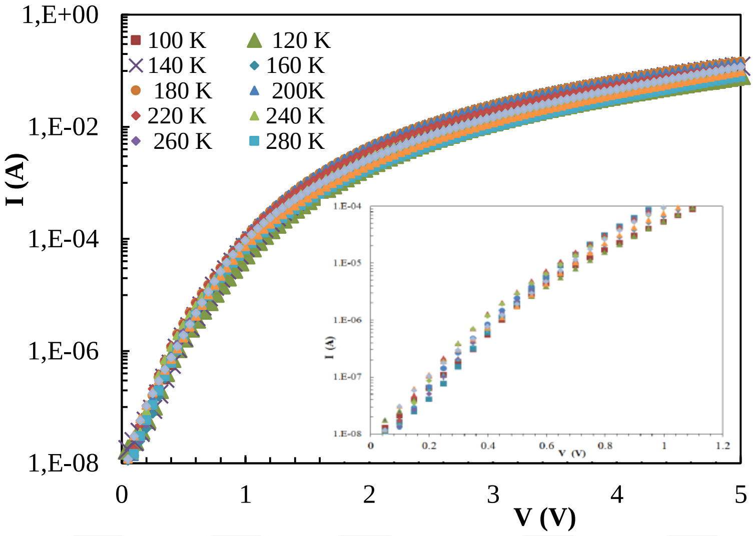

Figure 4.11. The semi-logarithmic *I-V* characteristics of the Au/(Zn-PVA) /n-4H-SiC (MPS) structure at various temperatures.

Table 4.3. The experimental values of I_o, n and Φ_{Bo} obtained from the forward bias *I-V* data for the LBR and MBR for the Au/(Zn-PVA)/n-4H-SiC (MPS) structures at various temperature.

LBR (Low Bias Region)				***MBR (Moderate Bias Region)***			
T (K)	**I_0 (A)**	**n**	**Φ_{B0} (eV)**	**T (K)**	**I_0 (A)**	**n**	**Φ_{B0} (eV)**
100	$7.70x10^{-9}$	10.99	0.24	100	$2.25x10^{-9}$	13.31	0.252
120	$7.00x10^{-9}$	8.55	0.29	120	$3.75x10^{-9}$	11.25	0.301
140	$1.00x10^{-9}$	7.40	0.34	140	$8.30x10^{-9}$	9.74	0.346
160	$1.80x10^{-9}$	6.039	0.40	160	$9.20x10^{-9}$	8.45	0.397
180	$2.30x10^{-9}$	4.529	0.47	180	$1.52x10^{-8}$	7.45	0.443
200	$3.0x10^{-9}$	3.99	0.52	200	$2.09x10^{-8}$	6.73	0.490
220	$3.05x10^{-9}$	3.63	0.57	220	$3.42x10^{-8}$	6.18	0.533
240	$3.10x10^{-9}$	3.42	0.63	240	$3.50x10^{-8}$	5.70	0.585
260	$3.50x10^{-9}$	3.29	0.69	260	$4.39x10^{-8}$	5.09	0.632
280	$5.00x10^{-9}$	3.27	0.74	280	$5.85x10^{-8}$	4.63	0.678
300	$7.21x10^{-9}$	3.24	0.77	300	$7.06x10^{-8}$	4.34	0.725
320	$1.68x10^{-8}$	3.08	0.83	320	$9.89x10^{-8}$	4.15	0.767

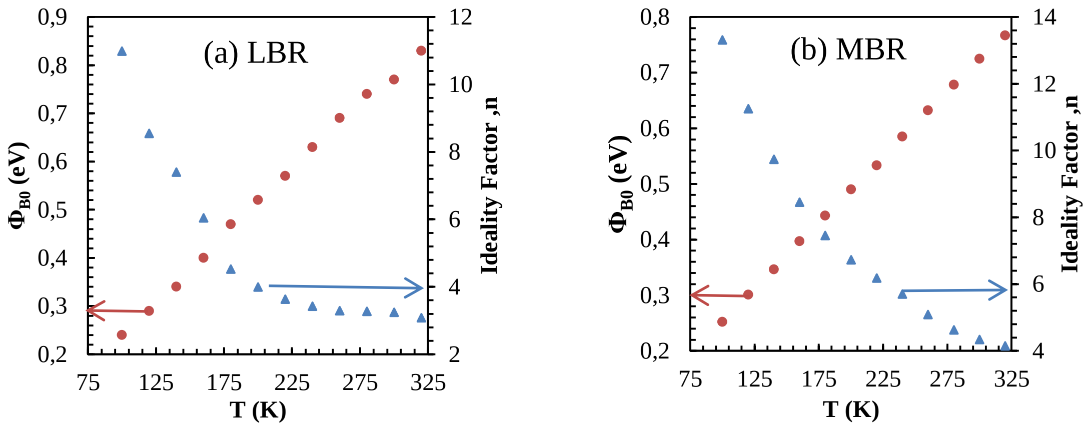

Figure 4.12. The temperature dependence of n and Φ_{Bo} of the Au/(Zn-PVA)/n-4H-SiC (MPS) structure for (a) LBR and (b) MBR region.

The others main important characteristics of the Au/(Zn-PVA)/n-4H-SiC (MPS) structure are series and shunt resistances (R_i and R_{sh}) which considerably influence the forward and reverse bias *I-V* characteristics. In ideal case, R_i =0 while the value of R_{sh} is about $10^{12}\Omega$. Therefore, in this study, the values of R_i and R_{sh} were calculated from Ohm's Law ($R_i=dV_i/dI_i$) for selected five different temperatures. The voltage dependent resistivity (R_i) of the structure for each temperature is shown in Fig.5. As shown in Fig. 5, at zero bias voltage, the value of R_i becomes almost constant for all taken temperatures that corresponds to the real value of R_{sh}. Similarly, at enough elevated forward bias voltage it also becomes almost constant for all taken temperatures, which is corresponding to the real value of R_s. Furthermore, R_s is effective at enough high forward bias regions, while R_{sh} is effective in the reverse bias region or near zero bias. Thus, the real values of R_s and R_{sh} for MPS structure were obtained as 27.40 Ω, 0.21 kΩ at 100 K and 20.78 Ω, 0.202 kΩ at 320 K, respectively. The low value of R_s can be accomplished by rather having low SBH at metal-semiconductor contact or by increase tunneling through the BH by using dense doped semiconductor ($\geq 10^{17}$ doping atoms per cm^{-3}) (Nicollian et al., 1982; Alialy et al., 2015,). Usually, the existence of R_s can arise from different sources which are the contacts at the back of semiconductor, the contact of the wire to the gate, the resistivity of the quasi-neutral bulk of semiconductor, impurities and random doping distribution in the semiconductor (Nicollian et al., 1982; Alialy et al., 2015). On the other hand, the existence of R_{sh} can originate from leakage current, leaky oxide channel along the interfacial layer between rectifier and ohmic back contacts, or by the shunt resistance that calculated from the shunt resistance within measuring instrumentation itself.

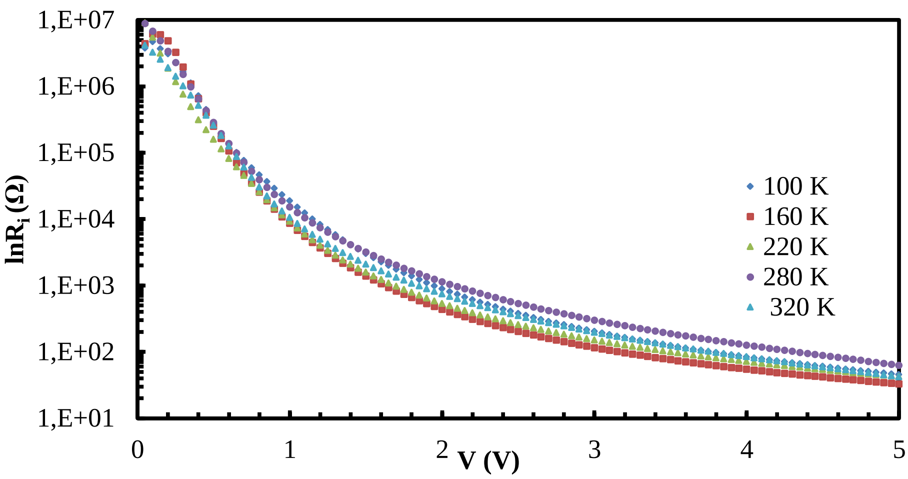

Figure 4.13. The R_i *vs* V plot for the Au/(Zn doped PVA)/n-4H-SiC (MPS) structure in the temperature range of (100-320 K) by 60 K steps.

The decrease in n and increase in Φ_{Bo} with increases of temperatures may clear that the reason of adeviation from the TE theory may be due to the exisistance of the thermionic field emission (TFE) and field emission (FE) mechanisms (Crowell et al., 1969; Nicollian et al., 1982; Tung, 1992; Alialy et al., 2014). It is well known that the requirements of FE and TFE mechanisms is the change in the tunneling current parameter E_o (=nkT/q) as a function of temperature which explaind by using Equations(2.10),(2.11) and(2.12) (Padovani et al., 1966; Crowell et al., 1969; Sullivan et al., 1991; Alialy et al., 2014).

By using Equation (2.12), the theoretical value of E_{oo} was calculated as 16.66 meV for room temperature. On the other hand, TFE should be accurate when $E_{oo} \approx$ kT/q; the TE if E_{oo} << kT/q and The FE if E_{oo} >>kT/q .Thus, if the FE dominates, then the E_o must be a straight line and so it is independent of temperatures (Padovani et al., 1966; Tung, 1992). In this case, E_o is equal to E_{oo}. Fig. 6 (a, b) shows E_{oo} (=nkT/q) vs kT/q plot of the Au/(Zn doped PVA)/n-4H-SiC (MPS) structure in the temperature domain of 100-320 K at LBR and MBR, respectively. From these figures the values of E_o were obtained 89.5 meV at LBR and 118.6 meV at MBR. These two values are higher than the theoretical values of E_{oo} (16.66 meV). These experimental values E_{oo} show that both the TFE and FE theories are possible CTMs especially at low temperatures.

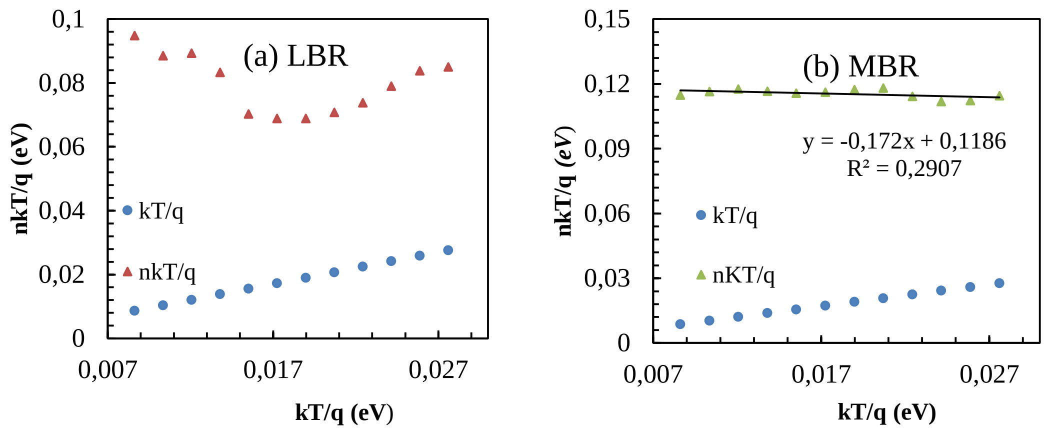

Figure 4.14. (a) Experimental and (b) theoretical nkT/q vs tunneling current parameter kT/q for Au/(Zn-doped PVA)/n-4H-SiC structure for (a) LBR and (b). MBR, respectively.

It is difficult to clarify such behavior of higher values of n especially due to low temperatures and positive temperature coefficient in BH by only TFE and FE theories. Therefore, we tried to clarify this non-ideal behavior of the forward-bias *I-V* characteristics in Au/(Zn-doped PVA/n-4H-SiC structure according to the basis of a TE mechanism with a Gaussian distribution (GD) of the BHs (Rhoderick ,1978; Song et al., 1986; Werner et al., 1991; Schmitsdrof et al., 1997; Mönch, 1999; Tung, 2001; Reddy et al.,2014). Usually, there are three basic reasons for the GD of BH which is Φ_{Bo} vs n, Φ_{bo} vs q/2kT and $(n^{-1}$-1) vs q/2kT plots. For this purpose, these figures were drawn to obtain an evident GD of the BHs and they represented in Figs. 4.15(a, b), 4.16(a, b) and 4.17(a, b) for both LBR and MBR, respectively.

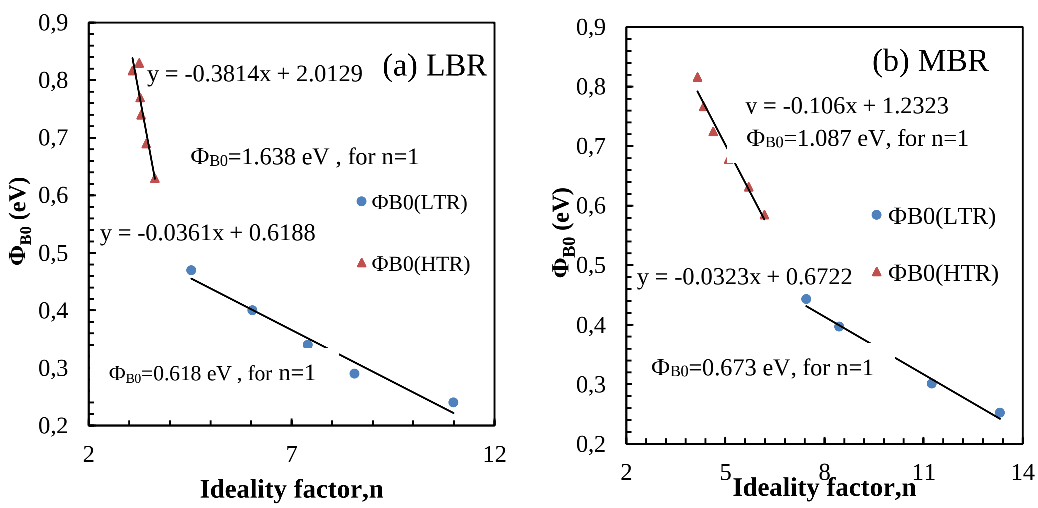

Figure 4.15. Plot of the Φ_{B0} vs n for Au/(Zn-doped PVA)/n-4H-SiC (MPS) structure for (a) LBR and (b) MBR, respectively.

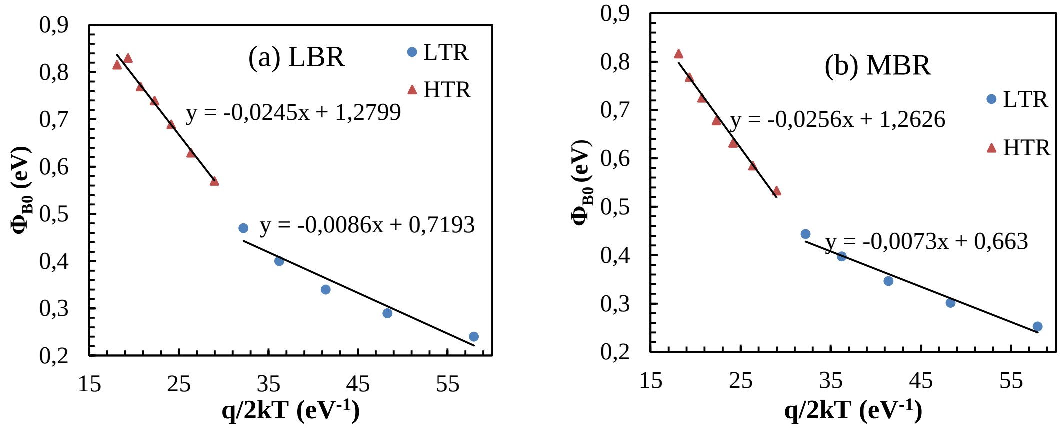

Figure 4.16. Plot of the Φ_{B0} vs $q/2kT$ for Au/(Zn-doped PVA)/n-4H-SiC (MPS) structure for (a) LBR and (b) MBR, respectively.

Mönch and coworkers (Schmitsdrof et al., 1997; Mönch, 1999) applied Tung's theoretical approach and they found a correlation between Φ_{Bo} and n which confirmed the existence of lateral inhomogeneities of the BHs at M/S interface. Furthermore, they found that the Φ_{Bo} vs n plot to n=1 has should be given a homogeneous BH. As can clearly be seen in Fig. 4.15 (a,b), Φ_{Bo} vs n plots for both LBR and HBR have two distinguished linear region with two slopes between (100-200 K) and (220-320 K) which are called low- and high- temperature domain (LTR and HTR), respectively. Such behavior of Φ_{Bo} vs n plots n can be clarified by the lateral inhomogeneities of the BHs. The extrapolation of the results of Φ_{B0} vs n plot Fig. 4.15(a) in LBR, for n=1 have given the values of 0.615 eV (at LTR) and 1.638 eV (at HTR), respectively. In the same way, these values for MBR were calculated as 0.673 eV and 1.087 eV, respectively. The experimental results offer the decrease in Φ_{Bo} and increase in n are perhaps caused by the BH inhomogeneities at M/S interface. According to the model recommended by Werner and Güttler (Werner et al., 1991), the total current for any forward bias V can be calculated by using Equations (2.17),(2.19)

Thus, the GD of the BH with a mean BH ($\bar{\Phi}_{Bo}$) and standard deviation (σ_o) can be calculated by using Equation (2.21).The other observed variation in the n as a function of temperature in the model can be obtained from Equation (2.22).

The values $\overline{\Phi}_{Bo}$ and σ_o can be calculated from the interception point of the Φ_{B0} axis and slope of vs $q/2kT$ plot respectively .As seen in Fig. 4.16 (a, b), the Φ_{ap} vs $q/2kT$ plot for both LBR and MBR has also obvious two linear regions at LTR and HTR. Thus the intercept and slope of these linear regimes for LBR have been two sets of values of Φ_{Bo} and σ_o as 0.0719 eV and 0.0086 V in the LTR, and as 1.27 eV and 0.024 V in the HTR, respectively. These values for MBR were calculated as 0.663 eV and 0.0073 V in the LTR, and as 1.262 eV and 0.025 V in the HTR, respectively. By using Equations (2.21) and (2.22), it is prospective that the adjusted value of $\overline{\Phi}_{Bo}$ and σ_o depend on applied bias voltage linearly by the equations $\Phi_B=\overline{\Phi}_{Bo}+\rho_2 V$ and $\sigma=\sigma_o+\rho_3 V$. In general, the value of σ_o is temperature independent value, therefore it can be neglected. In order to calculate the voltage deformation coefficients ρ_2 and larger, $(n_{ap}^{-1}-1)$ vs $q/2kT$ plots for LBR and MBR were drawn and given in the Fig. 4.17 (a) and (b), respectively. As shown in Fig. 4.17 (a, b), the $(n_{ap}^{-1}-1)$ vs $q/2kT$ plot must also have different characteristics in the two temperature ranges due to containing the diode of two BH distributions. The values of ρ_2 and ρ_3 are calculated from the intercepts and slope of the experimental $(n_{ap}^{-1}-1)$ vs $q/2kT$ plots both for LBR and MBR. Thus, for the LBR these values are found as -0.0054 V, -0.6175 V at LTR and as -0.0052 V, -0.5845 V at HTR, respectively. Similarly, for the MBR these values are found as -0.0025 V, -0.7866 V at LTR and as -0.0101 V, -0.5766 V at HTR, respectively.

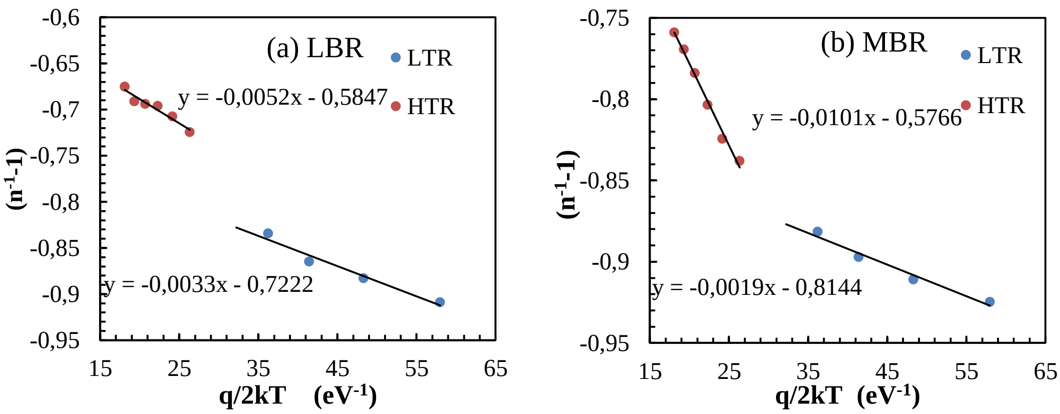

Figure 4.17. Plot of the $(n^{-1}-1)$vs $q/2kT$ for Au/(Zn-doped PVA)/n-4H-SiC (MPS) structure for (a) LBR and (b) MBR, respectively.

According to above discussions/ characterization, both the inhomogeneity and potential variation in the BH dramatically affect the forward-bias *I-V* characteristics especially at low temperatures. Right now, the classical Richardson/Arrhenius plot can be adjusted by uaing Equation (2.23).

The adjusted Richardson plots for LBR and MBR were shown in Fig.4.18 (a, b), respectively. As seen in these figures, these plots have two good linear lines with two slopes in the temperature domian of 100-320 K. These two regions are corresponding to LTR (100-200 K) and HTR (220-320 K), respectively.

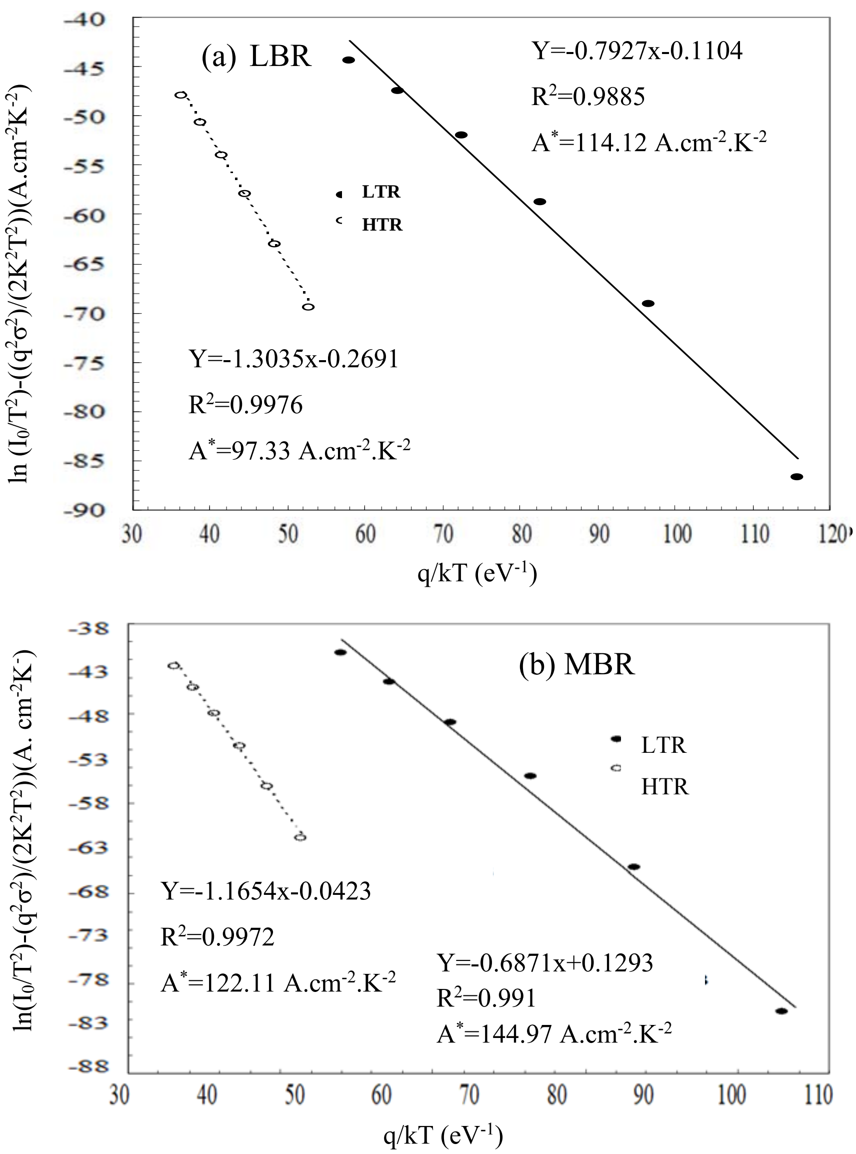

Figure 4.18. The adjusted Richardson plots of the Au/(Zn-doped PVA)/n-4H-SiC (MPS) structure for (a) LBR and (b) MBR, respectively.

The mean value of $\bar{\Phi}_{Bo}$ and effective Richardson constant (A^*) for LBR were obtained from slope and interception of these plots as 0.730 eV, 114.12 A.cm^{-2}K^{-2} at

LTR and 1.304 eV, 97.33 $A.cm^{-2}K^{-2}$ at HTR, respectively. Similarly, for MBR these values were found as 0.687 eV, 144.97 $A.cm^{-2}K^{-2}$ at LTR and 1.165 eV, 122.11 $A.cm^{-2}K^{-2}$ at HTR, respectively. the plots figures from 7 to 10 show a good two distinguished linear regions with two slopes behavior in the both LBR and MBR regions, respectively, which is evidence the presence of double GD of BHs of the Au/(Zn-doped PVA)/n-4H-SiC (MPS) structure. The obtained experimental values of $\bar{\Phi}_{Bo}$ from figures 4.15, 4.16 and 4.18 are consistent with each other for both the LBR and MBR. In addition, at HTR the mean value of BH is higher than when compared with those in LTR. These experimental results affirmed that the temperature dependent of the forward bias I-V characteristics of the manufactured Au/(Zn-doped PVA)/n-4H-SiC (MPS) structure can be successfully clarified on the basis of TE mechanism with a GD of BHs.

4.3. Dielectric Characteristics of Metal-Polymer-Semiconductor (MPS) Structure at wide Temperature Domain

4.3.1. Voltage and temperature dependence of capacitance and conductance at 1 MHz

From *C–V* and *G/ω–V* measurements, the main electric and dielectric properties of MPS structure were obtained at wide voltage and temperature ranges ,to give us all detalled information about these properties (Symth, 1955; Nicollian et al., 1965; Nicollian et al., 1967; Nicollian et al., 1982; Kar et al., 1982; Jonscher et al., 1988; Cheng, 1989; Wu et al., 1990; Penin, 1996; Akkal et al., 2000; Awadhia et al., 2006; Demirezen et al., 2013; Çetinkaya et al., 2015; Hemalatha et al., 2015; Chatterjee et al., 2016). *C-V-T* is shown in Fig. 4.19, while Fig.4.20 shows *G/ω–V-T* for MPS structure at high frequency (1 MHz), respectively.

Fig.4.19, shows the measured values of C were quite sensetive to applied bias voltage and temperature especially in the depletion region. As seen in Fig. 4.19 *C–V*-T plot has three regimes of accumulation–depletion–inversion region. Also, *C–V-T* plots especially at low temperature region (100K) show a higher peak in the depletion region than the other temperature curves and its position at about 2V, due to their structure and reordering charges at traps under temperature and applied voltage. The existence of the capacitance peak in the forward bias *C–V-T* plot is obtained by a number of practical searches on MIS and MOS structures (Nicollian et al., 1982; Karatas et al., 2011; Barış, 2013; Yucedağ et al., 2014; Kalandrgh et al., 2014; Hoque et al., 2014; Elfaleh et al., 2015). Furthermore, *C–V–T* peaks can be explained in term of the existence of R_s, inhomogeneities of the modified PVA interfacial layer doped by Zn nanoparticles. *C-V*-T plot shows rise in capacitance value until ~ 3V and then a decrease with increasing voltage for all temperatures, then the capacitance curves cross the voltage axis at a certain point and take negative values. Such behavior of capacitance at strong accumulation region is known negative capacitance (NC) or inductive behavior (Symth, 1955; Demirezen, 2013; Chatterjee et al., 2016). Penin structures has been considered as theoretical details of NC phenomena in homogeneous (barrier-free) semiconductor and it can appear for inertial conductivity (i.e. current retardation phase behind voltage phase) and conduction current is higher than the reactive component of the displacement current. The physical mechanisms of NC are depending on many parameters such as contact injection, interface state, minority carrier injection effects and applied voltage, ects.

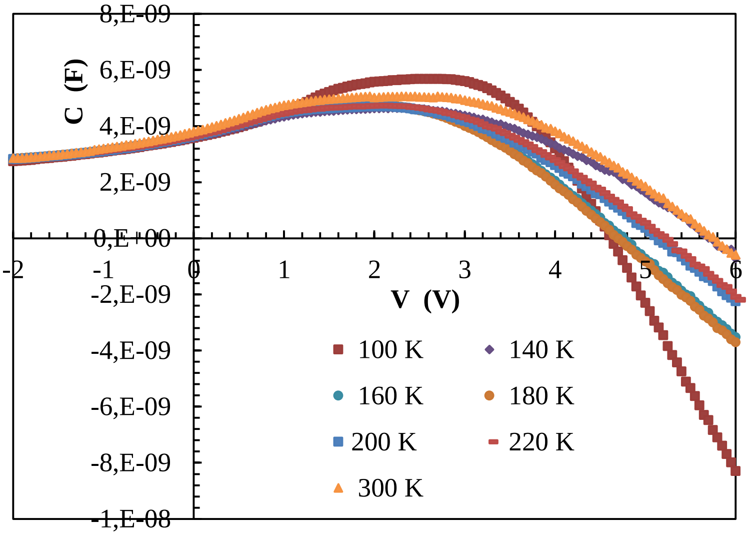

Figure 4.19. The *C–V-T* characteristics of the Au/ modified PVA interfacial layer doped by Zn nanoparticles / n-4H-SiC (MPS) structure.

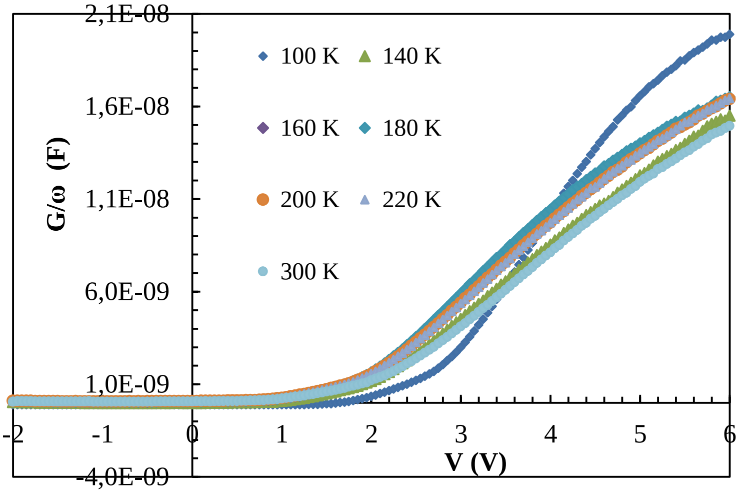

Figure 4.20. *G/ω–V-T* characteristics of the Au/ modified PVA interfacial layer doped by Zn nanoparticles / n-4H-SiC (MPS) structure.

G/ω–V-T curve in Fig.4.20 shows an increasing of conductance with the rising forward bias voltage. As seen in Fig. 4.20 the value of conductance increase with increasing voltage at high applied forward bias voltage V≥ 2V. Furthermore, the capacitance value decreases with increasing temperature due to forming of interfacial charge that can be effective at high temperature. At enough high bias voltage, C and G values are perfectly sensitive to temperatures (Kar et al., 1982; Nicollian et al., 1982).The presences of interface states at the M/S interface acts as recombination centers and produce a dispersal in capacitance. At low frequencies the interface traps can be caused by the ac signal and then yield an additional capacitance value, depends on the temperature and frequency. While at high frequency about (1MHz) the carrier life time τ is much higher than (1/2πf), the interface states cannot follow the ac signal, then the interface state capacitance can be neglected. Therefore, at high frequency the temperature become more effective on *C–V-T* and *G/ω–V-T* measurements (Mattsson et al., 1999; Akkal et al., 2000).The real value of R_i of the MPS structure are biased into strong accumulation which can be calculated from *C–V-T* and *G/ω–V-T* measurements at high enough frequency (1MHz) by using impedance or admittance methods as in Equation (2.39) (Symth,1955; Cheng, 1989; Wu et al., 1990; Çetinkaya et al, 2015).Then R_s value were calculated from the use of any measured C_m and G_m values by using Equation (4.11) for each temperature at wide applied bias voltage (-2V) to (+6V) interval as shown in Fig. 4.21. It is clear that R_s is sensitive to applied bias voltage and temperature.Fig.4.21 shows that the series resistance R_s values show increasing with increasing temperature and give a peak value at high applied bias voltage about (+3V) for all temperatures . It means that at high temperature the trap charges will have enough energy to leave the traps locating between M/S interface in SiC band gap. Furthermore, R_s values are independent of temperature at low applied bias voltage ≤1V.

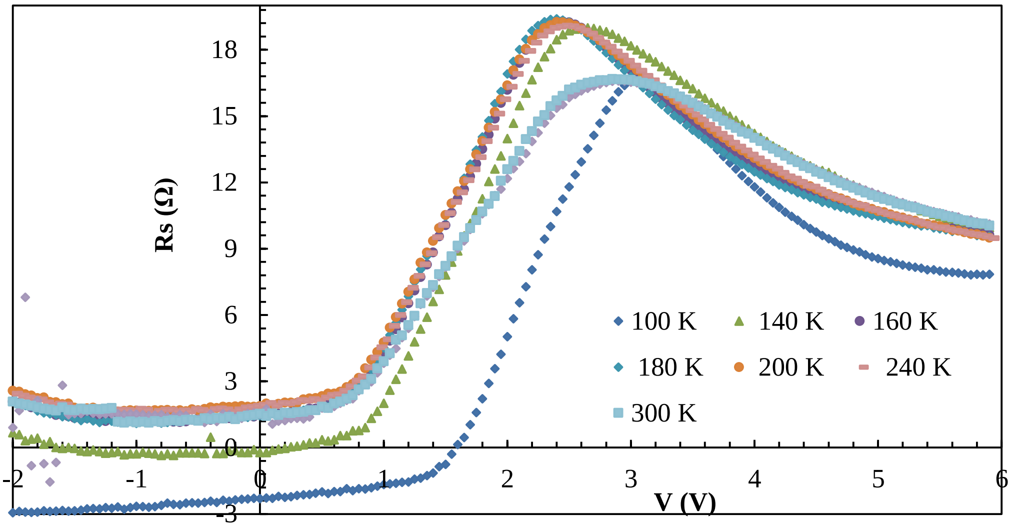

Figure 4.21. R_s-V-T plot of Au/ modified PVA interfacial layer doped by Zn nanoparticles / n-4H-SiC (MPS) structure at wide temperature range (100-300K).

4.3.2. Temperature dependence of dielectric parameters and Ac conductivity at 1 MHz

The complex permittivity of the interfacial polymer can be obtained from the Equation (2.41) (Symth, 1955; Penin, 1996; Jonscher et al., 1988; Cheng, 1989; Wu et al., 1990; Shekar et al., 1999; Awadhia et al., 2006; Çetinkaya et al., 2015; Hemalatha et al., 2015; Asar et al., 2015; Kaya et al., 2016; Chatterjee et al., 2016).

The values of ε′, ε" and tanδ can be calculated by using Equation (2.30),(2.47) and (2.49) respectivly (Symth, 1955; Penin, 1996; Jonscher et al., 1988; Cheng, 1989; Wu et al., 1990; Shekar et al., 1999; Awadhia et al., 2006; Çetinkaya et al., 2015; Hemalatha et al., 2015; Asar et al., 2015 ; Kaya et al., 2016 ; Chatterjee et al., 2016), where C_m in Equation (2.30) is the maximum capacitance at the strong accumulation region corresponds to the interfacial layer capacitance. The effect of temperatures on ε' and ε″ at (100-300K), 0.5V and1MHz are shown in Fig. 4.22 and 4.23, respectively. As seen in Figs. 4.22, 4.23 ε' and ε'' values increase by increasing of temperature .In addition, the value of ε' increases with increasing temperature and the value of ε" almost remain in the same value at range (100–230 K) then increase exponentially as increasing temperature at range (230–300 K).In other word, disorders occurred when the temperature rise in the lattice, this will cause a rise in the mobility of the majority carriers. Also the effect of temperature on the loss tangent (tanδ) for the structure at 0.5V is shown in Fig.4.24 in which the values of tanδ have almost constant value at low temperature range (100-230K) then increase with increasing temperature at (230-300K) (Saghrouni et al., 2014). In general, at high temperatures higher than 230 K, ε'' and tanδ show an exponential increase with increasing temperature. It perhaps belongs to polarization of the space–charge which are caused by impurities or interstitials modified PVA interfacial layer doped by Zn nanoparticles interface. Moreover, some charge carriers are trapped in some kinds of semiconductors, causing a polarization. The rise in temperature creates an expansion of molecules that lead to some increasing in the electronic polarization, as a result the amount of charge carriers at interfacial layer rises and submis more space–charge polarization and leads to a rise in the ε' and ε'' values of the dielectric materials (Symth, 1955; Penin, 1996; Jonscher et al., 1988; Cheng, 1989; Wu et al., 1990; Shekar et al., 1999; Awadhia et al., 2006; Çetinkaya et al., 2015; Hemalatha et al., 2015; Asar ,et al., 2015 ; Kaya et al., 2016 ; Chatterjee et al., 2016; Güçlü et al., 2016).

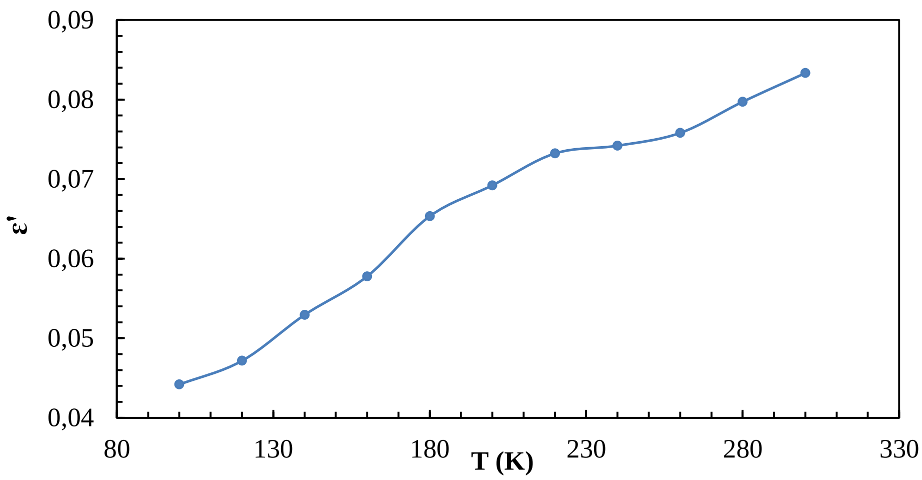

Figure 4.22. The effect of Temperature on dielectric constant Au/ modified PVA interfacial layer doped by Zn nanoparticles / n-4H-SiC (MPS) structure at 0.5V.

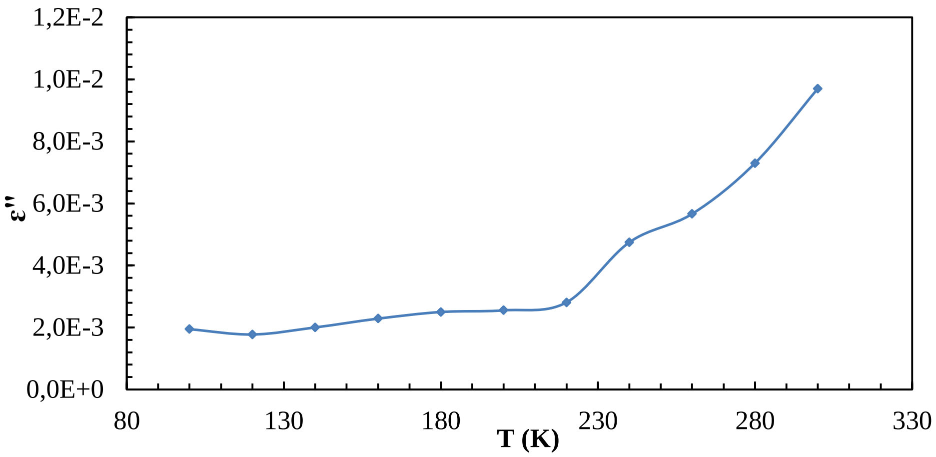

Figure 4.23. The effect of Temperature on dielectric loss of Au/ modified PVA interfacial layer doped by Zn nanoparticles / n-4H-SiC (MPS) structure at 0.5V.

The ac electrical conductivity σ_{ac} of Au/ modified PVA interfacial layer doped by Zn nanoparticles / n-4H-SiC (MPS) structure was calculated using by the following equation (Jonscher et al., 1988)

$$\sigma_{ac} = \omega C \tan\delta \left(\frac{d}{A}\right) = \varepsilon_o \omega \varepsilon'' \quad (4.15)$$

This suggests that the way of dielectric polarization in MPS structure happen by a same mechanism of conduction. It is obvious that σ_{ac} values rise with raising temperature because of the impurities or dislocations that remain at the grain boundaries. Same results have been obtained in the literature (Nicollian et al., 1965; Kar et al., 1982; Eroğlu et al., 2012).

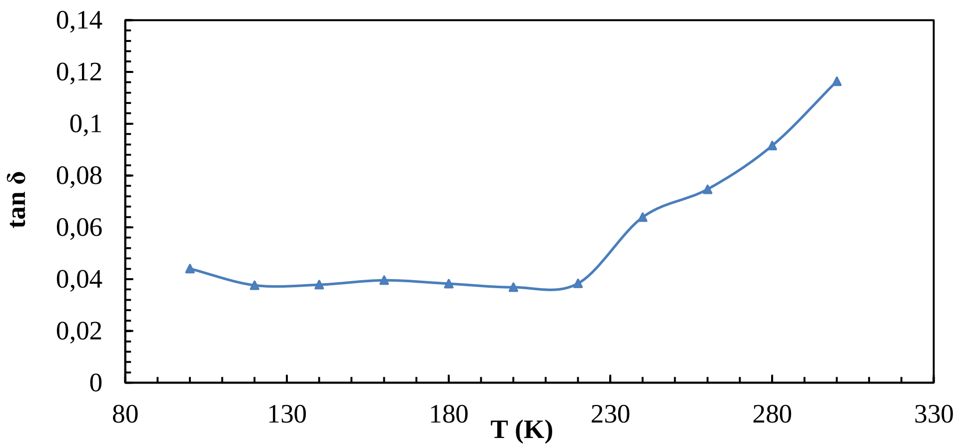

Figure 4.24. The variation of the tangent loss (tan δ) versus temperature of Au/ modified PVA interfacial layer doped by Zn nanoparticles / n-4H-SiC (MPS) structure at 0.5V.

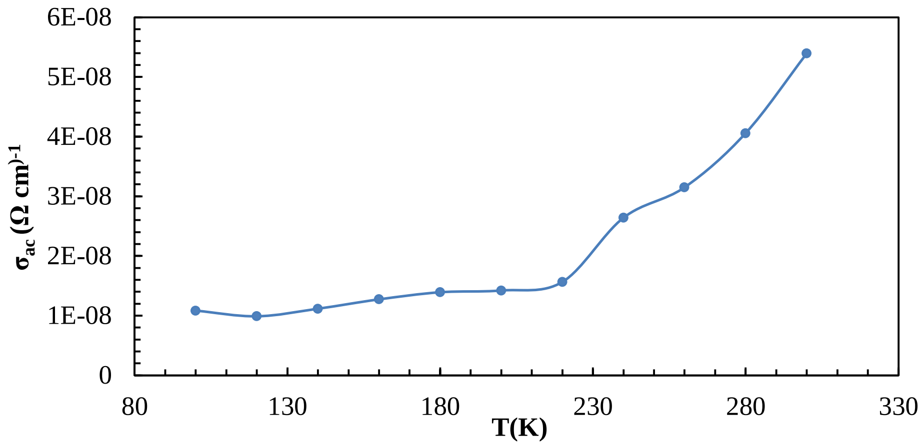

Figure 4.25. The temperature dependence of the ac electrical conductivity of Au/ modified PVA interfacial layer doped by Zn nanoparticles / n-4H-SiC (MPS) structure at 0.5V.

The formalism of electric modulus was used to eliminates the effect of electrode polarization and carrier charges transportation that lead to inaccurate (high values) of permittivity and conductivity especially at high temperatures. In other word, when the reciprocal complex permittivity was explained as an electrical analogue to the mechanical shear modulus (Jonscher et al., 1988; Wu et al., 1990). The physical opinion of the electrical modulus represents the electric field relaxation in the material when the electric displacement stays constant. Therefore, the modulus has unique advantage in the interpretation of slow relaxation phenomena processes such as MWS relaxation (Jonscher et al., 1988; Penin, 1996). For these reasons ,many searchers prefer to use the formalized electric modulus M^* as real dielectric relaxation process of the electric field in the materials that have constant electric displacement (Symth, 1955; Çetinkaya et al., 2015). The real component M' and the imaginary component M″ are measured by using ε' and ε″ data and Equation (2.52) (Symth, 1955; Çetinkaya et al., 2015;Chatterjee et al., 2016).

where M' and M″ are calculated for each temperature as seen in Fig. 4.26(a) and (b), respectively. Fig. 4.26(a) and (b) show that both M' and M" are strong temperature dependence especially in depleletion region. In *M'-T* plot, the values of *M'* inversely proportinal to the temperature. In other word, when temperature increase the value of *M'* decrease. In *M"-T* plot, *M"* values decrease with increasing temperature at low temperature range(100-230K) then increase in the range (230-300K) due to the contribution to interface trap charges. This attitude of *M'-T* and *M"-T* plots can be explained by the dielectric relaxation mechanism sensitivity to temperature instead of applied bias voltage. In other word, the conduction mechanism is different due to the change in temperature. (Symth,1955; Cheng, 1989; Akkal et al., 2000; Demirezen, 2013; Çetinkaya et al., 2015; Chatterjee et al., 2016).

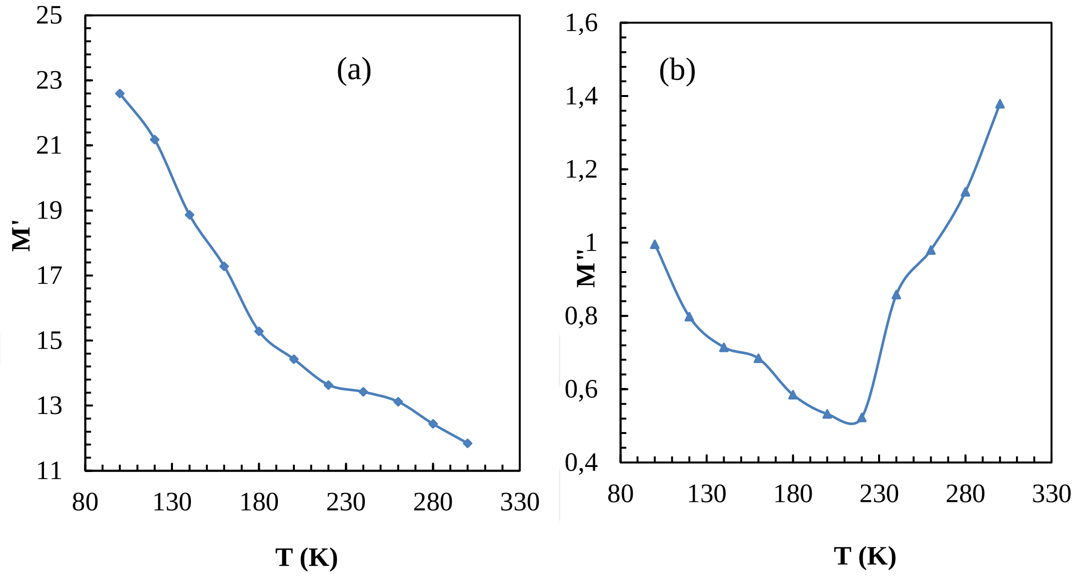

Figure 4.26. The (a)real part(M') and(b)imaginary part (M″) of the complex modulus versus temperature of Au/ modified PVA interfacial layer doped by Zn nanoparticles / n-4H-SiC (MPS) structure at 0.5V.

5. CONCLUSION

The research conducted in this thesis is primarily concerned with preparing and investigating the interfacial (Zn-doped PVA) layer effect on the electrical and dielectric characteristics. The research can be divided into three parts: (1) preparing the samples. (2) studying the effect of Zn doped PVA interfacial layer on the electrical characteristics in Au/n-4H SiC (MS) structures at high and low frequencies(1KHz and 1MHz) at room temperature.(3) studying the electric and dielectric properties and current transport mechanism of the structure at wide temperature and voltage ranges**.** First of all, Au/n-4H SiC (MS) and Au/ (Zn-doped PVA)/n-4H SiC (MPS) structures have been prepared and investigated. After that their main electrical parameters are obtained from *I-V*, *C-V* and *G/ω-V* characteristics at room temperature to compare of them. The main electrical parameters of these structures were obtained and show a considerably dependent on voltage as well as interfacial layer. From the reverse bias *C-V* data plot, the value of BH was obtained and shows a higher as compare with the value of BH that obtained from the forward bias *I-V* data for the two structures due to the nature of the measurement technique used. The obtained high values of n for two structures were attributed to the existence of the native and doped interfacial layer, lower barriers or patches around the mean value of BH and the existence of N_{ss} at interfacial layer/n-4H SiC interface. The energy density distribution profile of N_{ss} was obtained by using the forward bias *I-V* data by taking into account the voltage dependent BH and n for these two structures. The values of N_{ss} increase exponential from the mid-gap of n-4H SiC toward the bottom of its E_c. On the other hand, the voltage dependent profile of R_s for these structures was obtained from the *C-V* and *G/ω-V* data by using Nicollian and Brews method. These obtained experimental results confirmed that the existting of N_{ss}, R_s, and the interfacial layer are very effective on the electrical characteristics of the MS and MPS structures. In conclusion, when the main electrical parameters of MS and MPS structure are compared; the values of n, leakage current, R_s, Φ_{Bo} and N_{ss} for MPS structure are lower than those of the MS structure, but the values of R_{sh} and *RR* for MPS structure are higher than those of the MS structure due to the passivity role of Zn-PVA interfacial polymer layer. As a result, we can say that the (Zn doped-PVA) polymer material can be used as interfacial layer instead of conventional SiO_2 insulator layer to ameliorate the quality or performance of MS structure.

CTMs at room temperature cannot give all information about all dominant CTMs. Therefore, For the Au/(Zn-doped PVA)/n-4H-SiC (MPS) structures, the forward bias *I-V* characteristics of them were performed in the temperature range of 100-320 K by the steps of 20 K in order to obtain more information on the CTMs of the structure . The semi-logarithmic forward bias *I-V* curve has two distinct linear regions with different temperature for each temperature which are corresponding to LBR and MBR, respectively. While the values of n and Φ_{B0} are changed from 10.99 and 0.240 eV (at 100 K) to 3.08 and 0.0.830 eV (at 320 K) in the LBR, they changed from 13.31 and 0.252 eV (at 100 K) to 4.15 and 0.767 eV (at 320 K) in the MBR, respectively. The values of ($n.T$) or $n.(kT/q)$ especially at MBR are found almost constant at each temperature, and so it shows that the FE theory is possible conduction mechanism rather than the TE and TFE theories. On the other hand, the obtained higher values of n even at room temperatures cannot be explained by only FE theory. Therefore, Φ_{B0} vs n, Φ_{B0} vs q/2kT and $(n^{-1}-1)$ vs q/2kT plots were drawn to get evidence to the GD of BH. All these plots show also two distinct linear regions with different slopes which are corresponding to LTR (100-200 K) and HTR (220-320 K), respectively. Therefore, the conventional Richardson plots were also drawn for both the LBR and MBR and they show two linear regions which confirm the presence of double GD of BHs of the Au/(Zn-doped PVA)/n-4H-SiC (MPS) structure both in LBR and MBR, respectively. The values of $\overline{\Phi}_{bo}$ and A^* for LBR were obtained from slope and intercept of these plots as 0.730 eV, 114.12 $A.cm^{-2}K^{-2}$ at LTR and 1.304 eV, 97.33 $A.cm^{-2}K^{-2}$ at HTR, respectively. Similarly, for MBR, these values were found as 0.687 eV, 144.97 $A.cm^{-2}K^{-2}$ at LTR and 1.165 eV, 122.11 $A.cm^{-2}K^{-2}$ at HTR, respectively. It is clear that the obtained experimental values of A^* especially at low and moderate temperatures approaches to its theoretical value of 146 $A.cm^{-2}K^{-2}$ for n-4H-SiC. All experimental results confirmed that the *I-V-T* characteristics of the fabricated Au/(Zn-doped PVA)/n-4H-SiC (MPS) structure can be successfully explained on the basis of TE mechanism with a GD of BHs.

Furthermore, the effect of temperature and voltage on dielectric properties and ac conductivity of Au/Zn-doped PVA / n-4H-SiC (MPS) structure using impedance spectroscopy method in the wide temperature range (100–300 K) and at a constant frequency (1 MHz) have been investigated. It was shown that the dielectric properties of the C–V and G/ω–V characteristics of Au/Zn-doped PVA / n-4H-SiC (MPS) structure were found to be strongly dependent temperature and voltage. Also, the series resistance plot gives a peak, increasing with increasing temperature. It has been shown that the R_i strongly depends on voltage and temperature, and rapidly increases with increasing of high forward bias voltage V≥ 5V, and *C–V* and *G/ω–V* characteristics confirm that the series resistance is important parameters that strongly influence the dielectric properties in Au/Zn-doped PVA / n-4H-SiC (MPS) structure. In addition, we can conclude that the real and imaginary parts of dielectric constant ε'; ε″, electric modulus (M' and M″), loss tangent (tanδ), and σ_{ac} values were found to be strongly dependent on temperature and applied bias voltage especially in the depletion region. In addition, the electric modulus provides a good description of the dielectric relaxation. The representation of the dielectric properties in terms of the electric modulus is very sensitive and constitutes the features of relaxation peaks. Such occurred behavior of these plots certain of two different conduction mechanisms which attributed to the low and high temperature parts. All of these results confirmed that R_i, and Zn-doped PVA interfacial layer are very important parameters that strongly effect on electric and dielectric properties.

REFERENCES

Akkal, B., Benamara, Z., Gruzza, B., Bideux, L., 2000. Characterization of Interface States at Au/InSb/ InP(100) Schottky Barrier Diodes as a Function of Frequency. Vacuum, 57, 219-228.

Alialy, S., Altındal, Ş., Tanrıkulu, E.E., Yıldız, DE., 2014. Analysis of Temperature Dependent Current-Conduction Mechanisms in Au/TiO_2/n-4H-SiC Metal /Insulator /Semiconductor type Schottky Barrier Diodes. Journal of Applied Physics.1168:083709 ·

Alialy, S., Tecimer, H., Uslu, H., Altındal Ş., 2013. A Comparative Study on Electrical Characteristics of Au/N-Si Schottky Diodes, with and without Bi-doped PVA Interfacial Layer in Dark and under Illumination at Room Temperature. J Nanomed Nanotechol, 4, 3, 1000167.

Altındal, Ş., Yerişkin, M. Balbaşı, Demirezen, S., 2017. Temperature and Voltage Dependence of Barrier Height and Ideality Factor in Au/0.07 graphene-doped PVA/n-Si structures. Indian Journal of Physics, 91, 4, 421.

Altındal, Ş., Yeriskin, M. Balbaşı, A. Tataroğlu, 2016. Frequency and Voltage Dependence of Dielectric Properties, Complex Electric Modulus, and Electrical Conductivity in Au/7% graphene doped-PVA/n-Si MPS Structures. J. Appl. Polym. Sci. 133, 33, 43827.

Altındal, Ş., Sarı, B., Ünal, H.I, Yavas, N., 2009. Electrical Characteristics of Al/Polyindole Schottky Barrier Diodes. I. Temperature Dependence. J. Appl. Polym. Sci., 113 2955-2961.

Altındal, Ş., Uslu, H., 2011.The Origin of Anomalous Peak and Negative Capacitance in the Forward Bias Capacitance-Voltage Characteristics of Au/PVA/n-Si Structures. J. Appl. Phys., 109 074503-1 - 074503-7.

Altuntaş, H., Altındal, Ş., Özçelik, S., Shtrikman, H., 2009. Electrical Characteristics of Au/n-GaAs Schottky Barrier Diodes with and without SiO_2 Insulator Layer at Room Temperature. Vacuum Vol. 83, Issue 7, 1060–1065.

Altuntaş, H., Altındal, Ş., Shtrikman, H., Özçelik, S., 2009. A detailed Study of Current-Voltage Characteristics in Au/SiO_2/n-GaAs in Wide Temperature Range. Microelectronics Reliability, 498, 904-911.

Anis, A and Banthia, A.K, 2007. Preparation, Electrical and Dielectric Characterization of crosslinked Polyvinyl Alcohol-Phosphotungstic Acid. Nanocomposites Mater. Manuf. Process. 22, 737.

Aras, G., Orhan, E., Selçuk, A. B., Bilge, Ocak S., Erturul M., 2015. Dielectric Properties of Al/Poly methyl methacrylate PMMA/ p-Si Structures at Temperatures Below 300 K. Procedia - Social and Behavioral Sciences 195, 1740 – 1745.

Arora, R., Mosch, W., 1995. High Voltage Insulation Engineering: Behaviour of Dielectrics – their Properties & Applications, 1st Ed., New Age International Publishers: New Delhi, India.

Asar, Y., Safak, Asar, T., Altındal, Ş., Ozcelik S., 2015. Investigation of Dielectric

Relaxation and ac Electrical Conductivity using Impedance Spectroscopy Method in AuZn/TiO_2/p-GaAs110 Schottky Barrier Diodes. Journal of Alloys and Compounds, 628, 442–449.

Ataseven, T.,Tataroğlu, A., 2013. Temperature-Dependent Dielectric Properties of Au/Si3N4/n-Si Metal –Insulator- Semiconductor Structures. Chin. Phys. B, 22, 11, 117310.

Awadhia, A., Patel, S.K., Agrawal, S.L., 2006. Dielectric Investigations in PVA based gel electrolytes. Progress in Crystal Growth and Characterization of Materials, 52, 61-68.

Aydemir, U., Ilke, T., Altındal, Ş., Uslu I., 2013. Materials science in Semiconductor Processing, 16, 1865-1872.

Aydin, M E., Yildirim, N., Türüt A., 2007. Temperature-Dependent Behavior of Ni/4H-n-SiC Schottky Contacts. J. Appl.Phys.102, 043701-1.

Aydoğan, Ş., Sağlam, M., Türüt, A., 2005. The Effects of the Temperature on the some Parameters Obtained from Current–Voltage and Capacitance–Voltage Characteristics of polypyrrole/n-Si structure. Polymer 46, 563-568.

Behzad, B., 2013. Frequency Dependent Dielectric Properties in Schottky Diodes Based on Rubrene Organic Semiconductor. Physica E, 54, 171–176.

Belyaev, A.E., Boltovets, N.S., Konakova, R.V.,Ya., Kudryk Ya., Sachenko A.V, Sheremet V.N., 2010. Temperature Dependence of Contact Resistance of Au/Ti_2Pd_2Si/n+-Si Ohmic Contacts. Semiconductor Physics Quantum Electronics & Optoelectronics, 13, 4, 436.

Bethe, H. A., 1942. Theory of the Boundary Layer of Crystal Rectifiers MIT, Radiat. Lab. Rep. 43-12.

Bhattarai, P., Thapa, K., Basnet, R., Sharma S., 2014. Electrospinning: how to Produce Nanofibers using Most Inexpensive technique: an Insight into the Real Challenges of Electrospinning Such Nanofibers and its Application Areas. International Journal of Biomedical And Advance Research, 5, 9,401-405.

Bilge, Ocak, S., Selçuk, A.B., Bayram, S.B. Ozbay A., 2014. Frequency Dependent Dielectric Properties of Al/ maleic anhydride MA /p-Si Structures. J. of Opolectronics and Advance Materials, 16, 7-8, 956-963.

Bilkan, Ç., Azizian-Kalandaragh, Y., Altındal, Ş., Shokrani-Havigh R., 2016. Frequency and Voltage Dependence Dielectric Properties, ac Electrical Conductivity and Electric Modulus Profiles in Al/Co_3O_4-PVA/p-Si Structures. Physica B, 500, 154–160.

Bilkan, Ç., Gümüş, A., Altındal, Ş., 2015. The Source of Negative Capacitance and Anomalous Peak in The Forward Bias Capacitance-Voltage in Cr/p-si Schottky Barrier Diodes SBDs. Mater. Sci. Semicond.Proces., 39484-4911.

Bilkan, Ç., Zeyrek, S., San, S. E., Altındal, Ş., 2015. A Compare of Electrical Characteristics in Al/p-Si MS and Al/$C_{20}H_{12}$/p-Si MPS type Diodes using Current-Voltage I-V and Capacitance-Voltage C-V Measurements. Mater. Sci. and Semicon. Process, 32, 137-144.

Bowen, C., Fernardo, C., Klimeck, G., Chatterjee, A., Blanks, D., Lake, R., Hu J., Davis, J., Kulkarni, M., Hattangady, S., Chen, I., 1997. Physical Oxide thickness Extraction and Verification using Quantum Mechanical Simulation. IEDM Technical Digest, 869-872.

Butcher, K.S.A, Tansley, T.L, D., 1996. An Instrumental Solution to the Phenomenon of Negative Capacitances in Semiconductors. Solid-State Electron, 39, 333-336.

Bülbül, M.M., Bengi, S., Dökme, İ., Altındal, Ş., Tunç, T., 2010. Temperature Dependent Capacitance and Conductance-Voltage Characteristics of Au/polyvinyl alcoholCo, Zn/n-Si Schottky Diodes. J. Appl. Phys., 108, 034517-1 - 034517-6.

Card, H.C. and Rhoderick, E.H., 1971. Studies of Tunnel MOS diodes I. Interface effects on Silicon Schottky Diodes. J. Phys. D: Appl. Phys., 4, 1589-1602.

Casady, J.B., Johonson, R.W., 1996. Status of Silicon Carbide SiC as a Wide-Bangap Semiconductor for High-Temperature Applications A Review. Solid State Electronics, 39, 1409-1422.

Cetinkaya, H. G, Alialy, S., Altındal, S., Kaya, A., Uslu I., 2015. Investigation of Negative Dielectric Constant in Au/1 % graphene GP doped-$Ca_{1.9}Pr_{0.1}Co_4Ox$/n-Si Structures at Forward Biases using Impedance Spectroscopy Analysis. J Mater Sci: Mater Electron, 26, 3186–3195.

Chaari, M. Matoussi, Ad., 2014. Structural and Dielectric Properties of undoped ZnO Pellets Prepared by Solid State Route. Appl. Phys. A. 116, 1149–1160.

Champbell, A. J., Bradley, D. D. C., and Lidzey, D. G, 1997. Space-Charge Limited Conduction with Traps in Polyphenylene Vinylene Light Emitting Diodes. J. Appl. Phys., 82, 6326-6342.

Chand. S., Kumar, J., 1995. Current-Voltage Characteristics and Barrier Parameters of Pd_2Si/p-Si111 Schottky Diodes in a Wide Temperature Range. Semiconductor Science and Technology, 10, 12, 1680.

Chand, S., Kumar, J., 1997. Effects of Barrier Height Distribution on the Behavior of a Schottky Diode. J. Appl. Phys., 82, 5005-5010.

Chang, G., 2015. Synthesis and Performance Characterization of Polymer Semiconductors for Organic Thin Film Transistors PH.D thesis, 163 p, University of Waterloo, ON, Canada.

Charles, J. Scozzie, and James, M. McGarrity, 1998. Effects of Interface-Trapped Charge on the SiC MOSFET Characteristics, Proceedings: 4th International High Temperature Electrons Conference, p. 23.

Chatterjee, B., Kulshrestha, N., Gupta, P.N., 2016. Nano Composite Solid Polymer Electrolytes Based on Biodegradable Polymers Starch and Poly Vinyl Alcohol. Measurement, 82, 490–499.

Chen, T., 1994. Studies of Metal - Semiconductor Contacts: Current Transport, Photovoltage, Schottky Barries Heights and Fermi Level pinning PH.D thesis, 232 p, university of Hong Kong, Hong Kong.

Cheng, D., 1989. Field and Wave Electromagnetics, 515 p, second ed., Addison-Wesley, New York.

Cheung, S. K., Cheung, N. V., 1986. Extraction of Schottky Diode Parameters from Forward Current- Voltage Characteristics. Appl. Phys. Lett., 49 85-87.

Chiang, C. K., Fincher, C. R., Parker, J. Y. W., Heeger, A. J., Shirakawa, H. , Louis, E. J., Gau, S. C., and MacDiarmid, A. G., 1977. Electrical Conductivity in Doped Polyacetylene," Phys. Rev. Lett., 39, 17, 1098-1101.

Chiou, Y.L., Gambino J.P., Mohammad M., 2001. Determination of the Fowler-Nordheim Tunneling Parameters from the Fowler-Nordheim plot, Solid-State Electronics, 45, 1787-1791.

Chien, Fu, 2014. A Review on Conduction Mechanisms in Dielectric Films Hindawi Publishing Corporation Advances in Materials Science and Engineering ID 578168.

Choueib, M., Ayari A., Vincent, P., Perisanu, S., Purcell, S.T., 2011. Evidence for Poole Frenkel Conduction in Individual SiC Nanowiers by Field Emission Transport Measurments. Journal of Applied Physics, 109, 073709.

Clemenson, S., Leonard, D., Sage, D., David, L., Espuche E., 2007. Metal Nanocomposite Films Prepared In Situ from PVA and Silver Nitrate. Wiley Inter Science, 46, 6, 2062-2071.

Colinge, J. P., Colinge, C. A. 2002. Physics of Semiconductor devices, 431p, Kluwer Academic Publishers, New York.

Cooke, M. J. 1990 Semiconductor Devices, 339 p, Prentice Hall, New York.

Cova, P., Singh, A., 1990. Temperature Dependence of I-V and C-V Characteristics of Ni/n-CdF_2 Schottky Barrier Type Diodes. Solid-State Electron. 33, 11-19.

Çakar, M., Türüt A., Onganer Y., 2002. The Conductance- and Capacitance-Frequency Characteristics of the Rectifying Junctions Formed by Sublimation of Organic Pyronine-B on p-Type Silicon. J. Solid State Chem., 168, 1,169-174.

Çicek, Ö., Tecimer., H.,Uslu, Tanç S.O., Tecimer, H., Altındal, Ş., Uslu I., 2016. Evaluation of Electrical and Photovoltaic Behaviours as Comparative of Au/n-GaAs MS Diodes With and Without Pure and graphene Gr-doped polyvinyl alcohol PVA Interfacial Layer under Dark and Illuminated Conditions. Composites Part B, 98, 260-268.

Dakin, T. W., 2006. Conduction and Polarization Mechanisms and Trends in Dielectrics, IEEE Electrical Insulation Magazine, 22, 5, 11-20.

Demir, A., Yücedağ, İ., Ersöz, G., Altındal, Ş., Baraz, N., Kandaz, M. A., 2016. Comparative Study on the Main Electrical Parameters of Au/n-Si, Au/Biphenyl-CuPc/n-Si/and Au / Biphenylsubs -CoPc/n-Si/type Schottky Barrier Diodes, J. Nanoelectron and Optoelectron, 11,5,620-625.

Demirezen, S., Kaya, A., Vural, Ö., Altındal, Ş., 2015. The effect of Mo-doped PVC+ TCNQ Interfacial Layer on the Electrical Properties of Au/PVC+ TCNQ/p-Si Structures at Room Temperature. Materials Sci. in Semicond. Proces., 33, 140–148.

Demirezen, S., Kaya, A., Yerişkin, S. A., Balbaşı, M., Uslu, İ., 2016. Frequency and Voltage Dependent Profile of Dielectric Properties, Electric Modulus and ac Electrical Conductivity in the PrBaCoO Nanofiber Capacitors. Results in Phys, 6 180-185.

Dimitriadis, C.A., Logothetidis, S., Alexandrou, I., 1995. Schottky Barrier Contacts of Titanium Nitride on n-type Silicon. Applied Physics Letters, 66, 502-504

Dogish, M.Y. and Ho, F.D., 1992. A Comprehensive Analytical Model for Metal-Insulator Semiconductor MIS devices. IEEE Trans. Electron Dev., 39, 12, 2771-2780.

Dokme, I., Altındal, S., Tunc, T., 2010. Temperature Dependent Electrical and Dielectric Properties of Au/polyvinyl alcohol Ni, Zn-doped/n-Si Schottky diodes. Microelectronics Reliability, 50, 39–44.

Dökme, İ., Tunç, T., Uslu I., Altındal, Ş., 2011. The Au/polyvinyl alcohol Co, Zn-doped/n-type Silicon Schottky Barrier Devices Synthetic Metals 161,5- 6, 474-480.

Ejderha, K., Yıldırım, N., Albay, B., Turut, A., 2009. Examination by Interfacial Layer and Inhomogeneous Barrier Height Model of Temperature-Dependent I–V characteristics in Co/p- InP Contacts. Journal of Alloys and Compounds, 484, 870-876.

Eliana, A., Van Etten, Eder S. Ximenes, Lucas, T. Tarasconi, Irene T.S., Garcia Maria, M.C., Forte, Henri Boudinov, 2014. Insulating Characteristics of Polyvinyl Alcohol for Integrated Electronics. Thin Solid Films 568, 111–116.

Emil, A., and Dev Alok, 2001. Effect of Interface States on Electron Transport in 4H-SiC Inversion Layers. IEEE Trans. on Electron Devices, 48, 9, 1870-1877.

Eroğlu, A., Tataroğlu, A., Altındal, S., 2012. On the temperature dependent dielectric properties, conductivity and resistivity of MIS structures at 1 MHz. Microelectronic Engineering, 91, 154–158.

Ershov, N., Buchanan, M., Wasilewski, Z.R., Jonscher, A. K., 1998. Negative Capacitance Effect in Semiconductor Devices.IEEE Transactions on Electrical Devices 45, 10, 2196-2206.

Feng-Ping C., Yu-Ming Z., Yi-Men Z., Xiao-Yan T., Yue-Hu W. and Wen-Hao C., 2012. Temperature-Dependent Characteristics of 4H SiC Junction Barrier Schottky Diodes. Chin. Phys. B, 21, 3, 037304 .

Fowler, R., Nordheim L., 1928. Electron emission in intense electric fields, Proc. Roy. Soc. A, 119, 173-181.

Forrest, S.R., Kaplan, M.L., Schmidt, P.H., Feldmann, W.L., Yanowski E., 1982. Organic- on- inorganic semiconductor contact barrier devices. Appl. Phys. Lett., 41,1, 90-93.

Freeman, L.B., Dahlke W.E., 1970.Theory of Tunneling into Interface States, Solid-State Electronics, 13, 11, 1483-1503.

Gilliot, M., Hadjadh, A., Martin, J., 2015. Investigation of correlation between dielectric fuction thickness and morphology of nano-granular ZnO very thin film. Thin Solid Film, 597, 65-69.

Gökçen, M., Tunç, T., Altındal, Ş., Uslu, İ., 2012. Electrical and Photocurrent Characteristics of Au/PVA Co-doped/n-Si Photoconductive Diodes. Mater. Sci. and Eng. B., 177,416-420.

Guichelaar, PJ., 1997. Acheson Process. Carbide, Nitride and Boride Materials Synthesis and Processing, Weimer, A. W., Ed., Chapman and Hall, London, United Kingdom, 115-129.

Gupta, S. K., Pradhan, N., Shekhar, C., Akhtar, 2012. Design, Fabrication, and Characterization of Ni/4H-SiC 0001 Schottky Diodes Array Equipped With Field Plate and Floating Guard Ring Edge Termination Structures. J IEEE Trans. Semiconduct. Manufact.25, 4, 664-672.

Gupta, R.K. Singh, R.A., 2004. Electrical Properties of Junction Between Aluminium and Polyaniline–Polyvinyl Chloride Composite. Mater. Chem. Phys. 86, 2, 279-283.

Güçlü, Ç.Ş., Özdemir, A.F., Kökce A., Altindal Ş., 2016. Frequency and Voltage-Dependent Dielectric Properties and AC Electrical Conductivity of Au/Ti/Al_2O_3/n-GaAs with Thin Al_2O_3 Interfacial Layer at Room Temperature. Acta Physica Polonica A, 130, 1, 325-329.

Gülen, Y., Ejderha, K., Nuhoğlu, Ç., Türüt, A. 2011. Schottky barrier height modification in Au/n-type 6H–sic structures by pbs interfacial layer. Microelectronic Engineering, 881, 179-182

Gülü, Ö., Aydoğan, Türüt, Ş., A., 2012. Electronic Parameters of High Barrier Au/Rhodamine-101/n-Inp Schottky Diode with Organic Interlayer. Thin Solid Films, 520, 1944-1948.

Han, R., Xu X., Hu X., Yu N., Wang, J. Tan, Y. Huang, W., 2003. Development of Bulk SiC Single Crystal Grown by Physical Vapor Transport Method. Optical materials, 23, 415-420.

Hemalatha, K. S., Sriprakash, G., Ambika, Prasad M., V. N., Damle R., and Rukmani K. 2015. Temperature Dependent Dielectric and Conductivity Studies of Polyvinyl Alcohol-ZnO Nanocomposite Films by Impedance Spectroscopy. J. of Applied Physics 118, 15, 154103.

Hess, D. W., Jensen K. W., 1989. Microelectronics Processing: Chemical Engineering Aspects, 221 p, ACS Publication: Washington DC

Hoque, Md. Monwar, Dutta, Alo, Kumar, Sanjay, Sinha Tripurari Prasad, 2014. Dielectric Relaxation and Conductivity of $BaMg_{1/3}Ta_{2/3}O_3$and $BaZn_{1/3}Ta_{2/3}O_3$. J. Mater. Sci. Technol., 304, 311-320.

Horikosh S., Serpone, N., 2013. Microwaves in Nanoparticle Synthesis: Fundamentals and Applications, 325 p, Wiley-VCH Verlag GmbH & Co. KGaA.singapor.

Huang, Z. M., Zhang, Y.Z., Kotaki, M., Ramakrishna, S., 2003. A Review on Polymer Nanofibers by Electrospinning and their Applications in Nanocomposites. Composites Science and Technology, 63, 2223–2253.

Huang, X.L., Shin, Y. G., Lim. K.Y., Suh, E. K., Lee, H. J., Shen, S.C., 1997. Thermally Induced Capacitance and Electric Field Domains in GaAs/$Al_{0.3}Ga_{0.7}$As Quantum Well Infrared Photodedector. Solid-State Electron, 41, 845-850.

Hudait, M.K., Krupanidhi, S.B., 2001. Interface States Density Distribution in Au/n-GaAs Schottky Diodes on n-Ge and n-GaAs Substrates. Mat. Sci. Eng. B-Solid, 87 ,141-147.

Janardhanam, V., Jyoth,i I., Ahn Kwang-Soon, Choi, Chel-Jong, 2013. Temperature-Dependent Current–Voltage Characteristics of Se Schottky contact to n-type Ge. Thin Solid Films, 546, 63–68.

Jonscher, A. K. and M. N. Robinson, 1988. Dielectric Spectroscopy of Silicon Barrier Devices. Solid-State Electron, 31, 8, 1277-1288.

Kalandaragh, Y. Azizian, Aydmir, U., Altindal, S.¸ 2014. Dielectric and Optical Properties of CdS–Polymer Nanocomposites Prepared by the Successive Ionic Layer Adsorption and Reaction SILAR method. Journal of Electronic Materials, 43, 4, 1226-1231.

Kamoun, O., Boukhachem, A., Yumak, A., Petkova, P., Boubaker, K., and Amlouk, M., 2016. Europium Incorporation Dynamics and some Physical Investigations within ZnO Sprayed Thin Films. Materials Science in Semiconductor Processing, 43, 8-16.

Kang, M. S., Ahn, J. J., Moon, K. S., and Koo, SM., 2012. Metal work-function-dependent barrier height of Ni contacts with metal-embedded nanoparticles to 4H-Si. Nanoscale. Res. Lett., 7, 1, 75.

Kar, S., Panchal, K.M., Bhattacharya, S., Varma S., 1982. On the Mechanism of Carrier Transport in Metal-Thin-Oxide Semiconductor Diodes on Polycrystalline Silicon. IEEE Trans. Electron Devices, 29, 1839-1845.

Karim, R. M., Kwon, T. L., Chul J. L., Tauhidul, I. B., Hee, J. K., Lee, S. P., and Mu, S. L., 2007. Synthesis of Core-Shell Silver-Polyaniline Nanocomposite by Gamma Radiolysis Method. Polymer Science part A: Polymer Chemistry, 45, 5741-5747.

Kaya, A., Marıl, E., Altındal, Ş., Uslu, İ., 2016. The Comparative Electrical Characteristics of Au/n-Si MS Diodes With and Without a 2% graphene cobalt-doped $Ca_3Co_4Ga_{0.001}O_x$ Interfacial Layer at Room Temperature. Microelectronic Engineering, 149, 166–171.

Kaya, A., Alialy, S., Demirezen, S., Balbaş, M., Yerişkin, S.A., Aytimur, A., 2016. The Investigation of Dielectric Properties and ac Conductivity of Au/GO-doped PrBaCoO Nanoceramic/n-Si Capacitors using Impedance Spectroscopy Method. Ceramics International 42, 3322–3329.

Kaya, A., Sevgili, Ö., Altındal, S., Öztürk, M. K., 2015. Current-Conduction Mechanism in Au/n-4H-SiC Schottky Barrier Diodes. Indian Journal of Pure & Applied Physics, 53, 56-65.

Kaya, A., Yucedag, İ., Altındal, Ş., Altunpak, Y., Vural, Ö., 2016. On the Anomalous Peak and Negative Capacitance in the Forward-Bias C-V Plot in Al/Mo-doped PVC+TCNQ/p-Si MPS Capacitors. Journal of Materials and Electronic Devices 1, 6-13.

Khanna, P.K., Gokhale, R., Subbarao, V.V.V.S., Kasi, A., Das, B.K., Satyanarayana, C.V.V., 2005. PVA Stabilized Gold Nanoparticles by use of Unexplored Albeit Conventional Reducing Agent. Materials Chemistry and Physics, 92, 1, 29–233.

Kim, H., 2016. Capacitance-Voltage C-V Characteristics of Cu/n-type InP Schottky diodes.Transactions on Electrical and Electronic Materials, 17, 5, 293-296.

Kimoto, T., Cooper, J. A., 2014. Fundamentals of Silicon Carbide Technology, 538 p, 1.st Edn John Wiley & Sons Singapore.

Klauk, H., Zschieschang, U., Pflaum, J., and Halik, M., 2007. Ultralow-Power Organic Complementary Circuits. Nature, 445, 7129, 745-748.

Koehler M. Hümmelgen I. A., 1997. Temperature Dependent Tunnelling Current at Metal/Polymer Interfaces Potential Barrier Height Determination. Appl. Phys. Lett. 70, 24, 3254-3256.

Kondo, Takeshi, 2007. Current –Voltage characteristics of organic semiconductor: interfacial control between organic layer and electrodes PH.D thesis, 230 p, Georgia Institute of Technology, Georigia.

Köck, F.A.M., Garguilo, J.M., Brown, B., Nemanich, R.J., 2002. Enhanced low-temperature thermionic field emission from surface-treated N-doped diamond films. Diamond and Related Materials, 11, 774–779.

Kumar, V., Dahlke W.E., 1977. Characteristics of Cr-SiO_2-nSi Tunnel Diodes. Solid-State Electronics, 20, 2, 143152.

Lee, W.C. Hu C., 2000. Modeling gate and Substrate Currents due to Conduction and Valence Band Electron and Hole Tunneling, Digest Symposium on VLSI Technology Digest of Technical Papers. IEEE, New York, DOI: 10.1109/VLSIT.2000.852824

Lee, J.Y., Singh, S., Cooper, J.A., 2008. Demonstration and Characterization of Bipolar Monolithic Integrated Circuits in 4H-SiC. IEEE Trans. Electron. Devices, 55, 8, 1946–1953.

Lenzlinger, F.M. and Snow E.H., 1969. Fowler-Nordheim Tunneling into Thermally Grown SiO_2. J. Appl. Phys. 40, 1, 278- 283.

Li, Y., 2015. Organic Optoelectronic Materials, 392 p, Springer International publishing Switzerland.

Liu, Z., Chen, T. P., Liu Y., Yang, M., Wong, J. I., Cen, Z. H. and Zhang, S., 2012. Temperature-dependent charge transport in Al/Al nanocrystal embedded Al_2O_3 nanocomposite/p-Si diodes. ECS Solid State Lett., 1, 1, Q4-Q7.

Macedo, P.B., Moynihan, C.T., Bosz, R., 1972. Role of Ionic Diffusion in Polarization in Vitreous Ionic Conductors SOC Glass Technology. Phis. Chern. Glasses, 13, 6, 171-179.

Maheshwari, P., 2007. Electronic Components & Processes, New Age International Publishers: New Delhi, India.

Marco, Stella, 2006. Study of organic semiconductors for device applications, 221 p, PH.D thesis, university of DE Barcelona, Barcelona.

Marten, F.L., 2000. Vinly Alcohol Polymers Kirk-Othmer Encyclopedia of Chemical Technology, John Wiley&Sons Inc., New York, 1-16.

Michaelson, H.B., 1978. Relation Between an Atomic Electronegativity Scale and the Work Function. IBM J. of R&D, 22, 1,72-80.

Moissan, H., 1905. Etude du siliciure de carbone de la meteorite Canon Diablo. Comptes rendus Acad. sci., 140, 405-506.

Monch, W., 1990. On the Physics of Metal-Semiconductor Interfaces. Rep. Prog. Phys., 53, 221-278.

Moraki, K, Bengi, S., Zeyrek, S., Bülbül, M. M., Altındal, Ş., 2016. Temperature Dependence of Characteristic Parameters of the Au/C_20H_{12}/n-Si Schottky Barrier Diodes SBDs in the Wide Temperature Range. J Mater Sci: Mater Electron, 28, 5, 3987–3996.

Mott, N. F., 1938. Note on the Contact Between a Metal and an Insulator or Semiconductor. Proceedings of the Cambridge Philosophical Society, 34, 568-572

Mönch W., 1997. Barrier Heights of Real Schottky Contacts Explained by Metal-Induced Gap States and Lateral Inhomogeneities. J. Vac. Sci. Technol. B. 17, 4, 1867-1876.

Mukherjee, M., 2011. Silicon Carbide-Materials, Processing and Applications in Electronic Devices, 546 p, Croatia.

Mustafa, A., 2004. Electrical Transport in Metal-Oxide-Semicondutor Capacitors, Msc thesis,75 p, graduate school of natural and applied science, Middle East Technical University,Ankara.

Naik, S. Sankar, Reddy, V., Rajagopal, 2012. Temperature Dependency and Current Transport Mechanisms of Pd/V/n-type InP schottky rectifiers. Adv. Mat. Lett., 33, 188-196

Neamen, D. A., 1997. Semiconductor Physics and Devices 2nd ed., 618 p, Mc Graw-Hill, New York.

Nicollian, E.H., Goetzberger, A., 1965. MOS Conductance Technique for Measuring Surface State Parameters. Appl. Phys. Lett., 7, 8, 216-219.

Nicollian, E.H., Goetzberger A., 1967. The Si-SiO_2 Interface - Electrical Properties as Determined by the Metal-Insulator-Silicon. Conductance Technique Bell Syst. Tech. J., 46, 6, 1055-1133.

Nicollian, E.H., Brews, J.R., 1982. MOS Physics and Technology, 906 p, Wiley, New York.

Norde, H, A., 1979. Modified Forward I- V Plot for Schottky Diodes with High Series Resistance. J. Appl. Phys., 50, 5052-5053.

Oder, T. N., Martin, P., Adedji, A.V., Isaacs-Smith, T., and Williams, JR., 2007. Improved Schottky Contacts on n-type 4H-SiC using ZrB_2 Deposited at High Temperatures. J. Electron. Mater., 36,7, 805-811.

Okojie, R.S., Lukco, D., Spry, D., 2002. Reliability of Ti/TaSi /Pt ohmic contacts on 4H- and 6H-SiC after 1000 hours in air at 600 C. J. Appl. Phys., 91, 10, 6553-6559.

Okuyama, M., 2005. Ferroelectric Thin Films: Basic Properties and Device Physics for Memory Applications. 244p, Springer-Verlag, New York.

Orak, I., Kocyigit, A., Alındal, S., 2017. Electrical and Dielectric Characterization of Au/ZnO/n Si Device Depending Frequency and Voltage. Chin. Phys. B 26, 2, 028102 .

Osvald, J., 2009. Temperature Dependence of Barrier Height Parameters of Inhomogeneous Schottky Diodes. Microelectron. Eng. 86, 117-120.

Özavcı, E., Demirezen, S., Aydemir, U., Altındal, Ş., 2013. A Detailed Study on Current–Voltage Characteristics of Au/n-GaAs in Wide Temperature Range. Sensors and Actuators A, 194, 259-268.

Özdemir, A.F., Aydın, S. G, Aldemir, D. A., Görsoy, Ş. S., 2011. Electrical and Optical Properties of p-type Silicon Based on Polypyrrole-Derivative Polymer, Synth. Met., 161, 692-697.

Özden, Ş., Tozlu, C., Pakma, O., 2016. Temperature Dependent Electrical Transport in Al/Poly4-vinyl phenol/p-GaAs Metal-Oxide-Semiconductor by Sol-Gel Spin Coating Method. Hindawi Publishing Corporation International Journal of Photoenergy. ID 6157905,

Padovani, F., A., Sumner, G.G., 1965. Experimental Study of Gold- Gallium Arsenide Schottky Barriers. J. Appl. Phys. 36, 12, 3744-3747.

Pakma, O., Serin, N., Serin, T., Altındal, Ş., 2008. The Double Gaussian Distribution of Barrier Heights in Al/TiO_2/p-Si Metal-Insulator-Semiconductor Structures at Low Temperatures. J. Appl. Phys., 104, 014501-014506.

Pan H, Li, LM, Hu, L.,Cui X J., 2006. Continuous Aligned Polymer Fibers Produced by a Modified Electrospinning Method. Polymer, 47, 14, 4901- 4904.

Pawde, S.M., Deshmukh, K., Parab, S., 2008. Preparation and Characterization of Polyvinyl Alcohol and Gelatin Blend Films. J. Appl. Polym. Sci. 109, 1328.

Penin, N. A., 1996. Negative Capacitance in Semiconductor Structures, Semiconductors, 30, 4, 340–343.

Periasamy, V., Narayan B., Hak, Y. K., Douk, R. L., 2003. The Photoluminescence Properties of Zinc Oxide Nanofibres Prepared by Electrospinning. Nanotechnology, 15, 3, 320.

Popescu, M., Bunget, I., 1984. Physics of Solid Dielectrics, Elsevier, Amsterdam, 206-245, 282-291.

Reddy, Ch.V., Subba, Han X., Zhu Q. Y., Mai L.-Q., and Chen, W., 2006. Dielectric Spectroscopy Studies on PVP + PVA Polyblend Film. Microelctron. Eng., 83, 2, 281-285.

Reddy, V. R., 2014. Electrical Properties of Au/polyvinylidene fluoride /n-InP Schottky Diode With Polymer Interlayer. Thin Solid Films, 556, 300-306.

Reddy, M.S., Kang,.P. H.S, Lie J.H., Reddy, V.R., Jang, Ja. S., 2014. Electrical Properties and the Role of inhomogeneities at the Polyvinyl Alcohol/n-InP Schottky Barrier Interface. Appl. Polym. Sci., 131, 39773-1 -39773-10.

Resfa, A., Bourzig Y. S., Brahimi, R. Menezla, 2011. Study and Modeling of the Transport Mechanism in a Schottky Diode on the Basis of a GaAs Semiinsulator. Journal of Semiconductors, 32, 12, 124001-124006.

Rhoderick, E.H., Williams, R.H., 1988. Metal-Semiconductor Contacts, Clarendon Press, 247p, Oxford.

Rhoderick, E.H, 1978. Metal-Semiconductor Contacts, Oxford University Press, 217 p, Oxford.

Rybalkaö S.B., Krayushkinaö E.Yu., Demidov, A.A., Shishkina, O.A., Surin, B.P., 2017. Forward Current-Voltage Characteristics Simulation of 4H-SiC Silicon Carbide Schottky Diode for Power Electronics. International Journal of Physical Research, 5, 1, 11-13.

Sachenko, A.V., Belyaev, A.E., Boltovets, N.S, Kapitanchuk, L.M., Kladko V.P., Konakova, R.V., Kuchuk, A.V., Korostinskaya, T.V., Pilipchuk, A.S., Sheremet, V.N., Mazur, Yu.I., Ware, M.E., Salamo, G.J., 2013. Mechanism of Current Flow and Temperature Dependence of Contact Resistivity in Au-Pd-Ti-Pd-n+-GaN Ohmic Contacts. Semiconductor Physics, Quantum Electronics & Optoelectronics, 16, 4,313-321.

Saghrouni, H., Jomni, S., Belgacem, W., Elghoul, N., Beji, L., 2015. Temperature Dependent Electrical and Dielectric Properties of a Metal/Dy_2O_3/n-GaAs MOS Structure. Materials Science in Semiconductor Processing, 29, 307–314.

Saito, H., Stuhn, B., 1994. Dielectric Study of the Crystal-Amorphous Interphase in Poly vinylidene fluoride/poly methyl Methacrylate Blends. Polymer, 35, 3, 475-479.

Salace, G., Hadjadj, A., Petit, C., Ziane, D., 2000. The Image Force Effect on the Barrier Height in MOS Structures: Correlation of the Corrected Barrier Height with Temperature and the Oxide Thickness, Microelectronics Reliability, 40, 4, 763-766.

Salama AH, Dawys. M, Nada AMA, 2004. Studies on Dielectric Properties and AC-Conductivity of Cellulose Polyvinyl Alcohol Blends Polymer-Plast. Technol Eng., 43, 4, 1067-1083.

Sasidhar, S., 2011. Interfacial effect on dielectric properties of polymer particle nanocomposites, PH.D thesis, 174 p, Missouri university of science and technology, Missouri.

Saurabh, M., Dheeraj, M., Theresa, M., Vijay, N., Suman D., 2010. Temperature-Dependent I–V Characteristics of a Vertical $In_{0.53}Ga_{0.47}$as Tunnel FET. IEEE Electron Device Letters, 31, 6.564-566.

Schmitsdrof, R.F., Kampen, T.U., Mönch, W.,1997. Explanation of the Linear Correlation between Barrier Heights and Ideality Factors of Real Metal-Semiconductor Contacts by Laterally Nonuniform Schottky Barrier.s J. Vac. Sci.Technol. B, 15, 4, 1221-1226.

Schottky, W., 1938. Halbleitertheorie de Sperrschicht. Naturwissenschaften, 26, 843-870.

Schroeder, D., Avellan, A., 2003. Physical Explanation of the Barrier Height Temperature Dependence in Metal-Oxide-Semiconductor Leakage Current Models. Appl. Phys. Lett., 82, 25, 4510-4512.

Schuegraf, K.F., King, C.C., Hu, C., 1992. Ultra-thin silicon dioxide leakage current and scaling limit, Digest Symposium on VLSI, IEEE, New York, 18.

Selçuk, A. B., Ocak, S. B., Kahrama, G., and Selçuk, A. H., 2014. Investigation of Diode Parameters using I–V and C–V Characteristics of Al/maleic anhydride MA/p-Si Structure Bull. Mater. Sci., 37, 7, 1717–1724.

Selçuk, A.B., B., Ocak, S., Aras, G., Orhan, E., 2015. Frequency Dependent Dielectric Properties of PMMA Deposited on p-type Silicon. Materials Science in Semiconductor Processing, 38,119–125.

Selçuk, Demirezen, 2013. Frequency- and Voltage-Dependent Dielectric properties and Electrical Conductivity of Au/PVA Bi-doped/n-Si Schottky Barrier Diodes at Room Temperature. Appl. Phys. A, 112,827–833.

Sharma, M., Tripathi, S. K., 2012. Study of Barrier Inhomogeneities in I–V-T and C-V-T Characteristics of Al/Al_2O_3/PVA: n-ZnSe Metal–Oxide–Semiconductor Diode. J. of App. Phys., 112, 024521.

Sharma, B.L, 1984. Metal-semiconductor Schottky Barrier Junctions and their applications, 370 p, Plenum Press, New York and London,

Shehap, A., Abd Allah R.A, Basha A.F., and Abdel-Kader F.H. er, 1998. Electrical Properties of Gamma-Irradiated, Pure, and Nickel Chloride-doped Polyvinyl Alcohol Films. J. Appl. Polym. Sci., 68, 5, 687-698.

Shekar, B. C., Veeravazhuthi, V., Sakthivel, S., Mangalaraj, D., Narayandass, Sa. K., 1999. Growth, Structure, Dielectric and AC Conduction Properties of Solution grown PVA films. Thin Solid Films, 348, 122-129.

Singh, P. K., Gaur, M.S., Chauhan, R. S., 2015. Dielectric Properties of Sol–Gel Synthesized Polysulfone–ZnO Nanocomposites J.Therm Anal Calorim, 122, 2, 725-740.

Sochacki, M., Kolendo, A., Szmidt, J., Werbowy, 2005. A, Properties of Pt/4H-SiC Schottky Diodes with Interfacial Layer at Elevated Temperatures, Solid State Electron., 49,4, 585-590.

Song, Qing-Wen, Zhang Yu-Ming, Zhang Yi-Men, Chen Feng-Ping, Tang, Xiao-Yan, 2011. Investigation of Current Transport Parameters of Ti/4H–SiC MPS Diode with Inhomogeneous Barrier. Chin. Phys. B, 20, 5, 057301.

Sukru, K., Zekeriya K., 2011. Temperature Dependent Electrical and Dielectric Properties of Sn/p-Si Metal–Semiconductor MS Structures Microelectronics Reliability, 51, 2205–2209.

Sullivan, J. P., Tung, R. T., Pinto, M.R., Graham, W. R. 1991. Electron Transport of Inhomogeneous Schottky Barrier: A numerical study. Journal of Applied Physics, 70, 12, 7403-7423.

Symth, C.P., 1955. Dielectric behaviour and structure, 441 p, McGraw-Hill, New York.

Sze, S. M., and Kwok, K. Ng., 2007. Physics of Semiconductor Devices 3rd ed., 832 p, New Jersey: John Wiley & Sons, New Jersey.

Sze, S. M., 2002, Semiconductor Devices Physics and Technology, 574 p, John Wiley & Sons, 2nd ed..USA.

Sze, S. M., 1981, Physics of Semiconductor Devices, 830 p, John Wiley and Sons, Toronto.

Tairov, Yu.M., Tsvetkov, V.F., 1978. Investigation of Growth Processes of Ingots of Silicon Carbide Single Crystals. Journal of Crystal Growth, 432, 209-212.

Tanrıkulu, E. E., Yıldız, D. E., Günen, A., Altındal, Ş., 2015. Frequency and Voltage Dependence of Electric and Dielectric Properties of Au/TiO_2/ n-4H-SiC Metal-Insulator-Semiconductor type Schottky Barrier Diodes. Physica Scripta, 90, 9. 095801.

Tasciglu, İ., Farooq W.A., Turan, R., Altındal, Ş., yakuphanoglu, F., 2014. Charge Transport Mechanism and Density of Interface Traps in MnZnO/p-Si Diodes. Journal of Alloys and Compounds, 590, 157-161.

Taşçıoğlu, İ., Aydemir, U., Altındal, Ş., Kınacı, B., Özçelik, S., 2011. Analysis of the Forward and Reverse Bias I-V Characteristics on Au/PVA: Zn/n-Si Schottky Barrier Diodes in the Wide Temperature Range. J.Appl. Phys., 109, 054502.

Taşçıoğlu, İ., Tüzün., Ö., Sağban, H. M., Yağlıoğlu, E., Altındal, Ş., 2017. Frequency Dependent Electrical and Dielectric Properties of Au/P3HT: PCBM: F4-TCNQ/n-Si Schottky Barrier Diode. J. Electron. Mater, 46, 4, 2379–2386.

Tecimer, H., 2014. The Preparation of Au/Zn-Doped PVA/n-GaAs Structure and the Investigation of their Current Transport Mechanism in the Wide Temperature. Ph. D. thesis, 88 p, Gazi University,Ankara.

Tecimer, H., Turut A., Uslu, H., Altındal, S., Uslu, I., 2013. Temperature Dependent Current-Transport Mechanism in Au/Zn-dopedPVA/n-GaAs Schottky Barrier Diodes SBDs Sensors and Actuators A, 199, 194– 201.

Tecimer, H., Uslu, H., Alahmed, Z.A., Yakuphanoglu, F., Altındal, Ş., 2014. On the Frequency and Voltage Dependence of Admittance Characteristics of Al/PTCDA/P-Si MPS type Schottky Barrier Diodes SBDs. Composites Part B, 57, 25-30.

Tecimer, H., Türüt, A., Uslu, H., Altındal, Ş., Uslu, İ., 2013. Temperature Dependent Current-Transport Mechanism in Au/Zn-doped PVA/n-GaAs Schottky Barrier Diodes SBDs. Sensors and Actuators A : Physical, 199, 194-201.

Tiwari, D.C., Sen, V., Sharman, R., 2012. Temperature dependence studies of electric and dielectric properties of polythiophene based nano composite. Indian journal of pure &Applied physics, 50, 49-56.

Tripathi, S.K., Sharma, M., 2012. Analysis of the Forward and Reverse Bias I-V and C-V Characteristics on Al/PVA:n-PbSe Polymer Nanocomposites Schottky Diode J. Appl. Phys., 111, 074513.

Tunc, T.¸ Altindal, S., Dokme, I., Uslu, H., 2011. Anomalous Peak in the Forward-Bias C–V Plot and Temperature-Dependent Behavior of Au/PVA Ni,Zn-doped/n-Si(111) Structures. Journal of Electronic Materials, 40, 2,157-164.

Tunc, T., Altındal, Ş., Uslu, I., Dökme, I., 2011. Temperature Dependent Current–Voltage I–V Characteristics of Au/n-Si 111 Schottky Barrier Diodes with PVANi,Zn-doped Interfacial Layer. Mat. Sci. Sem. Proc., 14, 139-145.

Tunç, T., Gökçenö M., 2012. Preparation and Electrical Characterization of Au/n-Si (110) Structure with PVA–Nickel Acetate Composite Film Interfacial Layer. Journal of Composite Materials, 46, 22, 2843-2850.

Tung, R.T., 1992. Electron Transport at Metal-Semiconductor Interfaces General Theory. Phys. Rev. B-45, 23, 13509.

Tung, R.T., 2001. Recent Advances in Schottky Barrier Concepts, Materials Science and Engineering: R, 35, 1-3, 1-138.

Uslu, I., Dastan H., Altas A., Yayli, A., Atakol, O., Aksu, M., 2007. Preparation and Characterization of PVA/boron Polymer Produced by an Electrospinning Technique. e-Polymers, 133,1-6.

Uslu, İ., Başer, B., Yaylı A., and Aksu M.L., 2007. Preparation and Characterization of PVA/zinc acetate/ boron Composite Fibers. e-Polymers, 145, 1-6.

Uslu, H., Altındal, Ş., Dökme, İ., 2010. İllumumination Effect on Electrical Characteristics of Organic-Based Schottky Barrier Diodes. J. Appl. Phys., 108, 104501, 1-6.

Uslu, H, Altındal, Ş., Tunç, T., Uslu, İ., Mammadov, T., S., 2011. The Illumination Intensity and Applied Bias Voltage on Dielectric Properties of Au/polyvinyl alcohol Co, Zn- doped/n- Si Schottky Barrier Diodes, J. of Appl.Polym. Sci., 120, 1, 322-328.

Van Der Ziel, 1968. Solid State Physical Electronics, 654p, Prentich-Hall, New Jersey.

Von, R. A., 1959.Dielectrics and Waves, 284p, John Wiley & Sons, New York.

Wang, H., Lu X., Zhao Y., Wang C., 2006. Preparation and Characterization of ZnS: Cu/PVA Composite Nanofibers via Electrospinning. Materials Letters, 60, 2480–2484.

Werner, J.H., Güttler, H.H, 1991.Barrier Inhomogeneities at Schottky Contacts. J. Appl. Phys., 69, 3, 1522-1533.

Werner, J, Levi. A.F.J, Tung. R.T, Anzlowar. Pinto. M, M., 1988. Origin of the Excess Capacitance at Intimate Schottky Contacts. Phys. Rev. Lett., 60, 53-56.

Wert, C.A.,Thomson, R.M., 1970. Physics of Solids 2nd ed., 522 p, McGraw-Hill, New York.

Wittmer, M., Freeouf, J. L., 1994. Schottky Barriers and the Reactivity of The Interface. Europhysics Letters, 262, 135-140.

Wu J., Register L., Rosenbaum E., 1999. Trap Assisted Tunneling Current Through Ultra-Thin Oxide. Proc. IRPS Symposium, 389-395.

Wu, X, Yang, E. S., Evans, H. L., 1990. Negative Capacitance at Metal-Semiconductor Interfaces. J. Appl. Phys., 68, 6, 2845-2848.

Xiaa, Q., Chena X., Zhaoa K., Liu J., 2008. Synthesis and Characterizations of Polycrystalline Walnut-like CdS Nanoparticle by Solvo Thermal Method with PVP as Stabilizer. Materials Chemistry and Physics, 111, 1, 98-105.

Xu, Z., Huang, X.J., Wan, L., 2009. Surface Engineering of polymer Membranes, 329 p, Zhejiang University Press, Hangzhou and Springer-Verlag GmbH Berlin Heidelberg.

Yeriskin, S. A., Balbasi, M., Tataroglu, A., 2016. Frequency and Voltage Dependence of Dielectric Properties, Complex Electric Modulus, and Electrical Conductivity in Au/7% graphene doped-PVA/n-Si MPS Structures. J. Appl. Polym. Sci., 133, 43827.

Yucedağ, I., Kaya, A., Altındal, S., Uslu, I., 2014. Frequency and Voltage-Dependent Electrical and Dielectric Properties of Al/Co-doped PVA/p-Si Structures at Room Temperature. Chin. Phys. B, 23, 4, 047304.

Yucedağ, I., Kaya, A., Altındal S., Uslu I., 2014. Electrical and Dielectric Properties and Intersection Behavior of G/ω-V Plots for Al/Co-PVA/p-Si MPS Structures at Temperatures Below Room Temperature. Journal of the Korean Physical Society, 65, 12, 2082-2089.

Yun, M., 2009.Fabrication and abrication and characterization of polymer based metal-oxide – semiconductor and non-volatile memory device PH-D thesis, 160 p, Faculty of the Graduate School University of Missouri, Missouri.

Yücedağ, I., Kaya, A., Altındal, S., 2015. On the Anomalous Peak in the Forward Bias Capacitance and Dielectric Properties of the Al/Co-doped PVC+TCNQ/p-Si Structures as Function of Temperature. Journal of Nanoelectronics and Optoelectronics 10, 1–6.

Yücedağ, İ., Kaya, A., Tecimer, H., Altındal, Ş., 2014. Temperature and Voltage Dependences of Dielectric Properties and ac Electrical Conductivity in Au/ PVC+TCNQ /p-Si Structures. Materials Science in Semiconductor Processing 28, 37–42.

Zeghbroeck, B. Van., 2004. Principles of Semiconductor Devices. https://ecee.colorado.edu/~bart/book.

Zeng, Y.A., Softic, A., White M.H., 2001. Characterization of Interface Traps in Subthreshold Regions of Implanted 6H- and 4H-SiC MOSFETs. International Semiconductor Device Research Symposium, 213-215.

Zhu, C.Y., Feng,L.F., Wang, C.D., Cong, H.X., Zhang, G.Y., Yang, Z.J., Chen, Z.Z., 2009. Negative Capacitance in Light-Emitting Devices. Solid-State Electron, 53 324–328.

CURRICULUM VITAE

Personal Information:

Name	: Mohammad Hussein Ali AL-DAHROB
Place of Birth	: Iraq/Baghdad
Date of Birth	: 14/08/1979
Marital Status	: Married
Nationality	: Iraqi
Email	: mscmohammed@yahoo.com

Education: MSC in Physics /ALNahreein Uinversity /Baghdad/Iraq in 2002

Undergraduate Education : BSC in Physics /ALNahreein Uinversity / Baghdad / Iraq in 2000

ÖZGEÇMİŞ

Kişisel Bilgiler:

Adı ve Soyadı	: Mohammad Hussein Ali AL-DAHROB
Doğum Yeri ve Yılı	: Irak/Bağdat
Medeni Hali	: Evli
Uyruğu	: Irak
Yabancı Dili	: Arapça/Ingilizce
E-posta	: mscmohammed@yahoo.com

Eğitim Durumu**:**	Yüksek Lisans Fizik /ALNahreein Uinversity / Bağdat / Irak 2002
Lisans Öğrenimi	: Lisans Fizik /ALNahreein Uinversity / Bağdat / Irak 2000